AD NUMBER

AD000769

NEW LIMITATION CHANGE

TO

Approved for public release, distribution unlimited

FROM

Distribution no foreign.

AUTHORITY

ONR ltr., 26 Oct 1077

AD- 769

Second Annual Report of the work of the Bartol Research Foundation of the Franklin Institute

Performed under Contract N6ori-144
Task Order 1 - "NR 026-021"
September 30, 1952

SECOND ANNUAL REPORT

of the Work of the

BARTOL RESEARCH FOUNDATION

OF THE FRANKLIN INSTITUTE

Performed Under Contract N6ori-144

Task Order 1 - "NR 026-021"

with the

OFFICE OF NAVAL RESEARCH

W. F. G. Swann, Director

Swarthmore, Pennsylvania

September 30, 1952

TABLE OF CONTENTS

Personnel of the Bartol Research Foundation engaged in the work described in the Second Annual Report under Contract N6ori-144.

W. F. G. Swann, Director #

William E. Danforth, Assistant Director ##

Allocation of Staff Personnel:

Cosmic Rays:

H. O. Albrecht — D. W. Seymour ø+ — D. W. Kent ø
G. W. McClure + — F. J. Seymour ø+
M. A. Pomerantz — T. J. Tidd

Nuclear Physics:

L. Eisenbud — C. E. Mandeville +
H. W. Fricke #+ — E. C. Snowdon +
W. F. Gamp + — C. P. Swann +
R. W. Gunnett, Jr. + — W. D. Whitehead +

Investigations of Counters:

C. E. Mandeville + — W. C. Porter — W. E. Ramsey #
G. W. McClure +

Linear Accelerator:

J. F. Marshall — R. A. Shutes

Computing:

E. A. Seaman +

Shop: — R. C. Pfeiffer, Chief Mechanician +

G. A. Hay #+ — D. A. McCauley + — M. B. Peyton +
H. A. Lister + — R. J. Moore +

* The Director maintains active participation in the projects but receives no part of his salary from the Contract.

** Dr. Danforth also maintains interest in certain parts of the work under the Contract, but receives no part of his salary from this Contract.

* Part time charged to Contract.

\# Temporary or part-time.

\+ Terminated.

*** Dr. Marshall has participated in the development of the linear accelerator in connection with the use of this instrument for another project. No part of his time is charged to this Contract.

\' Part time roentgen ray work. Time not charged to this contract.

I. COSMIC RAYS

A. INDIA EXPEDITION

A considerable amount of time and effort has been spent in preparing apparatus for experiments to be conducted by Dr. M. A. Pomerantz in the Himalayan Mountains in India and in radiosonde flights in these locations. Dr. Pomerantz is at present en route to India under the auspices of a Fulbright Award. He has with him enough of the equipment to commence operations and further equipment is being sent to him.

The general nature of this work comprises measurements at high altitudes of the primary cosmic ray intensity utilizing Geiger counter techniques described in earlier reports and utilizing also, as part of the equipment, high-pressure ionization chambers devised by Dr. C. W. McClure and controlled by the Geiger counters aforesaid. It will be recalled that Dr. McClure's ionization chambers have already been tested and used by him in connection with flights made in polar regions. The purpose of these observations is, of course, to discriminate between the various kinds of ionizing primaries, with particular emphasis on the determination of the α-particle component. To the same end, some photographic plates will be flown.

In addition to the foregoing observations, the program includes measurements of neutron intensity with boron-trifluoride counters at various ground altitudes such as are obtainable in the Himalayan Mountains.

The total amount of equipment either at present with Dr. Pomerantz, en route to him, or in preparation for shipment, comprises the following: Twenty-six balloon-borne instruments containing Geiger-Muller counter telescopes in which various amounts of Fe absorber will be interposed, twenty-four balloon-borne instruments each containing a high-pressure ionization chamber controlled by a G-M counter telescope, and two neutron counting systems for ground observations. In addition to the actual recording instruments, numerous pieces of equipment required for thorough tests of the performance of these instruments are included among the supplies.

B. A DETERMINATION OF μ-MESOTRON REST LIFETIME AND A VERIFICATION OF THE RELATIVISTIC EXPRESSION FOR VARIATION OF LIFETIME WITH MOMENTUM

In the First Annual Report reference was made to an experiment which, at that time, had been completed, and concerned with an investigation described in the title. A copy of the completed paper on this matter, which has been sent in for publication, is appended to this Report.

C. COLLABORATION IN THE EXPEDITION TO GREENLAND SPONSORED BY THE OFFICE OF NAVAL RESEARCH

Four three-pound packets of nuclear emulsion were prepared for the balloon flight and delivered by Mr. Donald Kent to Lt. Erickson, Air Traffic Liaison Officer, Westover Air Force Base, on July 26, 1952. The construction of a typical packet is shown in the accompanying figure. The packets were arranged to obtain as much data as practicable concerning particles having a charge $z > 2$ in the primary cosmic radiation at high magnetic latitudes. Instructions were given to fly one packet on each of the four projected flights, in the interests of maximum opportunity for recovering some emulsion material.

The packets consisted of pairs of 6" X 6" plates coated with thick sensitive and insensitive emulsions. The emulsion surfaces were separated by paper spacers at the sides and were held firmly

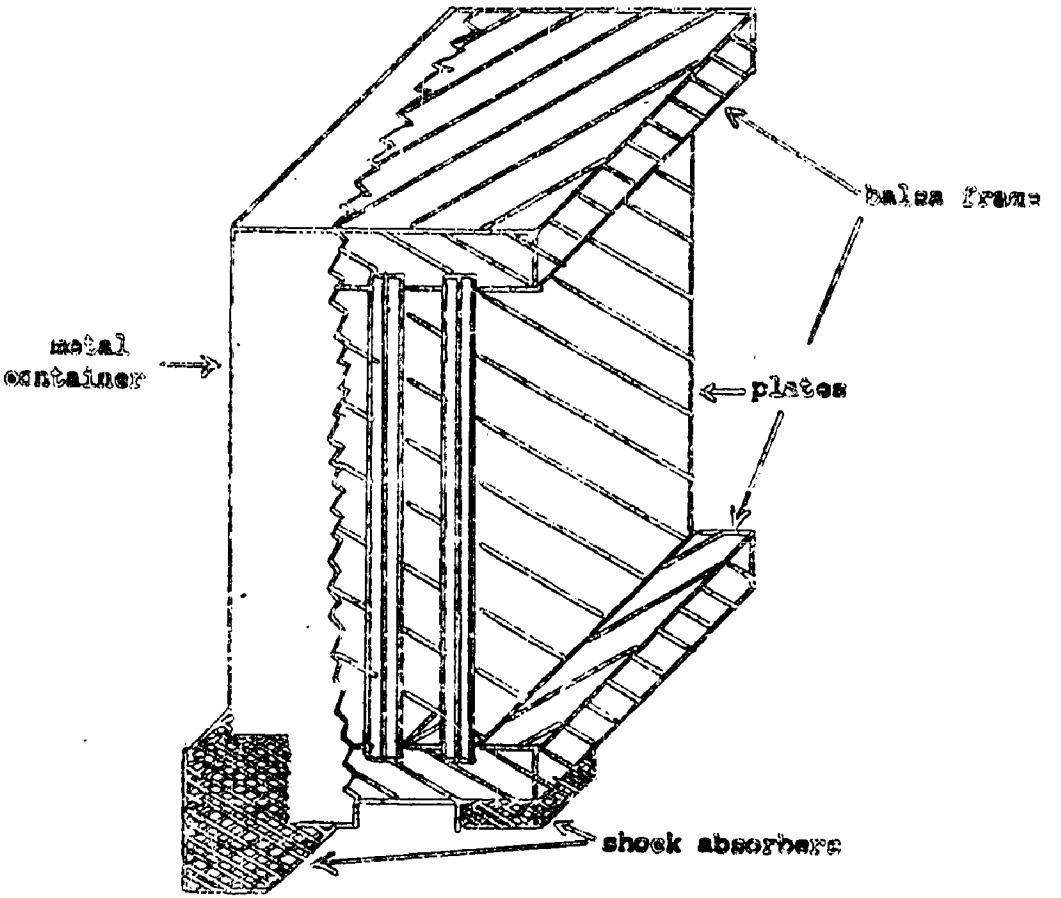

SCHEMATIC REPRESENTATION OF PLATE ORIENTATION IN A TYPICAL PACKET

together by a band of plastic tape around the glass backing. Three pairs of plates were enclosed in each box, supported in a grooved framework of balsa wood. The purpose of this framework was to insure that each pair be exposed so that a measurable track in one pair of plates could not have passed through any other pair, thus increasing the number of independent observations available for determination of the flux. To establish the value of the charge of a heavy primary, it is necessary, in general, to observe the track over a length greater than 3 mms in the emulsion. Thus only those tracks which lie near to the plane of the emulsion are useful in determining the charge distribution of the flux.

The plates used in making up the pairs were Ilford G5, 400μ and 600μ and Ilford C2, 200μ. There were also some Eastman Kodak NTB3 plates 250μ, 6" X 6". The purpose of the insensitive C2 plates is to permit a better measurement of the more heavily ionizing particles. The arrangement allows a threefold measurement to be made on each track: 1) δ-ray counts are made in the electron sensitive emulsion, 2) grain density measurement is made on the portion of the track which appears in the facing insensitive emulsion, 3) multiple coulomb scattering and, in some cases, range determinations are made to establish the velocity of the particle. From these measurements the charge can then be determined.

An "emulsion cloud chamber" consisting of 48 Eastman pellicles was included in one of the packets. The pellicles were 1" X 3" X 250μ; sensitive and insensitive emulsions were interleaved. This assembly permits following a track through as much

as a set of emulsions without passing through an intervening glass backing. The advantage of this arrangement is that the particle need not be in any particular plane to allow extensive measurement of the ionization. The disadvantage is difficulty in insuring uniform development throughout the 48 emulsions, so that ionization measurements can be made comparable in accuracy to those in the plates.

Two of the four projected flights were successful, one remaining at 90,000 feet for three hours. The equipment descended by parachute in one case to Ellesmere Island and in the other to the Greenland icecap. Unfortunately, in both cases, adverse weather conditions prevented recovery of the plates. There is some possibility that the packages may be salvaged in the spring, and a reward of $100 has been posted by Dr. Marcel Schein.

II. NUCLEAR PHYSICS

A. INSTRUMENTATION AND SOME NUCLEAR REACTIONS RELATING TO THE VAN DE GRAAFF GENERATOR.

For the first part of the report-year the operation of the small Van de Graaff was fairly satisfactory, and some progress was made in measuring the total neutron scattering cross sections of some of the elements. In the early spring several difficulties developed which culminated in the complete failure of the arc-type ion source due to poisoning of the filament. Some time was spent trying to find the source of the trouble without success and finally an RF ion source was installed in the existing head. This improved the situation but several leaks in the vacuum tube and an inability to focus the beam above 400 Kv prevented operation. A new head was installed with higher focusing voltage supplies, new focusing electrodes were installed and the leaks were gradually found and cured, and by late summer the generator was back in operation.

The RF ion source was of the type developed in this laboratory by Swann and Swingle and used in the large

Van de Graaff generator. The focusing electrode assembly was very similar to that in the large generator except that the high voltage electrode had to be modified because of the smaller diameter of the tube. In the final focusing assembly the intermediate electrode, the high voltage electrode and the first tube electrode are all the same diameter.

The new head, which was designed for ruggedness, compactness and convenience of servicing, has all of its components mounted on four plates which are assembled one above the other with spacer rods. The bottom plate supports the belt pulley and the high voltage electrode and is connected to the high voltage focusing electrode. This plate is electrically insulated from the second by lucite rods and a rubber V-belt which drives the 400 cycle generator. The second plate contains the 400 cycle generator, the oscillator, the oscillator power supply and the blowers all of which are complete units and can be separately removed from the plate. Originally, the second plate supported an aluminum electrode which shielded the upper plates from the high voltage electrode but this was found unnecessary. The third and fourth plates are back to back, the third supports the control varistor and the palladium leak and the associated vacuum system, the fourth is the chassis for the 30 Kv focusing supply, the 10 Kv focusing supply and the probe supply.

There are also valves in the vacuum system so that the entire head can be removed without opening the main vacuum.

The poisoning of the filament in the ion source and the clogging of the 20 mil hole in the first RF source indicated that the source of the contamination was the vacuum tube. We tried to reduce this effect with a dry ice-acetone cold trap in the main vacuum system and larger diameter pumping lead between the diffusion pump and the fore pump. The capillary in the RF source was enlarged to 40 mils; these two steps cured the contamination trouble.

Several changes and improvements have been made to try to improve the stability of the generator. Electrostatic deflectors have been installed in the vacuum tube to center the beam on the analyzing magnet. New connectors between the true electrodes and the rings have been installed. The target end of the vacuum tube has been completely rebuilt and a small diffusion pump added at the target. The corona stabilizer system has been overhauled and a Selsyn driver probe has been installed.

On the long term basis a new magnet box is being designed which will incorporate two sets of beam defining slits and a torsion balance so that the magnet can be used as an energy analyzer. The torsion balance is under construction. The parts for a new tube are completed, and will be assembled in the near future; the new tube will be installed when the situation warrants it.

The voltage scale of the generator beam was calibrated using the $F^{19}(p,\alpha\gamma)O^{16}$ resonance at 0.305 Mv, the $Li^7(p,\gamma)$ resonance at 441, the $Al^{27}(p,\gamma)$ at 992, and the $H^3(p,n)He^3$ threshold at 1.019 Mev. A measure of the energy spread in the beam was determined from the half widths of the resonance peaks and must be less than 2 Kv. The RF ion source has given a maximum current of 15 μa of analyzed protons, but the best stability is obtained between 2 μa and 5 μa, but there is still a certain amount of instability in the position of the beam. The high voltage has been up to 1.62 Mev but was unstable. However, data has been taken at 1.52 Mev, and with more operation the higher voltage will probably be attained. With the corona regulator working properly, the voltage is constant to ± 2 Kv.

Total Neutron Cross Sections

The measurement of the total neutron cross sections of some of the elements is being continued by measuring the transmission of discs for monoenergic neutrons from the $T(p,n)He^3$ reaction. The cross sections for copper and magnesium have been measured to test the technique and the apparatus, and we have completed the measurement of the cross section of gold from 300 Kv to 700 Kv.

The experimental apparatus and the manner in which the results were obtained. The neutrons were detected with a boron trifluoride counter surrounded by a block of paraffin and a cadmium shield. The counter is 1½ inches from the target, and the sample which has a transmission of about 50%, is 1 1/2 inches from the target. The sample position was determined experimentally to give a minimum scattering in correction. The following procedure was used for taking data, the neutron flux was determined with no sample, the flux was determined with sample, the background was determined with sample in place and a paraffin cone between it and the counter. The resolution, as measured by the threshold curve for the $T(p,n)He^3$, was 35 Kv, this also checks very well with the cross section for the resonances in Mg. The cross sections were computed, making corrections for inscattering and background.

Proton Spectrometer

A balance for measuring the magnetic field, a target chamber and a scintillation detector and amplifier have been constructed and tested. The balance has been calibrated using the α-particles from polonium and the edge of the beam is reproducible to better than 0.02%. The target chamber has slits to define the beam, a movable target support, an

α-particle source which can be inserted in place of the target, and a movable slit system to measure the angle between the incoming beam and the outgoing particles. The detector is a stilbene crystal mounted on a 5819 photomultiplier and magnetically shielded. The proton spectrometer is essentially complete and we plan to use it as soon as we can make the generator operation more stable.

Neutrons from the Disintegration of Neon by Deuterons

The stable isotopes of neon are Ne^{20}, Ne^{21}, and Ne^{22}, the relative abundance of Ne^{20} being more than 90%. The high concentration of this isotope in naturally occurring neon makes it possible to study certain reactions without the use of stable isotopes. When Ne^{20} is irradiated by neutrons, one of the several competing nuclear reactions is

$$(1) \quad Ne^{20} + D \rightarrow Na^{21} + H^1 + Q$$

where Q is the energy release of the reaction. This Q-value can be calculated from several other nuclear reactions which are already known. These are,

$$(2) \quad Ne^{20} (D, H^1) Ne^{21} \qquad Q = +4.529 \pm 0.009 \text{ Mev}$$

$$(3) \quad Na^{21} (\beta^+) Ne^{21} \qquad Q = 3.522 \pm 0.020 \text{ Mev}$$

$$(4) \quad N (\beta^-) H^1 \qquad Q = 0.782 \pm 0.001 \text{ Mev}$$

If reactions (3) and (4) are subtracted from reaction (2), the result is

(5) Ne^{20} (D,n) Na^{21} $\quad Q = 0.225 \pm 0.022$ Mev

The calculated Q-value of equation (5) should agree with that observed in reaction (1).

A thin gaseous target of neon was irradiated by deuterons of mean energy 1.0 Mev, supplied by the Bartol Van de Graaff statitron. The emitted neutrons were observed at angles of zero and 90^0 with the incident deuterons by the method of recoil protons in Eastman NTA plates. The observed neutron spectrum for 0^0 and 90^0 is shown in Figure 1. Emulsion thicknesses of 100 μ and 200 μ were employed. The most pronounced group of particles is attributed to Ne^{20} (D,n) Na^{21}. The position of neutrons from carbon contamination is indicated as is the position of the group from Ne^{20} (D,n) Na^{21}, calculated from the Q-value of +0.22 Mev. It is evident that the observed position is in disagreement with the calculated one. In the forward direction, two groups of neutrons are assigned to $C^{12}(D,n)$ N^{13}, one being assumed to have originated on the high energy side of the foil of the gas target chamber. The geometry was so arranged that such neutrons would not be recorded in the plates at 90^0. The observed Q-value is -0.17 ± 0.05 Mev, 0.39 Mev smaller than that calculated in equation (5).

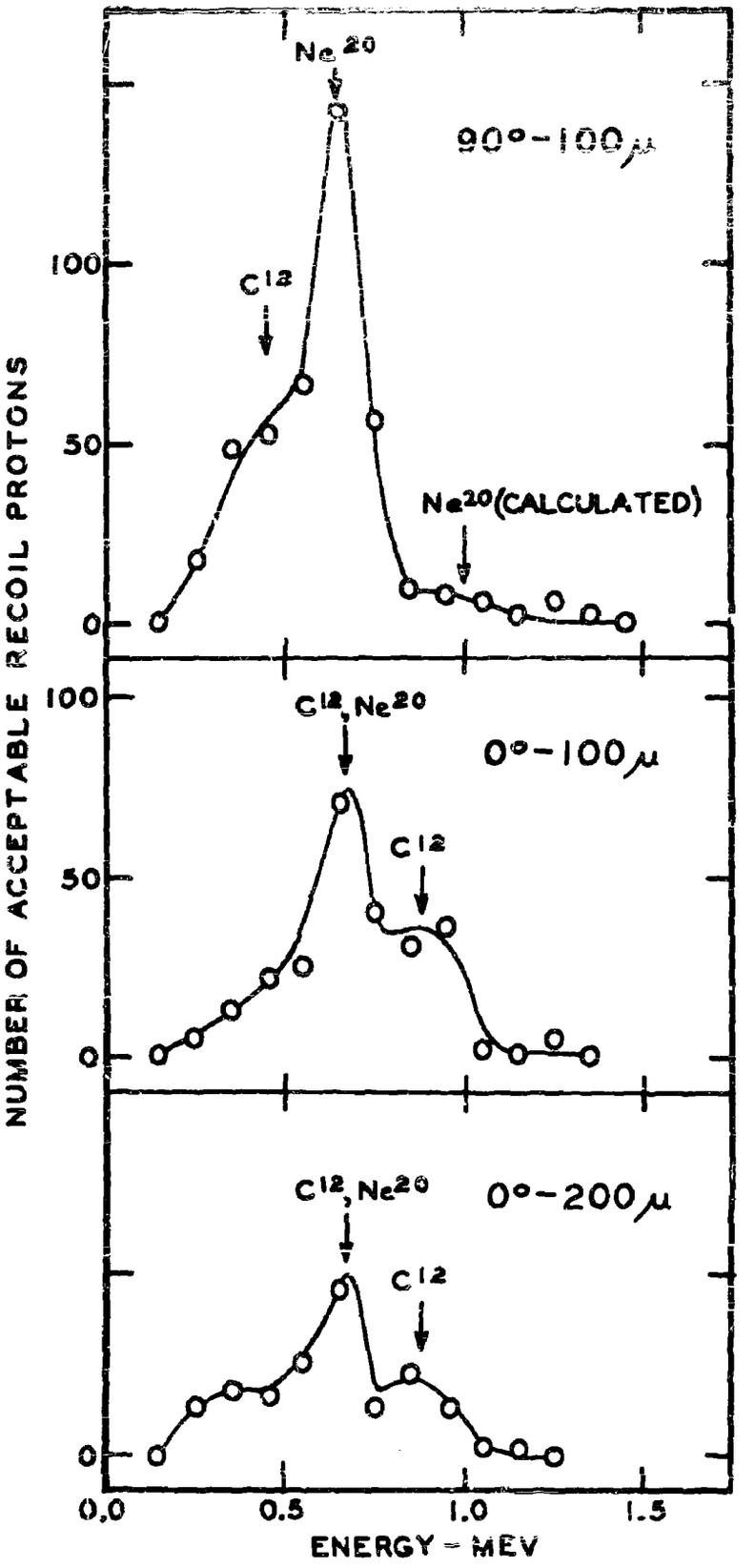

Fig. 1 Recoil proton spectrum of neutrons emitted in the disintegration of neon by deuterons.

A possible explanation for the discrepancy would be that the positrons of Na^{21} are followed by about 390 Kev of gamma ray energy. However, log ft. for Na^{21} is 3.6, placing the spectrum in the category of the super allowed transitions. This type of transition would be expected to occur between the ground states of Na^{21} and Ne^{21}; so no gamma radiation should be present. A private communication from J. R. Richardson and associates at UCLA has been received to the effect that no gamma rays from Na^{21} have been detected in a scintillation spectrometer. Only annihilation radiation was present.

The foil thickness and target thickness were calculated several times independently by several different members of the Bartol Staff. The bombarding energy was 1.35 Mev; the foil thickness was 300 Kev; and the target thickness was 100 Kev, giving an average effective deuteron energy of 1.35 - 0.30 - 0.05 = 1.0 Mev.

8. RADIOACTIVITY. Gamma Radioactivity from Zr^{95} and Nb^{95}.

Introduction

It has been shown that the 65 ± 2 day Zr^{95} and the 35 ± 1 day Nb^{95} are formed in several different nuclear reactions[1].

In a magnetic spectrograph[2], the energies of the gamma rays emitted by Zr^{95} have been measured at 0.75 Mev (93 per cent), 0.23 Mev (93 per cent), and 0.92 Mev (7 per cent). Approximately 2 per cent of the beta ray disintegrations of Zr^{95} have been shown to terminate at a 90 hour metas. is level[3] of the residual nucleus, radioactive Nb^{95}. The energy of the isomeric transition has been measured as 0.236 Mev[4] and 0.24 Mev[3]. The radiation is totally converted. The energy of the relatively hard abundant gamma ray of Zr^{95} has also been measured as 0.738 Mev[4].

Spectrometric measurements have yielded quantum energies of 0.75 Mev[6], 0.758 Mev[4] and 0.77 Mev[7] for the single gamma ray of Nb^{95}, the 35-day daughter element. The energy of this gamma ray was also measured as 0.92 Mev by the method of coincidence absorption[6]. In these latter measurements, the gamma ray which appeared to have an energy of 0.92 Mev was found in both the zirconium and niobium fractions. However, the beta-gamma coincidence

rate of Zr^{95} was such as to suggest that on the average, each beta of Zr^{95} is followed by less than 0.3 Mev of gamma-ray energy. When a carefully purified source of Nb^{95} yielded a beta-gamma coincidence rate sufficiently large to account for the presence of the hard gamma ray thought to be of energy 0.92 Mev, it was concluded that the presence of this gamma ray in the zirconium fraction arose from an incomplete chemical separation and that it is actually only associated with the daughter element. Because of the various conflicting reports concerning the gamma radiations, the properties of Zr^{95} - Nb^{95} have been reinvestigated.

Procedure and Results

A source of Zr^{95} - Nb^{95} was produced in the fission process at the Oak Ridge pile. Pure separated sources of Zr^{95} and Nb^{95} were prepared repeatedly by Steinberg's oxalate procedure[9]. The gamma rays of Nb^{95}, Zr^{95}, and Zr^{95} - Nb^{95} were absorbed in lead as shown in Figure 1. From the slopes of the curves it is evident that the gamma rays emitted by the three different radioactive sources are essentially the same in energy. No evidence appears on any of the absorption curves to suggest the presence of any gamma rays of lower energy and comparable intensity. Repeated chemical separations always gave

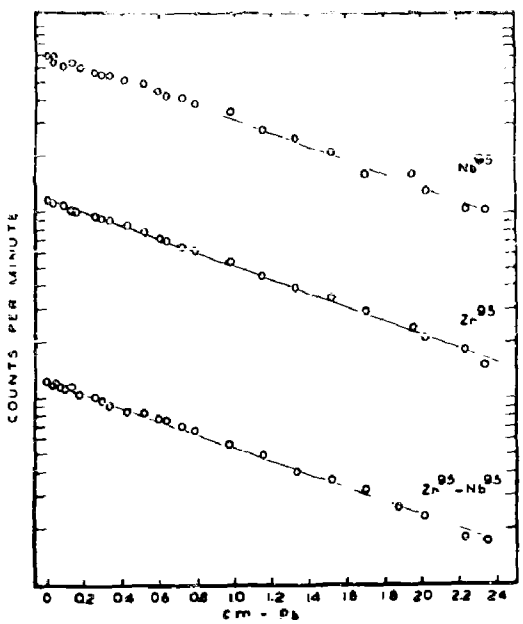

Fig. 1 Absorption in lead of the gamma rays of Nb^{95}, Zr^{95}, and $Zr^{95} - Nb^{95}$.

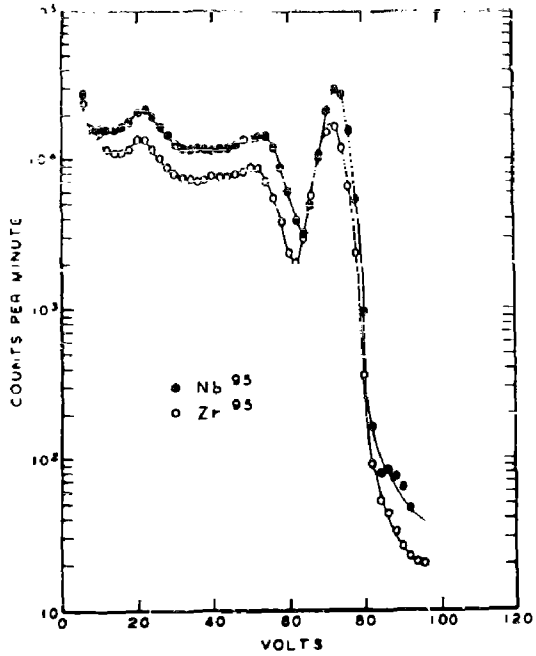

Fig. 2 Pulse height distribution of gamma rays from Zr^{95} and Nb^{95} on NaI - Tl .

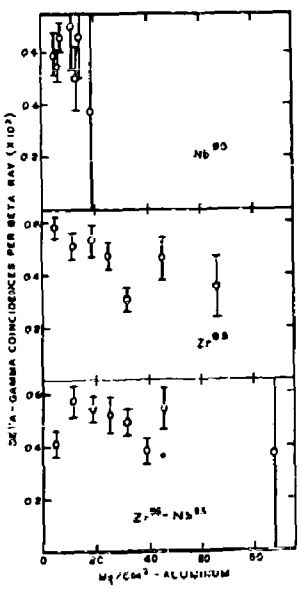

Fig. 3 Beta-gamma coincidence rate of Nb^{95}, Zr^{95} and $Zr^{95} - Nb^{95}$ as a function of aluminum absorber thickness before the beta ray counter.

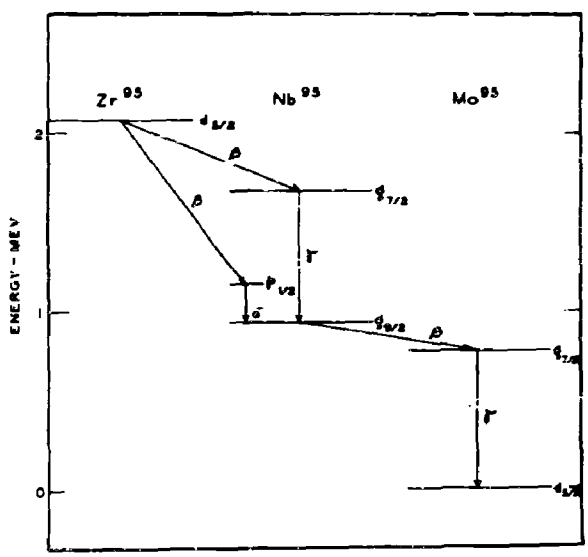

Fig. 4 Disintegration Scheme for Zr^{95} and Nb^{95}.

absorption curves similar to those of Figure 1. The quantum energy taken from the slope of the curve is 0.69 ± 0.05 Mev.

With the aid of a scintillation spectrometer, the photoelectric lines of the gamma rays of freshly separated Zr^{95} and Nb^{95} were observed in a crystal of NaI - Tl. The pulse height distributions are shown in Figure 2, where it is clear that the gamma ray of Nb^{95} is somewhat more energetic than that of Zr^{95}. Calibration of the spectrometer with the gamma rays from Au^{198}, Na^{22}, Cs^{137}, Sc^{46}, and Co^{60} yielded quantum energies of 0.73 ± 0.02 Mev and 0.76 ± 0.02.

The beta-gamma coincidence rates of Nb^{95}, Zr^{95}, and Zr^{95} - Nb^{95}, as a function of aluminum absorber thickness before the beta-ray counter, are shown in Figure 3. It is evident that the average value of the coincidence rate is approximately the same in the three cases, confirming that most of the beta rays of Zr^{95} are followed, on the average, by approximately the same amount of gamma-ray energy (0.71 Mev) as are the beta rays of Nb^{95}. The beta-gamma coincidence counting arrangement was calibrated by the beta-gamma coincidence rate of Sc^{46}. In a separate group of coincidence measurements at certain selected thicknesses of absorbers before the beta-ray

counter, the amounts of gamma ray energy per beta ray of Table I were obtained.

Table I - Average gamma-ray energy per beta ray

Radionuclide	Absorber thickness	Gamma-ray energy (Mev)
Nb^{95}	5 mg/cm^2	0.71 ± 0.09
Zr^{95}	40 mg/cm^2	0.67 ± 0.08
Zr^{95} - Nb^{95}	40 mg/cm^2	0.73 ± 0.09

The Disintegration Scheme

The 1.0 Mev beta spectrum of Zr^{95} ($\Delta I = 2$, yes!)[10] terminates at the 90-hr. level of Nb^{95} ($p_{1/2}$)[11]; as the orbital of the last odd nucleon of Zr^{95} is taken to be $d_{5/2}$. Log ft[12] for the most abundant beta spectrum of Zr^{95} is 6.62, permitting the interpretation that the spectrum may be once forbidden ($\Delta j = 0, \pm 1$, yes!) or λ-forbidden ($\Delta j = 1$, no!, $\Delta \ell = 2$). According to the former classification, the excited level at 0.73 ± 0.02 Mev in the residual nucleus, Nb^{95}, could have the orbital $p_{3/2}$, $f_{5/2}$ or $f_{7/2}$. Were it either of the first two values, a relatively intense gamma ray of energy ~0.5 Mev would be expected to appear among the radiations of Zr^{95}, emitted in the transition between the level at 0.73 ± 0.02 Mev and the 0.21 Mev metastable level of the 90-hr. Nb^{95}

(see Figure 4). Only in the case of $i_{7/2} \rightarrow f_{9/2}$ does the probability of a transition to the ground state of Nb^{95} exceed that of a transition to the metastable level ($f_{7/2} \rightarrow p_{1/2}$). Since no gamma radiation at 0.5 Mev is observed, the most likely of the three orbitals associated with the assumption of a once forbidden transition is $f_{7/2}$.

If an ℓ-forbidden beta transition is assumed, the orbital assignment of the 0.73 $\pm$ 0.02 Mev level is uniquely $g_{7/2}$. The transition $g_{7/2} \rightarrow g_{9/2}$ is, of course, far more probable than $g_{7/2} \rightarrow p_{1/2}$. Since the $f_{7/2}$ shell closes at 28 nucleons, the $g_{7/2}$ sub-shell, closing at 58 nucleons, is favored.

From shell model considerations and the conversion coefficients of the 0.76 $\pm$ 0.02 Mev gamma ray of Nb^{95}, it has been previously shown[13] that the decay of Nb^{95} to Mo^{95} can be characterized by $g_{9/2} \rightarrow g_{7/2} \rightarrow d_{5/2}$.

Footnotes

\# The present coincidence rates and associated gamma-ray energies are in contradiction with the previous report (reference 8) that the beta rays of Zr^{95} are coincident with less than 0.3 Mev of gamma-ray energy. The earlier results must be ascribed to the presence of unidentified impurities having relatively low beta-gamma coincidence rates.

When a radionuclide is grown from a parent element of comparable half-life, it can be shown that if a chemical separation is effected at a considerable length of time after onset of growth, the disintegration rates are in the ratio of

$$\frac{C_D}{C_P} = \frac{\lambda_D}{\lambda_D - \lambda_P}$$

where the subscripts P and D refer to parent and daughter, and the λ's are the decay constants. For the 65-day Zr^{95} and the 35-day Nb^{95}, this ratio is 2.16 ± 0.2. In the present investigation the ratio of the gamma-ray activities was observed in both scintillation counters and Geiger counters and found to be 2.2 ± 0.1, confirming a good separation if the gamma radiations of the parent and daughter are essentially the same.

References

1. Sagane, Kojima, Miyamoto and Ikawa, Phys. Rev. 57, 1180 (1940). B. L. Goldschmidt and I. Perlman, Radiochemical Studies: The Fission Products (McGraw-Hill Book Company, Inc., New York, 1951), Paper No. 84, National Nuclear Energy Series Plutonium Project Record, Vol. 9, Div. IV.

Brady, Engelhemier, and Steinberg, Ibid.,
Papers 85 and 88.

L. Jacobson and R. Overstreet, Ibid., Paper 91. The volume in which these latter references may be found will hereafter be referred to as NNES 9.

2. V. A. Nedzel, NNES 9, Paper 87.

3. D. W. Engelhemier and E. L. Brady, NNES 9, Paper 92. E. P. Steinberg, NNES 9, Paper 93.

4. Hudgens and Lyons, Phys. Rev. 75, 206 (1949).

5. J. S. Levinger, NNES 9, Paper 94.

6. W. Rall and R. G. Wilkinson, Phys. Rev. 71, 321 (1947).

7. V. A. Nedzel, NNES 9, Paper 90.

8. C. E. Mandeville and M. V. Scherb, Phys. Rev. 73, 1434 (1948).

9. E. P. Steinberg, NNES 9, Paper 243.

10. Mayer, Moszkowski and Nordheim, Revs. Modern Phys. 23, 315 (1951).

11. Goldhaber and Sunyar, Phys. Rev. 83, 906 (1951).

12. A. M. Feingold, Revs. Modern Phys. 23, 19 (1951).

13. C. Y. Fan, Phys. Rev. 81, 252 (1952).

C. CONCERNING COUNTERS

During the past year the counter group has dealt primarily with the problem of reducing dead-times in G-M counters and with measurements of the specific primary ionization of various gases by β-rays. In addition to the main investigations, a preliminary study has been made of the operation of counters in the neighborhood of the Geiger-Mueller threshold.

The dead-time investigations have lead to the development of simple cutoff circuit which limits the spreading of the discharge in a self-quenching counter to a small fraction of the wire length, thereby allowing the counter to respond to an ionizing ray as soon as 1.5 μ sec. after an earlier discharge. A detailed description of this circuit and the various tests which have been performed to test its effect on G-M counter-behavior is attached to the report in the form of a reprint. A review article now in preparation for publication in Nucleonics deals with the general problem of G-M counter dead-time and discusses the relative merits of the various methods which have been devised for dead-time reduction. An apparatus for measuring the relative efficiency of a counter at short times after a discharge has been devised, and will be described in this paper, together with some of the results it has yielded on counters with and without the cutoff circuit attached.

In an effort to obtain information for use in the design of low pressure G-M counters, a refined technique for measuring the specific primary ionization of gases has been developed. The method consists in measuring the probability that a low pressure counter filled with the gas under investigation will be discharged by a β-ray having a known energy (variable between 0.2 and 1.6 Mev) and a well-defined path-length in the counter. The discharge probability together with the path-length and gas pressure comprise information sufficient for the determination of the specific primary ionization of the gas contained in the counter.

Although the method of measurement is not new, certain improvements in apparatus design - notably a reduction of the upper and lower limits of the path-length -- provide the conditions necessary for more accurate specific primary ionization measurements than have heretofore been accomplished in the energy range concerned.

Successful measurements on H_2, He, Ne, and A -- described in detail in a paper which follows -- have been completed, and preparations are now being made to extend the investigation to the organic vapors used in self-quenching counters.

Specific Primary Ionization of H_2, He, Ne, and A by High Energy Electrons

Mono-energetic electrons magnetically separated from the continuous spectrum of a radioactive β-ray source are directed through a series of 3 G-M counters separated by thin Al windows. A measurement of the efficiency of the first counter by the coincidence method yields information from which the specific primary ionization of its contained gas is calculated.

Measurements on H_2, He, Ne, and A over the range of incident electron energies 0.2 to 1.6 Mev have been made and the data compared with the Bethe theory of primary ionization. By adjustment of two constants contained in the theoretical formula it is possible to fit the data for each of the four gases within the experimental errors. The adjusted formulae appear to predict accurate values of the specific primary ionization over a range of energies considerably greater than that investigated.

Introduction

Measurements of the specific primary ionization of gases by charged particles have been conducted by a number of investigators[1-7] over a considerable range of incident particle energies. There have, in some instances, been large discrepancies between the results obtained with

different methods of measurement, and the experimental errors have thus far precluded a critical quantitative comparison between the measurements and the predictions of the theory.

In view of the many applications of knowledge concerning the ionization of gases in various fields of experimental physics it was considered worthwhile to conduct a new set of precise measurements on several gases in the neighborhood of minimum ionization using β-particles from a radioactive source as the primary ionizing radiation. The measurements reported herein extend over a sufficient range of energies to make possible a determination of the parameters which enter into the Bethe theory of primary ionization and indicate the degree to which the theory may be relied upon as a tool for extrapolating experimental data.

Experimental Procedure.

The experimental procedure consists of measuring the probability that a G-M counter filled with the gas under investigation will be discharged by a β-ray having a known energy and a well-defined path-length in the counter. The relation between counting efficiency, $\mathcal{E}$, and the average number of primary ion pairs, X_0 produced by a β-ray in traversing the counter is

$$\mathcal{E} = 1 - e^{-X_0} \qquad (1)$$

and the specific primary ionization, i_p, at N. T. P. is given by

$$i = \frac{XT}{\ell p 273} \qquad (2)$$

where ℓ is the path-length, p the gas pressure in atmospheres and T the temperature in degrees K.

The validity of equation (1) rests upon the following assumptions: 1) that the primary ion pairs are statistically distributed in location along the path of an electron according to the Poisson law, 2) that the counter is certain to be discharged by any electron which produces one or more ion pairs in the gas, 3) that the probability of an electron being knocked out of the wall by an incident ray is negligible in comparison with the probability of production of a primary ion in the gas. Assumptions 1) and 2) appear to be well-founded on theoretical grounds, and 3) has been checked by examining the variation of ε with pressure as will be discussed below.

The experimental arrangement as shown in Figure 1 consists essentially of a 180° β-ray spectrograph (evacuated to 10^{-2} mm Hg) and a set of G-M counters C_1 C_2 and C_3. A radioactive cerium source at S gives rise to a continuous spectrum of β-rays ranging in energy from zero to 3 Mev. The series of baffles B selects from the continuous spectrum a mono-energetic beam of β-rays which

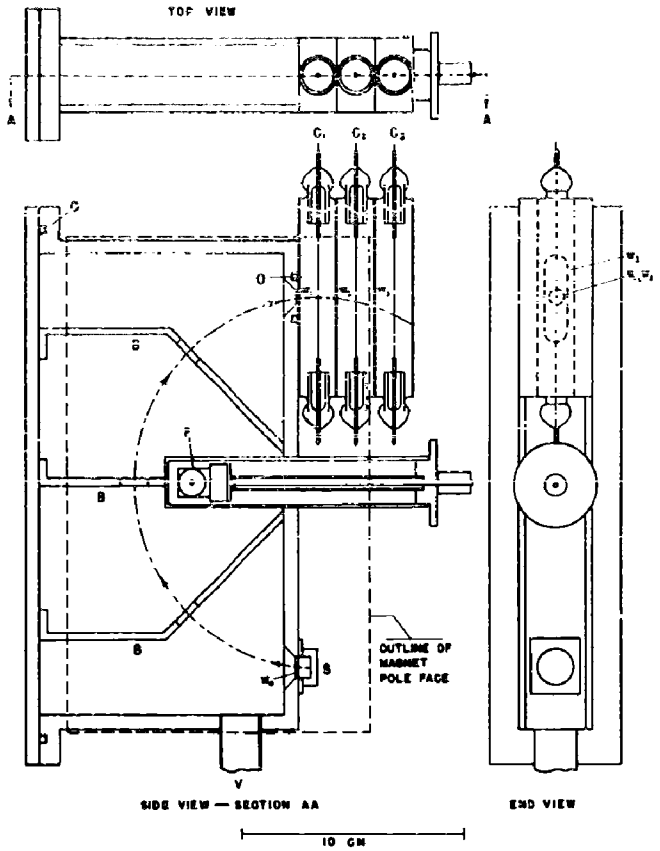

Fig. 1. - Appartus for determination of the specific primary ionization of gases by β-rays in the energy range 0.2 to 1.6 Mev.

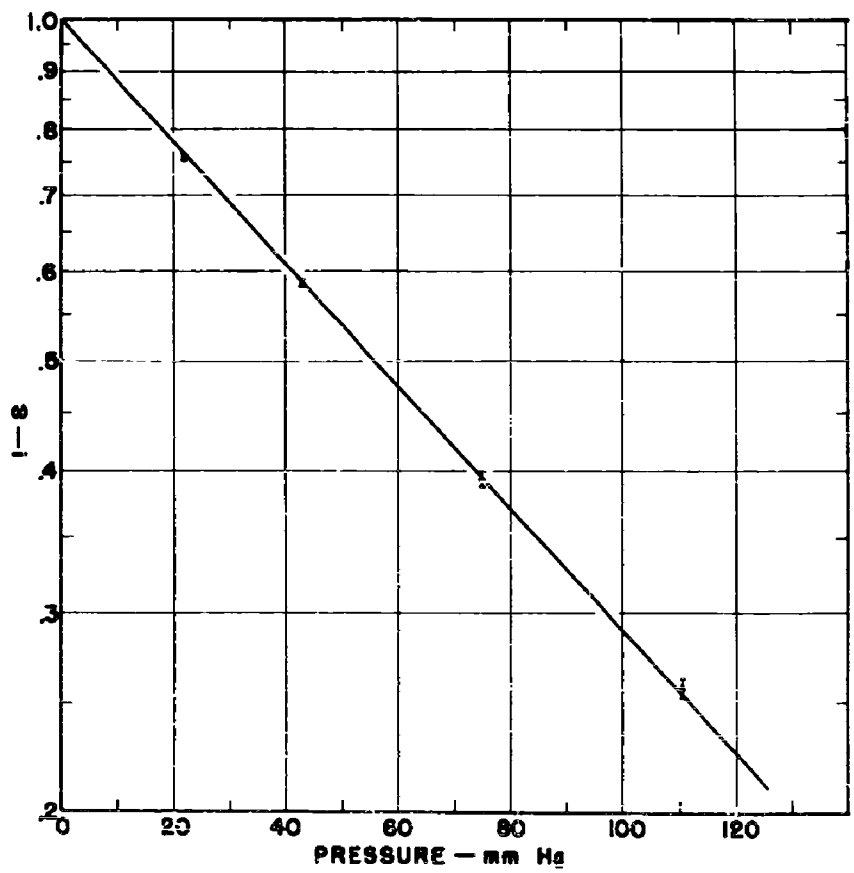

Fig. 2. - Variation of the quantity $(1-\varepsilon)$ as a function of the pressure of H_2 contained in counter C_1. (.855 Mev. β-rays)

pass through the counter train via a series of .1 mil aluminum windows W_1, W_2 and W_3. The magnetic field, which determines the momentum of the selected β-ray beam, is measured by means of a ballistic galvanometer connected to a flip coil F.

The β-ray energy range which can be covered with this apparatus is limited to about 200 kv at the low end, and to 1.6 Mev at the high end. The lower limit is determined by the total thickness of the three aluminum counter windows, and the upper limit by the maximum magnetic field attainable. The momentum resolution of the spectrograph is approximately $\pm$ 5 per cent.

Corrections for energy loss of the β-rays in the .001" Al window W_1 were made on the basis of the range vs energy curves for electrons in Al. For the lowest energy β-rays considered in the present investigation this correction amounts to approximately 4 per cent while for the highest energy rays the correction is approximately one per cent.

The counter C_1 is filled with a gas or mixture of gases whose primary ionization is to be measured. The gas pressure is chosen so that the β-rays in the spectrograph energy range are counted with an efficiency of about 0.3 - a condition which results in the least required operating time for determining the primary ionization to a given statistical accuracy. Counters

C_2 and C_3, which are filled with a self-quenching argon-butane mixture, serve to count the number of β-ray traversals of counter C_1.

The counters are connected to an external circuit which simultaneously records the number of 3-fold coincidences (C_1 C_2 C_3) and the number of 2-fold coincidences (C_2 C_3). The efficiency of C_1 for counting the β-rays which traverse it within the solid angle of windows W_1 and W_2 is given by

$$\varepsilon = \frac{(C_1C_2C_3) - (C_1C_2C_3)_o}{(C_2C_3) - (C_2C_3)_o} \qquad (3)$$

where the quantities with "o" subscripts represent the background coincidence rates recorded with the magnetic field of the spectrograph reduced to zero. The background rates were less than 10 per cent of the β-ray counting rates for all of the measurements reported here.

It was necessary to operate the counter C_1 as a resistance-quenched counter with all of the gases used in this investigation. Because of the rather large size of quenching resistance ($\sim 10^{10}$ ohms) required in some instances, a precaution was necessary to insure that the attendant dead-time of the counter did not give rise to a loss of real coincidences ($C_1C_2C_3$). The procedure which was finally adopted after the trial of several

alternative scheme was the following. A d.c. coupled anti-coincidence circuit was introduced between the wire of C_1 and the coincidence selection circuits so as to prevent the recording of any coincidences (C_2C_3) or ($C_1C_2C_3$) which occurred at a time when the wire potential of C_1 was more than 5 volts below its normal (quiescent) potential. This imposed the condition that counter C_1 be completely recovered from any preceding discharge before a coincidence could be recorded, and thus rendered the experimentally-determined efficiencies independent of the dead-time of C_1.

The background rates used in equation (3) to evaluate the efficiencies were corrected to compensate for the inactive time of the recording circuits introduced by the action of the anti-coincidence circuit during the β-ray data runs.

As a test of the over-all reliability of the experimental procedure, a curve of efficiency vs pressure was taken on the counter C_1 with hydrogen as the filling gas. Figure 2 is a semi-logarithmic plot of the measured values of $(1-\varepsilon)$ as a function of the hydrogen pressure. It is seen that the experimental points lie along a straight line which extrapolates to $(1-\varepsilon) = 0$ at $p = 0$ as expected from equations (1) and (2). If there were any significant contribution to the counting rate of C_1 from secondaries knocked out of the windows W_1 or W_2, one

would expect that the curve would not have the theoretical asymptotic shape predicted by the equations, but that λ would approach a value $\lambda = \frac{1}{2}$ less than unity at $p = 0$. The experimental errors due to wall effects are considered to be less than the statistical errors for all of the primary ionization measurement reported here.

The thicknesses of the walls of counter C_1 are sufficient to prevent the passage of β-rays either into or out of the counter except through the 1 mil Al windows W_1 and W_2. Thus, for a β-ray to cause a coincidence (C_2 C_3) it is necessary that the ray traverse C_1 within the solid angle of windows W_1 and W_2. These windows are 0.250" in diameter and the plane surfaces on which they are mounted are separated by a distance, l_0 = .688". There are two effects which cause the mean path-length of rays traversing C_1 to depart slightly from the length l_0. The first is scattering of the beam in the entrance window W_1. For β-rays of the energy range considered here, the mean scattering angle in W_1 is sufficiently large that each point of window may be considered as an isotropic source of rays in a calculation of the mean path-length l, of rays traveling between two windows. Such a calculation yields the result $l = 1.03\frac{1}{2}\ l_0$.

The second effect arises from a slight, approximately spherical distortion of window W_2 which resulted

from unintentionally subjecting the window W_1 to a one atmosphere pressure differential. This distortion has the effect of reducing the average path-length to a value approximately 0.5 per cent less than that indicated above for the case of a plane window surface. Consideration of the combined effects of scattering and window indicates that the mean path-length differs from the value ℓ_0 by less than 0.8 per cent. Since the error introduced into the final result by setting $\bar{\ell} = \ell_0$ is of the same order of magnitude as the statistical errors, ℓ in equation (2) has been set equal to ℓ_0 in all of the specific primary ionization calculations.

The pressures of gases introduced into the Counter C_1 were measured with a mercury manometer constructed of glass tubing of sufficiently large diameter (0.5 in.) to eliminate errors arising from unequal meniscus shapes in the two columns of the manometer. An anti-parallax method was used in comparing the heights of the mercury columns with a fixed scale, graduated in mm. Errors in the measured specific primary ionization values caused by inaccuracies in pressure readings were less than or equal to the statistical errors in all of the measurements.

Spectroscopically pure gases supplied by the Linde Air Products Company were used through the investigation. Counter C_1 exhibited a good efficiency vs voltage plateau (slope $< 1\%$ per 100 volts) with fillings of pure H_2 but

did not perform satisfactorily with fillings of pure He, Ne, or A. The addition of small amounts of H_2 to the latter gases was found to yield efficiency vs. voltage plateaux as good as that obtained with pure H_2. Consequently the addition of H_2 was adopted as the most practical procedure for overcoming the difficulties encountered with the pure gases. The specific primary ionization values obtained for He, Ne and A with hydrogen added were corrected by using the primary ionization values for pure H_2. These corrections amounted to 10%, 16% and 5% for the three gases, respectively.

Experimental results.

The results of the specific primary ionization measurements on H_2, He, Ne and A are presented in Table I. The experimental errors indicated in the Table are the statistical standard deviations which in all cases are comparable percentagewise with the independent uncertainties associated with the pressure and path-length determinations. The relative magnitude of the specific primary ionization values obtained for any individual gas are considered to be accurate within the statistical errors. Uncertainties in the absolute values are conservatively estimated at $\pm$ 3 per cent. Repeat runs on H_2, He and A, after removing the original gas filling and introducing new filling of the same pressures indicated that the measurements were reproducible within the statistical errors.

Table I. Measured values of the specific primary ionization of H_2, He, Ne and A for various β-ray energies.

Energy (Mev.)	$\frac{p}{Mc}$	Specific Primary Ionization-ions/cm at N.T.P			
		H_2	He	Ne	A
0.205	0.98	8.45 ± .095	7.56 ± .16	18.45 ± .36	41.7 ± .77
0.500	1.71	6.04 ± .065	5.58 ± .066	13.4 ± .17	30.5 ± .34
0.855	2.49	5.44 ± .054	5.08 ± .043	12.5 ± .14	27.7 ± .31
1.17	3.15	5.30 ± .053	- - - - -	- - - - -	- - - - -
1.55	3.90	5.32 ± .059	5.02 ± .060	12.4 ± .13	27.8 ± .31

Comparison of the Experimental Results with the Theory

The theory of primary ionization has been treated both classically and quantum-mechanically in various degrees of approximation by a number of authors. The most recent and comprehensive treatment of the subject -- given by Bethe[8] -- yields the following formula for the variation of specific primary ionization with the velocity of the incident particle:

$$S = 2\pi r_o^2 mc^2 N.z^2 \frac{Za}{Io} \frac{1}{\beta^2} \left[\ln^2 \frac{mc^2\beta^2}{I_o(1-\beta^2)} + b - \beta^2 \right] \quad (4)$$

where

S = number of primary ions per cm of path

$r_o = \frac{e^2}{mc^2}$ (classical electron radius)

m = electron rest mass

c = velocity of light

N = number of atoms per cc at N.T.P.

z = incident particle charge

Z = atomic number of gas

I_c = ionization potential of the gas

β = incident particle velocity / c.

a, b = constants dependent upon the electronic structure of the gas

For the particular case of atomic hydrogen (I_c = 13.5 ev., z = 1) Bethe has calculated the values of the constants in this equation to be: a = 0.285, b = 3.04. For gases other than atomic hydrogen, the calculation of the constants cannot be readily accomplished without introducing rather rough approximations regarding the form of the wave functions of the bound electrons.

In the derivation of equation (4) the assumption is made that the incident particle is undeviated by individual collision with the atoms of the gas. This approximation leads to rather large errors at low energies, but should not seriously affect the validity of the formula at electron energies greater than a few kv.

The form of equation (4) indicates that for a given gas, S depends only upon the velocity v and the charge z of the incident ionising particle. By making the substitution

$$\beta = \left(\frac{\left(\frac{p}{mc}\right)^2}{\left(\frac{p}{mc}\right)^2 + 1} \right)^{1/2} \qquad (5)$$

and lumping the constant coefficients in equation (4) one obtains the expression:

$$S = A \left[\frac{\left(\frac{p}{mc}\right)^2 + 1}{\left(\frac{p}{mc}\right)^2} \ln\left(\frac{p}{mc}\right)^2 - 1 \right] + C \left[\frac{\left(\frac{p}{mc}\right)^2 + 1}{\left(\frac{p}{mc}\right)^2} \right] \qquad (6)$$

where p is the incident particle momentum and m the incident particle rest mass. In terms of the constants of equation (4)

$$A = 2\pi r_o^2 mc^2 N z^2 \frac{Za}{I_o}$$

$$C = A \left(b + \ln m^2 \frac{mc^2}{I_o} \right)$$

In order to compare the theory with the experimental results the constants A and C have been empirically determined for each of the gases investigated so that equation (6) yields the best agreement with the experimental results. The values of A and C determined by least squares fits are given in Table II and the plots of equation (6) evaluated with the tabulated constants are shown in Figures 3, 4, 5 and 6. (solid curves). The dashed curves also shown in the figures indicate the extremes of a family of theoretical curves which fit all of the experimental values determined in the present investigation within one statistical standard deviation. The amounts by which the constants A and C corresponding to the two extreme curves deviate from the least squares values are indicated in Table II by the increments to the right of the $\pm$ and $\mp$ signs. One of the extreme sets of parameters is obtained by taking the upper signs and the other by taking the lower signs.

Table II Values of the parameter A and C calculated by fitting Eq. 6 to the experimental data. The limits indicate the range of variation of the parameters consistent with the statistical errors in the experimental results.

	H_2	He	Ne	A
A	0.356 $\pm$ .03	.422 $\pm$ .038	1.13 $\pm$ .09	2.37 $\pm$ .27
C	4.39 $\mp$ .02	7.98 $\mp$ .02	9.64 $\mp$ .11	21.8 $\mp$ .20

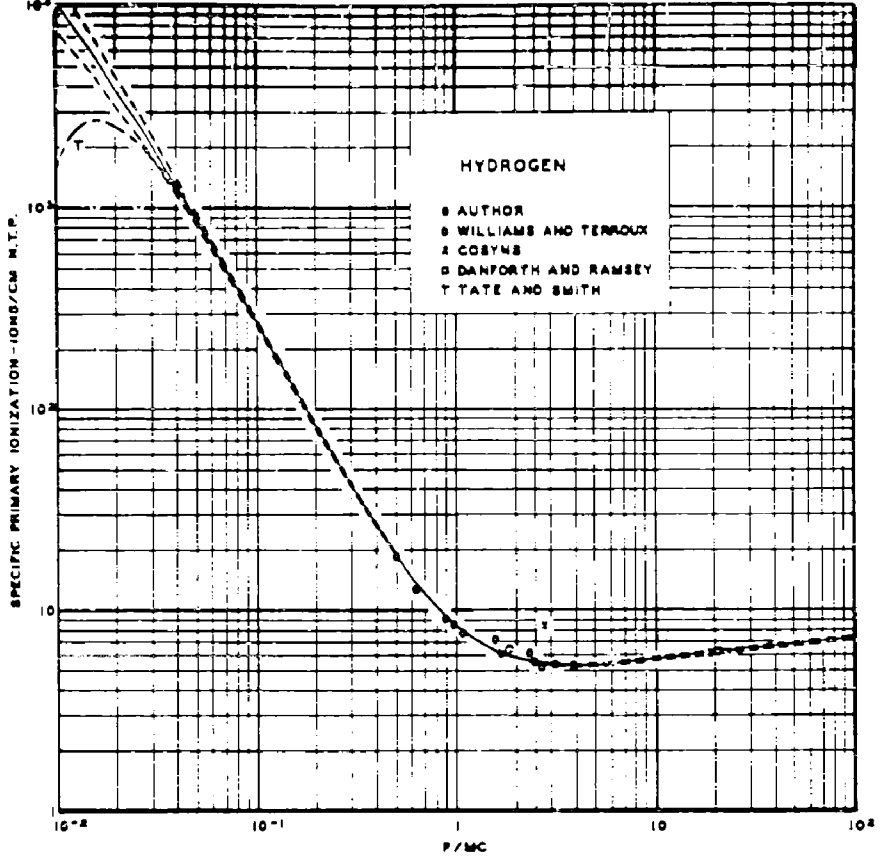

Fig. 3. - Composite plot of the present hydrogen data together with the results of Williams and Terroux[1], Tate and Smith[3], Danforth and Ramsey[4], and Cosyns[5,6]. Curves —— and - - - are theoretical.

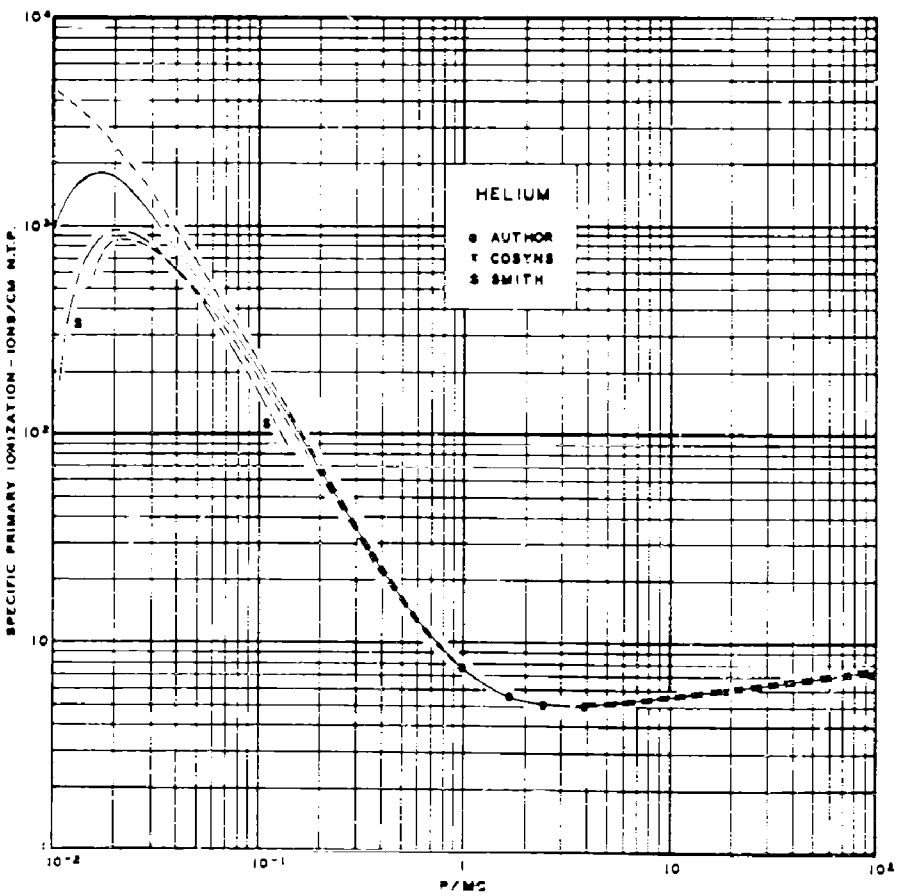

Fig. 4. - Composite plot of the present helium data together with the results of Smith[2] and Cosyns[5]. Curves —— and - - - are theoretical

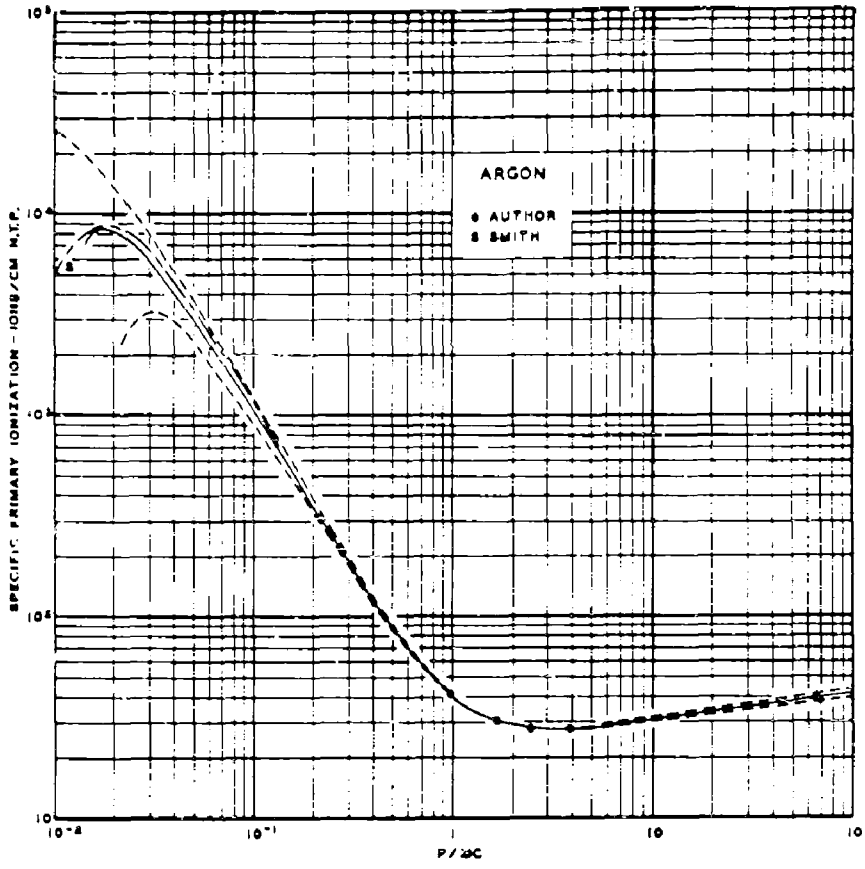

Fig. 5. - Composite plot of the present argon data together with the results of Smith[2]. Curves —— and - - - are theoretical.

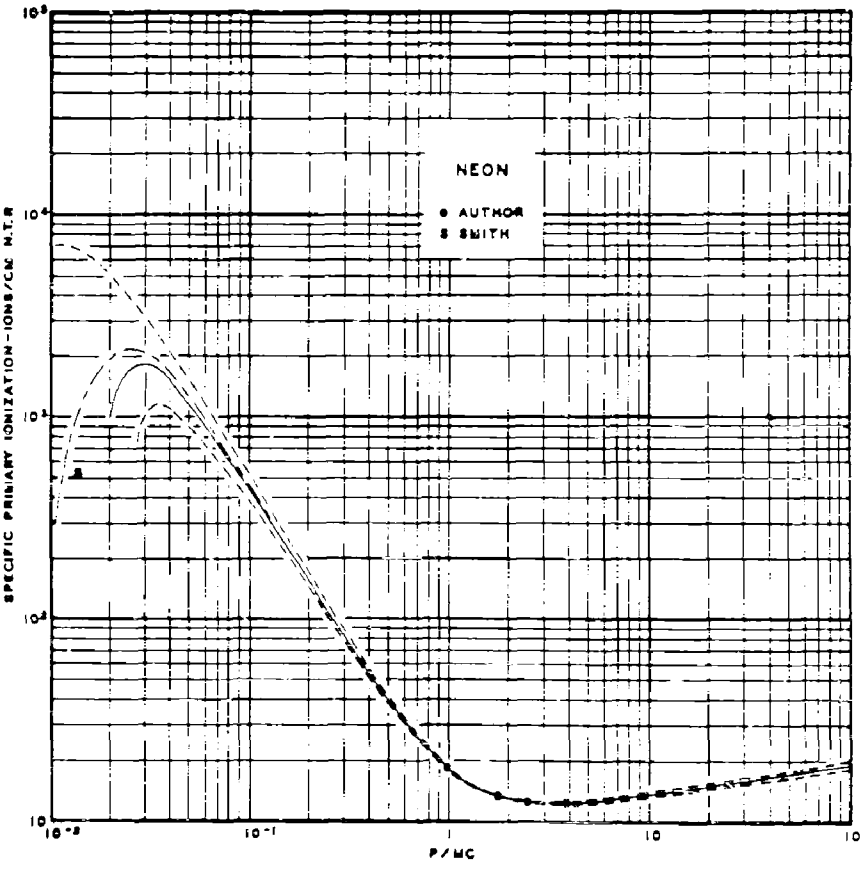

Fig. 6. - Composite plot of the present neon data together with the results of Smith[2]. Curves —— and - - - are theoretical.

Discussion

a) Hydrogen. The least squares fit of the Bethe formula (solid curve Fig. 3) to the hydrogen data obtained in the present investigation merges smoothly with the experimental data of Tate and Smith[3] at $p/mc = 0.054$ (electron energy of 750 volts) but diverges gradually at lower energies toward primary ionization values in excess of the Tate and Smith values. The experimental points of Cosyns[5] and of Danforth and Ramsey[4] for cosmic-ray mesons (average value of $\frac{p}{mc} \simeq .49$) agree with the solid curve within the experimental errors. The cloud chamber data of Williams and Terroux[3] scatter somewhat broadly above and below the curve indicating the presence of rather large experimental uncertainties, however the over-all agreement with the present results is quite satisfactory.

Hereford[7] has conducted an extensive low-pressure counter study of the primary ionization of H_2 by β-rays and cosmic-ray mesons. These results (not plotted in Fig. 3) although consistent with the other work as regards the ionization of cosmic rays show considerable discrepancies with the present work in the β-ray energy range. A series of values obtained by Hereford for β-rays of near-minimum ionization are about 18 per cent lower than the present data in the same range. Aside from the possibility that real

coincidences were lost by excessive dead-time of the H_2 counters used in Hereford's apparatus, no explanation for the disagreement is apparent.

b) Helium. In the case of helium, there is a rather large discrepancy between the solid curve and the low energy data of Smith[2]. This seems rather surprising in view of the relatively high accuracy with which the formula joins the high energy data with the low energy data for the other gases. The cosmic-ray point obtained by Cosyns[5] for helium agrees with the solid curve within the experimental errors.

The gradual relativistic increase in primary ionization at high energies predicted by the Bethe formula is confirmed in both H_2 and He by the consistency of the cosmic-ray data of Cosyns and of Danforth and Ramsey, with the theoretical extrapolation of the β-ray data.

c) Argon and Neon. In order to compare Smith's results[2] for argon and neon with the present measurements, it is necessary to observe that the quantity measured by Smith is not in general exactly equivalent to specific primary ionization. While the specific primary ionization, S, measured in the present experiment is defined as the number of ionizing collisions per unit path-length, the "ionization probability", P, measured by Smith may be defined as the number of electrons released in ionizing collisions per unit of path-length.

Conclusion.

The comparison made between the existing experimental results and the adjusted Bethe formula indicate a rather comprehensive agreement over an extremely large energy range. Although it is unfortunate that not all of the factors which enter into the mechanism of ionization can be precisely calculated from first principles, the Bethe formula appears to be a reliable tool for interpolating between measured values of specific primary ionization at energies in excess of a few kv.

The data obtained in the present investigation, in addition to serving as a useful guide toward further development of the theory of ionization, should be of value both in the design of low-efficiency G-M counters and in the analysis of cloud chamber photographs containing the tracks of fast particles.

Measurements of the specific primary ionization of several other simple gases and of some of the complex organic vapors utilized in G-M counters will be carried out in the near future.

References.

1) E. J. Williams and F. R. Terroux, Proc. Roy. Soc. 126, 289 (1929)

2) P. T. Smith, Phys. Rev. 36, 1293 (1930)

3) J. T. Tate and P. T. Smith, Phys. Rev. 39, 272 (1932)

4) W. E. Danforth and W. E. Ramsey, Phys. Rev. 49, 854 (1936)

5) M. G. E. Cosyns, Nature 138, 284 (1936)

6) M. G. E. Cosyns, Nature 139, 802 (1937)

7) F. L. Hereford, Phys. Rev. 74, 574 (1948)

8) H. A. Bethe, Hand. d. Physik 24,1, 515 (1933)

9) W. Bleakney, Phys. Rev. 36, 1303 (1930)
Phys. Rev. 35, 1180 (1930)

The Spreading of the Discharge in Self-Quenching Counters Operated Below the G-M Threshold

Introduction

A number of investigations[1,2,3] of the absorption of the photons which are released in the discharge of self-quenching G-M counters have lead to the conclusion that a very large percentage of such photons have absorption mean free paths of the order of a few millimeters in ordinary gas mixtures. The same conclusion may be reached indirectly on the basis of the fact that a small glass bead fused to the center wire of a counter can prevent a discharge which is initiated on one side of the bead from spreading beyond the bead.

In addition to the short-range photon component there has been observed by some investigators[1,2] a relatively long-range photon group capable of releasing photo electrons at a distance of several cm from their point of formation. In the course of a recent study of the behavior of G-M counters operated in the transition region between the proportional and Geiger regions additional evidence for the creation of photons of very long range has been obtained. While some of the broader aspects of this investigation have not yet been brought to a conclusion, it seems worthwhile to describe the experimental arrangement and to present the evidence pertaining to the presence of long-range photons in a communication at this time.

Apparatus

The apparatus (Figure 1) consisted of a counter with segmented cathodes 1 cm diameter, and 1 cm long spaced approximately 0.1 cm apart. The cylinders were made of copper, and the wire was 0.005 inch diameter tungsten. A coincidence circuit, also shown in Figure 1, was connected to segments C and K while all intermediate segments were connected together, and attached to a variable voltage source. Segments A, B and the end-segments were maintained at ground potential to eliminate inductive coupling between them and the coincidence segments, while the coincidence segments were held at -3 volts by the grid bias batteries of the coincidence input tubes.

The experiment was devised to measure the probability that a discharge initiated in the vicinity of segment A would spread to segment K as a function of the voltage applied to the intermediate cathode section D through J. Discharges were initiated in the upper end of the counter by admitting photons through a thin window in the vicinity of segment A. Each discharge spread downward to segment C causing a count to be recorded on scaler 1. If one or more photo-electrons were released in segment K (which was operated well above the G-M threshold) within 20 μ sec after the discharge of segment C, a two-fold coincidence (C, K) was recorded by scaler 2. Thus, the ratio of the

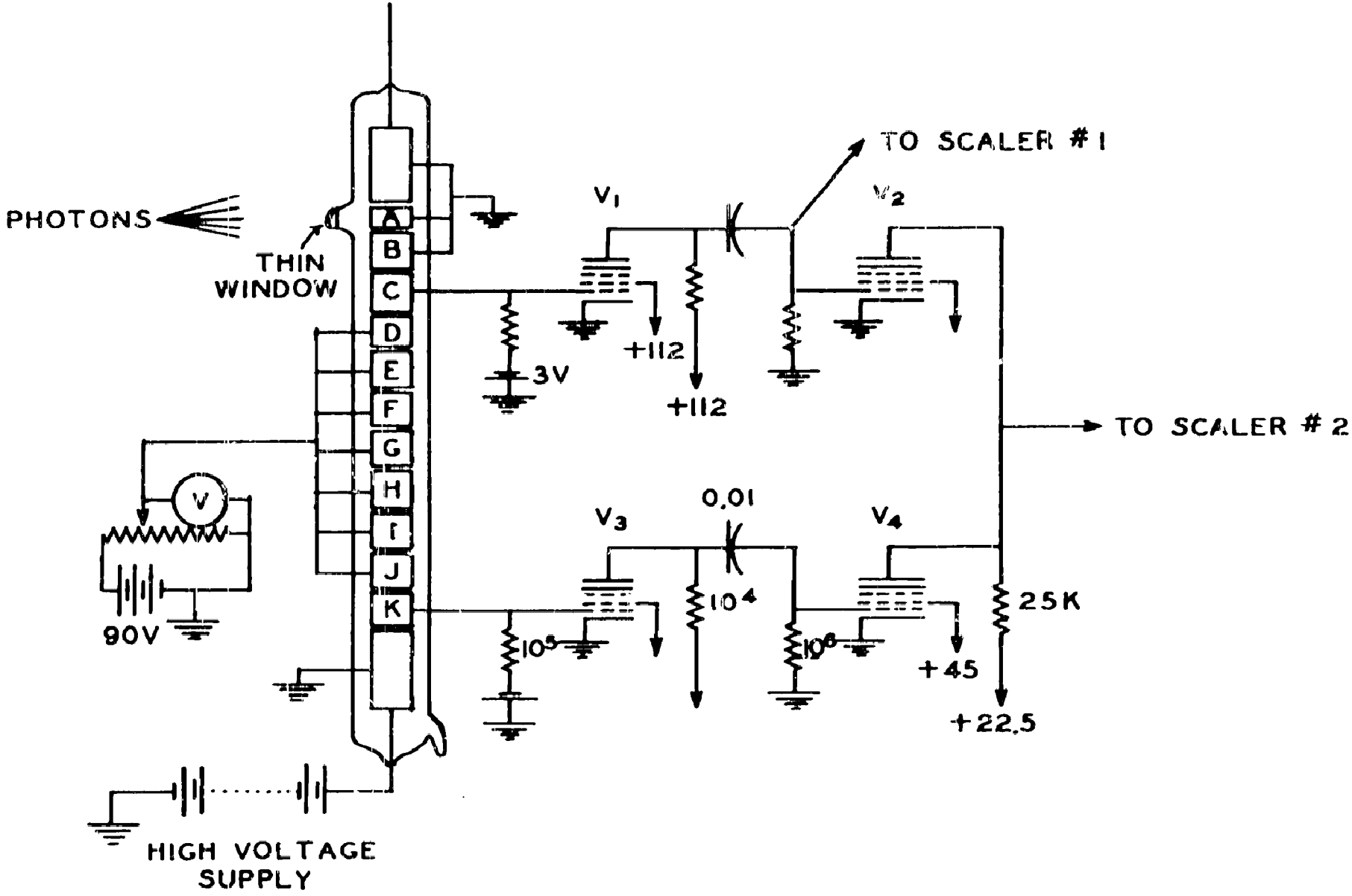

Figure 1 - G-M counter and coincidence circuit

number of counts recorded on scaler 1 to that recorded on scaler 2 was equal to the spreading probability which was to be determined. The standard mixtures used in this laboratory at various total pressures were investigated.

Preliminary Tests

Since a coincidence circuit was involved in these measurements, a test for chance coincidences was made. The time duration τ of the output coincidence-pulse was measured. A record of the individual rates of segments C and K, as well as the coincidence rate, was obtained with segments D through J, well below the Geiger region. Using the familiar expression for accidental coincidences $F_c = 2N_cN_k\tau$, it was found that the accidental rate N_c was less than 10^{-2} times the smallest coincidence rate recorded. Because of the smallness of contribution of accidental coincidences to the observed effects, no corrections for accidentals were made.

Observations of the variation in the size of output pulses from segments C and K as a function of the potential applied to the intermediate cathode section indicated that no appreciable fringing effects were present over the range of voltage utilized in the experiments.

Experimental Results

Typical families of curves for argon-butane and argon-ether are shown in Figures 2 and 3, respectively. The center

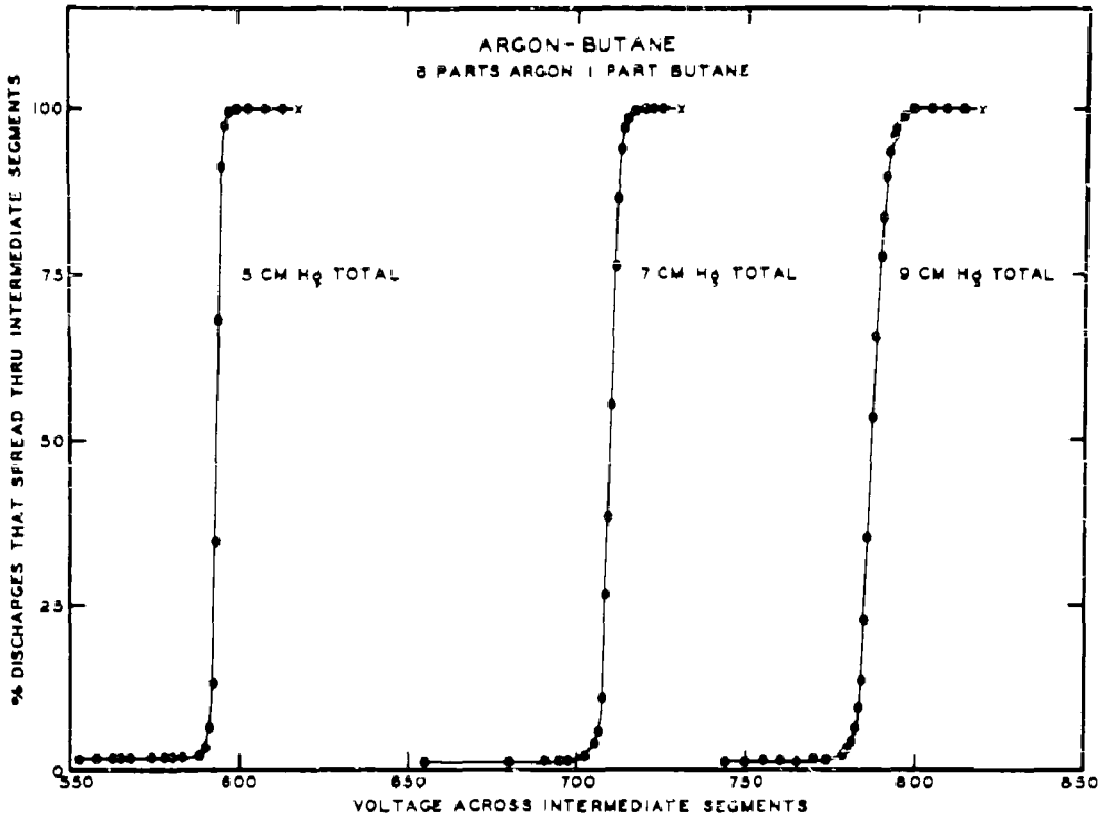

Figure 2 - Probability of discharge spread in Argon-Butane

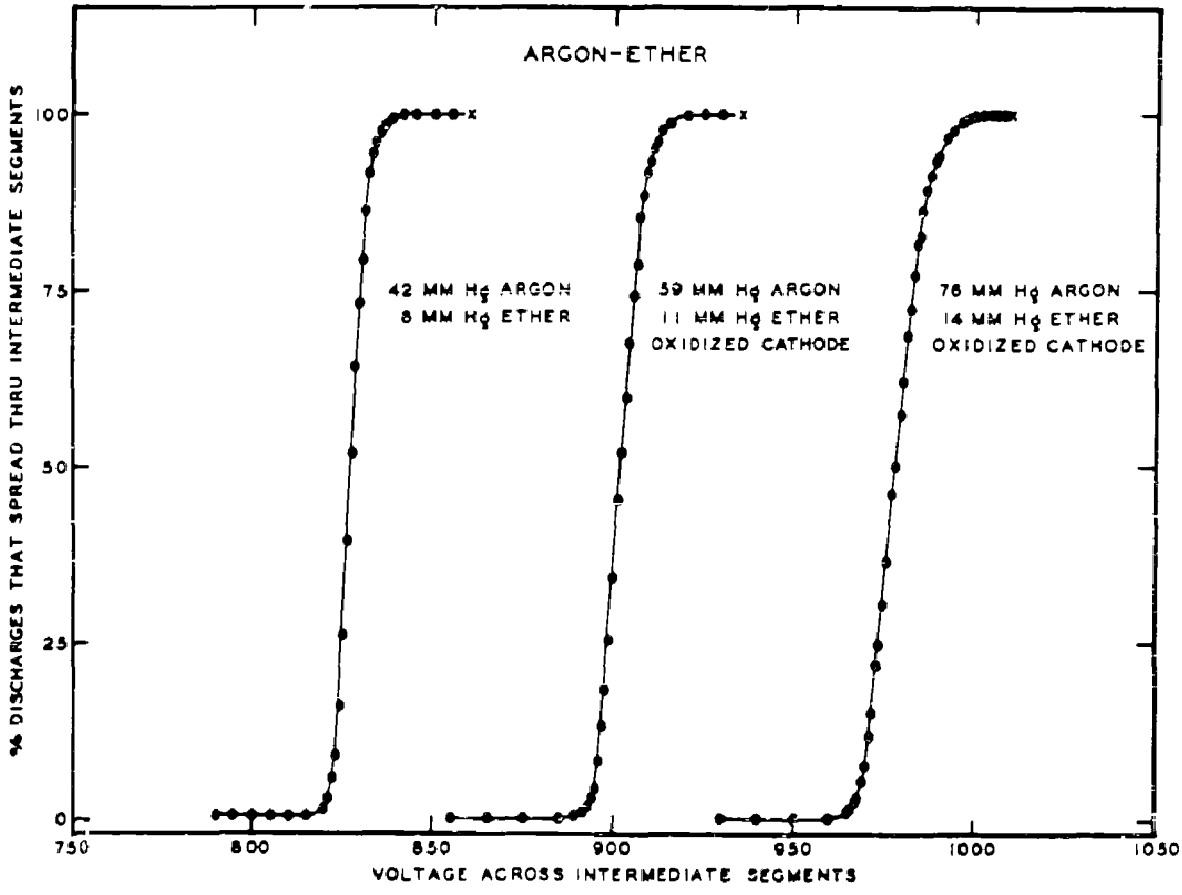

Figure 3 - Probability of discharge spread in Argon-Ether

wire potentials employed in obtaining these curves are indicated by the abscissal coordinates of the points X.

All of the gas mixtures investigated have certain qualitative features in common. With sufficiently high overvoltages, 100 per cent of the discharges spread the full length of the counter. As the potential on the middle segments is reduced, the spreading probability decreases--slowly at first, and then quite rapidly. With still lower voltages, the spreading probability tends to level off again over a span of at least 30 to 40 volts. In this region, the chance of a full-length spread depends critically upon the composition and total pressure of the gas mixture. However, it seems to be established that with fixed proportions of argon and quenching gas, the spreading probability in the lower "plateau" increases as the total pressure is decreased.

An oscilloscope observation of the time-delays between the discharges of segments C and K disclosed that the delays in the lower plateau regions were less than 10^{-8} sec, whereas the delays in the upper plateau (or G-M region) were predominately of the order of several microseconds depending upon the applied voltage and the gas mixture utilized.

In view of the critical voltage appendence of gas amplification in the proportional region, it appears unlikely that the spreading in the lower plateau regions can arise from a chain of photon-initiated avalanches along the length of segments D through J. If such chains existed, we

should expect the spreading probabilities to drop off rapidly below the knees of the curve, rather than to level off, as observed. The most plausible explanation for the level-off of the curves at low voltage seems to be that a small percentage of the photons generated in the discharge of segments A, B and C penetrate the full length of the gas column in the intervening segments D through J and release photo-electrons in segment K.

As the spreading of the discharge along the length of a G-M counter is propagated by photons, the uniformity of the spreading must depend critically upon the photon range distribution. Thus, it would be expected that the shapes of the current pulses occurring during intervals of electron collection should display jagged discontinuities differing from pulse to pulse when long range photons are generated in the discharge.

Such discontinuities have been observed with a number of counters tested in this laboratory and seem to have a reasonable explanation in terms of the presence of long-range photons.

Certain other anomalies in the behavior of G-M counters (in particular, the production of multiple pulses in large diameter counters controlled by the Porter and Ramsay[4] cutoff circuit) may also be related to the generation of long-range photons in the discharge.

References

1) S. H. Liebson, Phys. Rev. 72, 602 (1947)

2) C. Balakrishnan, J. D. Craggs and A. A. Jaffe, Phys. Rev. 74, 410 (194)

3) F. Aldes, E. Baldinger, P. Huber and F. Metzger, Helv. Phys. Acta 20, 73 (1947)

4) W. C. Porter and W. E. Ramsey, Jour. Frank. Inst. 254, 153-163 (1952).

D. PHOSPHORESCENCE STUDIES

The Alpha Particle Induced Phosphorescence of Silver Activated Sodium Chloride

Introduction

In several earlier communications, the writers have discussed the fluorescence and phosphorescence of NaCl -Ag irradiated by nuclear particles[1,2]. The phosphorescent effects have also been studied qualitatively by Furst and Kallman[3] and by Bittman, Furst, and Kallmann[4]. The light emission is known to occur in two bands centered at 2500 A and 4000 A, respectively[2,3]. It has been known for some time that these two bands are emitted when ultraviolet light is employed as the primary excitant[5]. A discussion of previous papers on ultraviolet excitation of NaCl-Ag may be found in the aforementioned reference[5].

In the present investigation, the phosphorescence of NaCl-Ag irradiated by alpha-particles and ultraviolet light has been observed, using as detectors photosensitive Geiger counters, RCA-1P28 photomultiplier tubes, and RCA-5819 photomultipliers.

The G-M tubes were constructed of copper cathodes, and the phosphorescent emission was usually introduced into the counters through a thin window of pyrex (3 mg/cm^2) or through a side wall of thickness one millimeter, made of

Corning 9741 glass. The counters employed exhibited a maximum of spectral response at ~2500 Å with no detectable response whatever above ~3000 Å. Measurements with the C-K tubes thus always constituted observation of the decay of the short-wave band alone. With the strongest phosphorescent sources used, the counting-rate of the photosensitive C-K tubes dropped to cosmic-ray background when one millimeter of soft glass was inserted before the counter, indicating only response to the ultraviolet of the short-wave band.

The RCA-5819 photomultiplier was utilized for detection of the long-wave band. Although these tubes are not expected to respond below 3000 Å, two millimeters of soft glass were interposed between source and phototube as an additional precaution. The DC current flowing in the photomultiplier was taken as a measure of the phosphorescent intensity. The current was measured in a fast galvanometer (T = 4 sec), and measurements were not commenced until several seconds after cessation of irradiation, so that ballistic corrections were small. The deflection of the galvanometer and the readings of a stop-watch were photographed simultaneously with a Sept camera. Measurements with an RCA-1P28 tube were also carried out. This detector is sensitive to light emitted in both bands. The decay curve of the combined emission of both bands is of interest for reasons to be later discussed.

The measurements of the present paper are concerned with the normal unstimulated phosphorescent decay of NaCl-Ag. This type of phosphorescent decay is to be distinguished from that arising from the release of stored light by thermostimulation[6] and photostimulation[7].

In general, the properties of two types of crystals were investigated. Single crystals of NaCl + 1% AgCl were obtained from the Harshaw Chemical Co. (hereafter referred to as "Harshaw"), and polycrystalline melts of NaCl + 0.5% AgCl prepared at the Bartol Research Foundation (hereafter referred to as "Bartol").

Results

The decay of NaCl-Ag (Bartol), irradiated by ultraviolet light from a germicidal lamp is shown in Figure 1. Curve A shows the decay of the short-wave band as measured in a Geiger counter, and curve B the decay of the long-wave band as observed with the RCA-5819 tube. The two curves were obtained after successive irradiations of the same melt, the conditions of the two irradiations being identical. The excited crystal was carefully totally de-excited by photostimulation before the second exposure to the ultraviolet source. The curves are log-log plots of the phosphorescent intensity versus the time. At large values of the time, the curves are seen to assume a slope of $-(2.63 \pm 0.05)$ on the log-log plot. The usual "power law" decay is assumed to have the form

$$I = \frac{I_0}{(1 + \alpha t)^n}$$

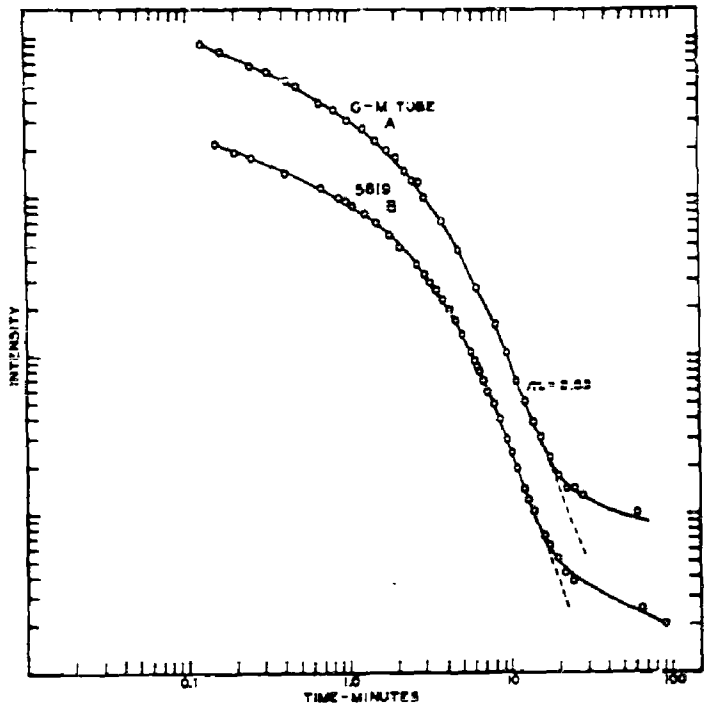

Figure 1 - Phosphorescent decay curves of NaC + 1/2% AgC (polycrystalline melt) irradiated for five seconds with ultra violet light from a germicidal lamp. Curve A gives the decay of the lower band (2500 A), curve B that of the upper band (4000 A).

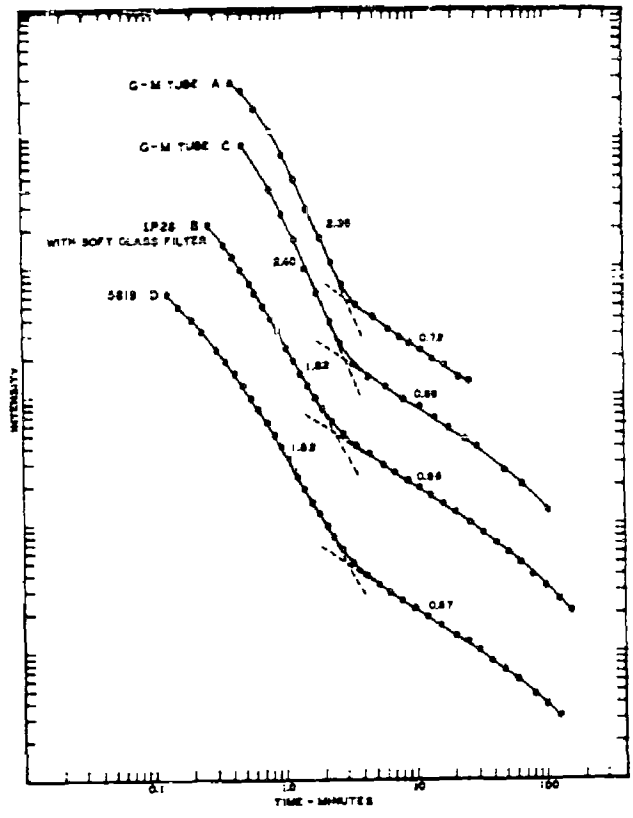

Figure 2- Phosphorescence of NaC+1% AgC (single crystal) irradiated for five seconds by alpha particles. The same crystal was bombarded repeatedly. The curves are lettered in chronological order, A & C being the decay of the shortwave band as detected by a photosensitive G-M tube, B and D the decay of the long wave band as measured with an RCA 1P28 with filter and an RCA - 5819 phototube.

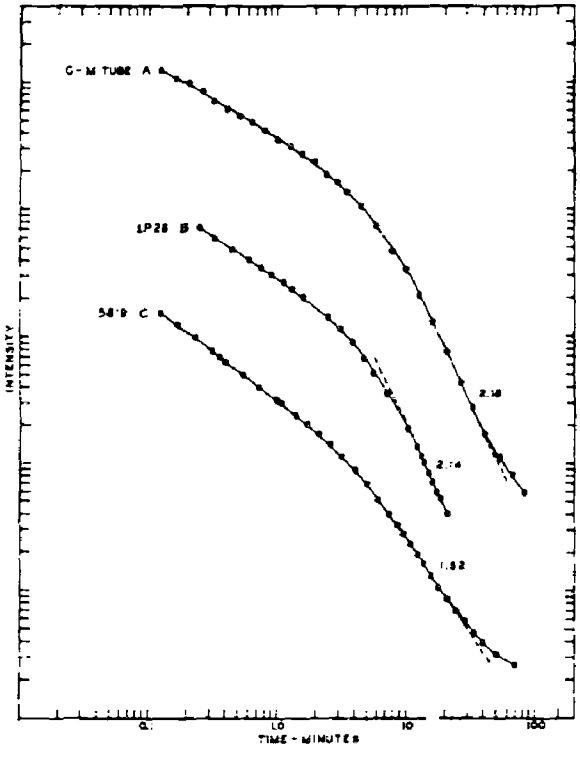

Figure 3 - Bartol polycrystalline mass irradiated by alpha particles. The ultraviolet band, predominant in the 1P28 and detected alone in the Geiger, decays with the steeper slope.

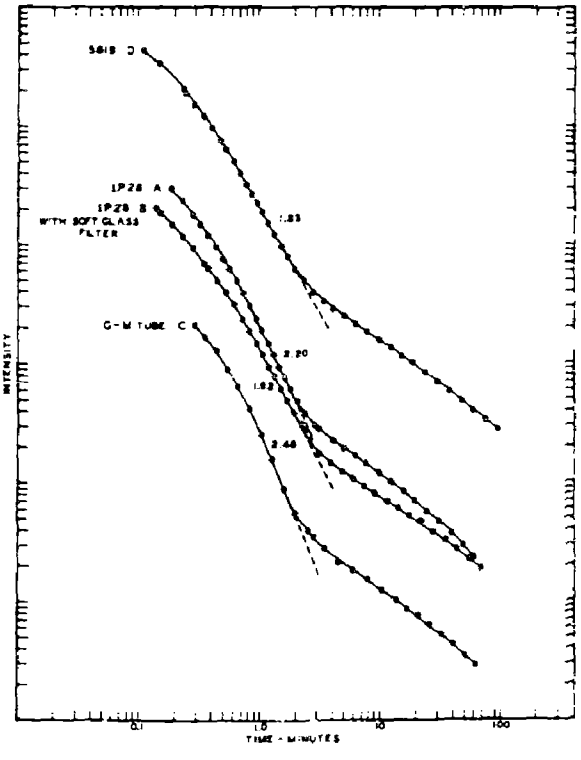

Figure 4 - Decay curves of a single crystal of NaC+ 1% AgC irradiated by alpha particles. Curves are lettered in chronological order.

where, theoretically, n does not exceed 2. A survey of the available literature has shown that negative slopes of more than (-3) are seldom observed. A slope of -2.09 has been reported[8] at 80° C in the decay of ZnS excited by ultraviolet light. All of the measurements of the present paper were performed at temperatures less than 25° C. In the particular case of Figure 1, the decay curves for the two emission bands have the same slope and the same general shape, indicating that the electrons which give rise to the two bands have a common origin in the same trap distribution. As will be subsequently seen, not all of the crystals examined exhibited this property.

The phosphorescent decay-curves of a single crystal (Harshaw) are shown in Figure 2. The primary excitant was in this case the alpha-particles of polonium. The same crystal was irradiated repeatedly for five seconds at a time to obtain the curves. The source strength was twenty-five millicuries. It is thought that very nearly complete de-excitation was obtained between successive bombardments. The curves are lettered in chronological order. The short-wave band detected with a photosensitive Geiger counter is seen to decay with a negative slope of ~ 2.38 whereas the long-wave band as noted in phototubes decays with a slope of -1.82. A slower mode of decay is also in evidence of the approximate form $I = I_0 t^{-0.7}$. Since the absolute value of the negative slope is less than 1, this mode of decay could not persist indefinitely. A likely

interpretation[9] is that it occurs in a "transition region".

A polycrystalline melt (Bartol) was irradiated three times with alpha-particles to obtain the curves of Figure 3. Curve A is the decay curve of the short-wave band alone in a photosensitive Geiger counter; Curve B is that of the two bands combined, and Curve C that of the long-wave band. The similarity of curves A and B shows that although the spectral response of the 1P28 is such as to favor the long-wave band, the short-wave one is predominant because of its greater intensity. As in the case of Figure 2, the ultraviolet band appears to decay with the steeper slope.

Since considerable variation in silver content has been noted in Harshaw crystals, a second one was irradiated, and the decay curves of Figure 4 were obtained. Here again, it is clear that the decay slope is greater for the short-wave band as detected in the Geiger counter and 1P28 without filter than for the long-wave band as measured in the 5819 and 1P28 with filter.

Figures 2, 3, and 4 show a tendency toward steeper slopes for the decay of the short-wave band. Decay-curves of several other single crystals (Harshaw) not included in this paper substantiate this tendency. No fast rule can be developed, however. The curves of Figure 1 are an exception, and in the course of studying a crystalline melt (Bartol) at the conclusion of these measurements, a reverse trend was encountered. Slopes of -2 were observed in the

decay of the long-wave band whereas the absolute value of the decay of the short-wave band did not exceed 1.5.

A general conclusion which can be drawn from these measurements is that for a given set of conditions of excitation, the two bands decay with differing power laws. It has been previously shown[5] that the long-wave band arises from the presence of paired silver ions in the crystal lattice. It is concluded that the trap distribution associated with the paired silver ions is different from that related to the single silver ions[10].

References.

1) C. E. Mandeville and H. O. Albrecht, Phys. Rev. 79, 2010 (1950); ibid. 80, 117 (1950); ibid. 80, 299 (1950); ibid. 80, 300 (1950).

2) H. O. Albrecht and C. E. Mandeville, Phys. Rev. 81, 163 (1951); Rev. Scient. Inst. 22, 855 (1951).

3) Furst and Kallmann, Phys. Rev. 82, 964 (1951); ibid. 83, 674 (1951).

4) Bittman, Furst, and Kallmann, Phys. Rev. 87, 85 (1952).

5) Etzel, Schulman, Ginther, and Claffy, Phys. Rev. 85, 1063 (1952).

6) H. Friedman and C. P. Glover, Nucleonics 10, No. 6, 24 (1952).

7) Kallmann, Furst, and Sidran, Nucleonics 10, No. 9, 15 (1952).

8) W. W. Antonow - Romanowsky, Phys. Zeits. d. Sowjetunion 7, 366 (1935).

9) Mott and Gurney, Electronic Processes in Ionic Crystals (Oxford University Press, London, England, 1948), second edition, p. 215.

10) See Preparation and Characteristics of Solid Luminescent Materials: Cornell Symposium of the American Physical Society (John Wiley and Sons, Inc. New York 1948) and remarks by Garlick, Pringsheim, and Maurer, p. 397; also statements by Garlick, paper no. 3, p. 111.

B. THE LARGE VAN DE GRAAFF GENERATOR.

At the time of the last report, we were in the process of installing the Bartol ion source into the test section of the large generator. Photo #1 is a photograph of the ion source and allied circuitry as it appears in the generator. A description of the set-up and data on the performance appears in the section entitled "An R. F. Ion Source". After having passed through fourteen feet, however, the beam was about 3/4 inch off center.

Following this installation further tests were conducted relative to the tube behavior with and without baffles. Because of the off-centered beam, however, we were unable to bring the beam through the 1/2 inch holes in the baffles. The reason for the off-centered beam was determined to be the result of a bend in the tube caused by a misalignment in the tube assembly gig.

In addition to the bend in the tube, too much Vynal Seal had been used in the assembly and not enough care had been taken to keep the tube clean. Consequently, it was decided to fabricate a second tube.

This also gave us a chance to check the behavior of the generator without a tube. While the tube was in with the source operating, we made a voltage calibration,

Photo 1 – "Ion source and allied equipment in central electrode of large generator".

using the [illegible] resistors. Thus, with the voltmeter calibrated, we were able to get an accurate value on the limit of the generator. With 80# pressure, the generator operated very well at 3 Mev. whereas at 3.25 Mev sparking began to take place between the rings. Insofar as 3 Mev on this section represented 19 Mev for the full machine, we did not increase the pressure to attain higher voltages.

The resistors between the equipotentials were modified during these tests. As previously reported, the IRC barber pole resistors had been changed to SS White resistors. Twelve SS White resistors were required to replace the IRC resistors. This was originally done by soldering knobs on the ends of the resistors, stacking these inside a glass tube and then putting buttons into the ends of the tube. The whole resistor was then pressed together by the spring in the holder attached to the equipotential. This push contact was determined to be inadequate; consequently the knobs were all soldered together. In the final assembly the wires of the resistors are soldered into a single spacer.

The tube connectors have been modified twice since the modification last reported. These modifications have been made in order to rid the resistor current readings of little kicks. Originally the connectors were

long stainless steel springs which rested on the electrodes of the tube, the two ends of the spring being connected to the equipotential. These were changed to short springs, one end of which was connected to the tube electrode and the other to the equipotential. Next aluminum shields were put over the springs, one end of the shield being connected to one end of the springs and the other end free so that any current still had to pass through the spring. The difficulty, however, with these springs seems to be the inability for them to take high frequency surges. Finally, the free end of the shield was connected so that the shield now shorted out the spring. As a result, in the final assembly the stainless steel springs will be replaced by a couple of turns of #12 copper wire.

The new tube section turned out very well. Without any baffles, steady voltages up to about 2 Mev were obtained after running for some 50 hours; any effect of the beam on the voltage was not observed. Following this test, a baffle consisting of three overlapping annular rings each supported by three arms were inserted in the three electrodes in about the middle of the tube. After a few hours of running, steady voltages of about 2 1/4 Mev were obtained, which is not an appreciable gain over the case without the baffle. Nevertheless, there was certainly no inverse effect and, of course, it is possible that the limitation is not due to tube loading.

The actual length of the accelerating tube in these tests was 6 feet.

In connection with the tube loading effect, the following test was conducted. A 6" dia. copper plate was placed at a 45° angle in the main tube plumbing system at the tee going into the diffusion-pump-baffle system; the angle was such as to prevent any back-diffusion up into the accelerating tube proper. This plate was connected to a 3/4" copper rod which passed out of the vacuum system through a Kovar tube. This plate was -- first, cooled by a dry-ice-acetone mixture -- second, brought to room temperature -- third, raised to about 200° C. The voltage was brought up on the machine for each condition without any beam. During all the previous tests very little vacuum effect was observed with increase in voltage. In the first case above, there was an appreciable increase in vacuum with increase in voltage; in the second case, there was no appreciable effect; in the third case, the effect was again observed. Undoubtedly, if still higher temperatures were tried, the effect would have decreased again. The reason for this effect does not seem difficult to understand, but the fact that the ground-end of the generator extends seven feet below the end of the accelerating tube is of importance.

When the full tube is installed, a baffle will be put at the base of the accelerating tube and a suppressor will be placed under this baffle. This will tend to shield the accelerating tube from the large amount of plumbing surface as well as to shield the electrostatic deflector plates for centering the beam from stray beam-particles.

The analyzing magnet has been assembled. Photo #2 shows this assembly. The magnet is much the same as the magnet used on the Los Alamos generator. The control circuit has also been installed and the degree of stability of the current in the coils is now being checked. The control consists of a magnesium resistor in series with the magnet winding. The voltage from this resistor is compared with a standard voltage and the error amplified by a chopper amplifier to control the field of an amplidyne which in turn controls the field of the M-G set energizing the coils. As may be seen from the photo, the magnet is mounted on a turret to allow for positioning of magnet.

At present, assembly of the complete generator is under way. Initially, electrostatic tests will be run to determine the ultimate voltage obtainable. The generating voltmeter, and a voltage controlling corona probe are completed and will be used during these tests.

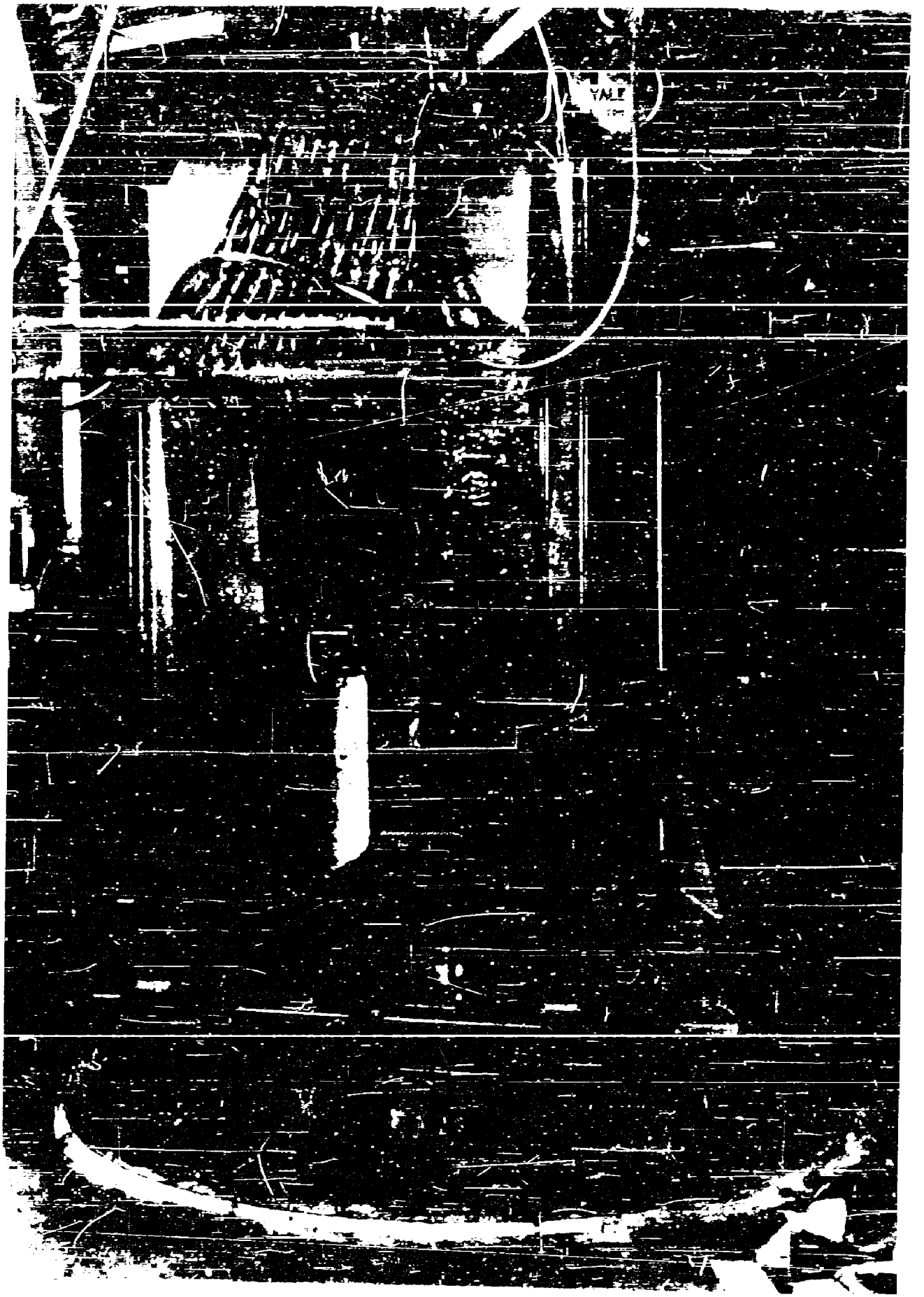

Photo 2 – "Analyzing magnet for large generator".

The vacuum system is also essentially complete. This envolves the suppressor, the electrostatic beam positioning device, two sets of energy defining air-cooled slits capable of withstanding 100 watts per slit, slits to collimate the beam entering the magnet box, the magnet box, and the necessary valves.

One other revision has been made in the bolting arrangement for the cap of the tank. Originally, nuts were welded on the underside of the flange on the tank proper, and the studs were screwed permanently into these. However, it was found difficult to position the cap precisely over these studs. Consequently, all the nuts were taken off and a platform installed below the lower flange so that the studs may be dropped to the level of the joint, thus avoiding the difficulty of alignment.

III. LINEAR ACCELERATOR.

Introduction.

The work of the linear accelerator project has been divided between investigations of secondary emission from thin metal foils and engineering improvements designed to improve the stability of the machine and to eliminate radiation hazards to the operating personnel.

1. Secondary emission measurements.

The linear accelerator is being used as a source of electrons of from 300 Kev to 1.5 Mev in the measurement of secondary emission from thin metal foils.

In order that the secondary yields obtained shall be characteristic of the material being investigated and not of surface impurities, vacuum conditions must be much better than those prevailing in the linear accelerator. Consequently, a tube, of which a photograph is shown in Figure 1, has been designed which permits the injection of the high energy electrons through a thin glass window. This tube is of a sealed-off construction with a vacuum of better than 10^{-7} mm Hg. It consists essentially of four electrodes, a collimator, a collector for measuring electrons emitted from the back face of the target, an

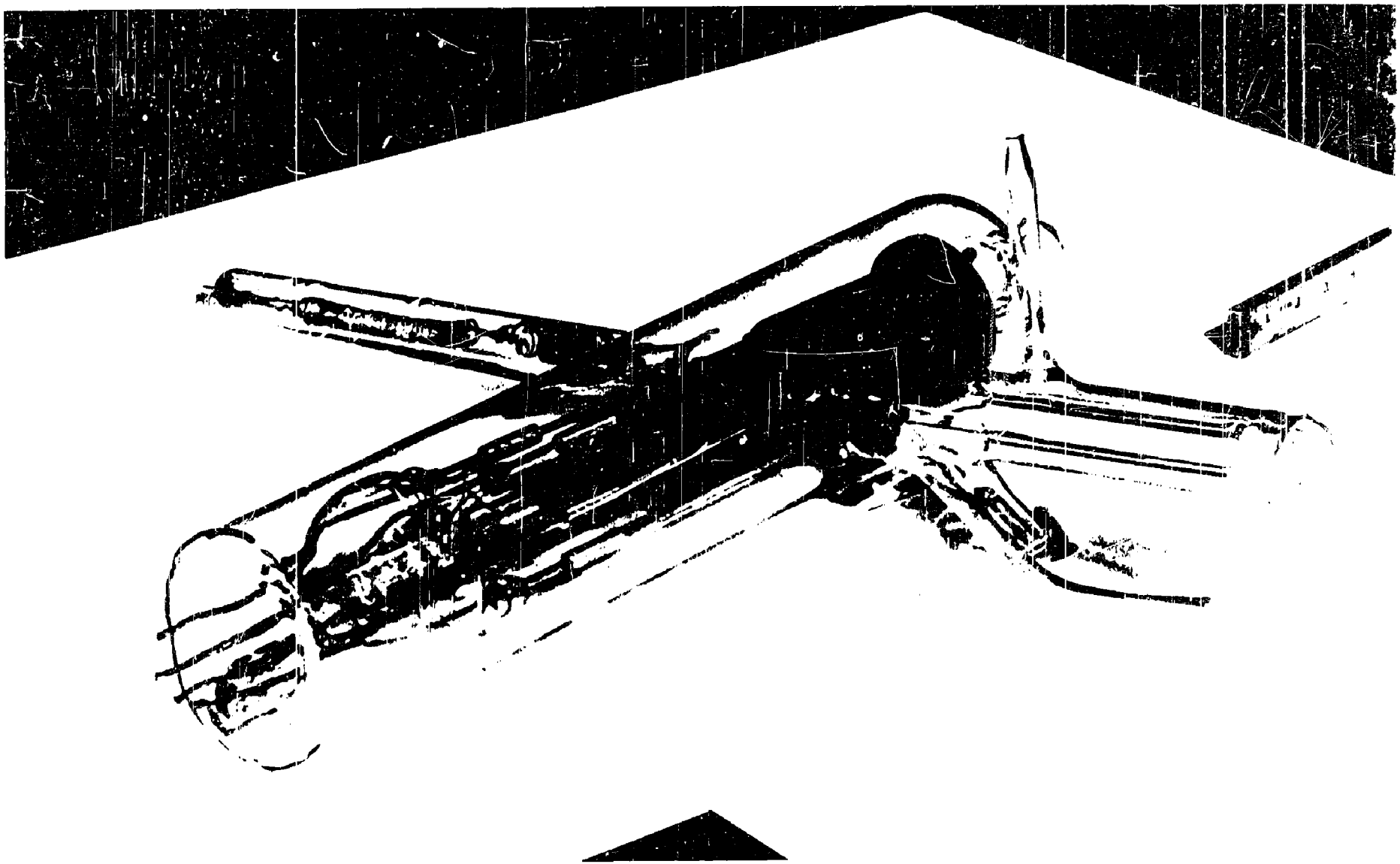

Figure 1 - Secondary Emmission Tube.

adjustable target assembly which permits measurements on several targets without opening the tube, and a trap for measuring the primary current and the secondaries from the front face of the target. With the exception of the target assembly, all of the electrodes are made of graphite in order to minimize extraneous secondary emission and scattering. In the processing of the tube, particular attention has been given to proper de-gassing of the electrodes, especially the targets, in order to exclude surface adsorbtion phenomena. For this purpose, an auxilliary tungsten cathode has been incorporated in the tube to permit heating of the targets by electron bombardment.

To date, measurements have been made on nickel foils of 1 and 2 mil thickness. Because of ambiguities arising from the fact that part of the primary beam strikes the target supports, only a lower limit has been obtained for the total secondary yield from the front and back faces of the target. This lower limit for the secondary yield (about 5%) is of considerable interest, since it is considerably higher than one would expect from simple theoretical considerations concerning the energy loss of the primary beam.

Engineering improvements in the linear accelerator and modification of the design of the target assembly

which have been made should remove many of the ambiguities present in these experiments, and more precise results are expected in the near future.

2. Design changes in the linear accelerator.

Certain general difficulties with the operation of the linear accelerator which are now being eliminated, have arisen in connection with the above experiments.

First, because of the necessity for changing several variables during a set of measurements, the operator has to remain in the vicinity of the accelerator during the experiment. This results in a high rate of irradiation of the operating personnel, and from safety considerations, experiments must be infrequent and of short duration. This situation is being corrected by the introduction of a remote control system.

Secondly, the stability of the accelerator is rather poor because of the ef heating of the accelerating cavities. A temperature change of 1° C in a cavity produces a change of about 60 kc in its resonant frequency. Because of the high Q this small change produces a large phase shift (about 1/2 radian). Thus, a temperature difference, between cavities, of a few degrees C seriously upsets the phasing conditions and is accompanied by a drop in the output energy. This situation has been remedied by water-cooling the cavities and magnetron.

Test runs show that with this water-cooling the rf heating changes the cavity temperature by only a fraction of a degree C while with air-cooling, the change is about 10° C. By this means the warm-up period has been reduced from one hour to a few minutes.

A third difficulty has been experienced with the dielectric phase shifters used to load the wave-guide in order to obtain the proper phasing conditions in the cavities. Occasional arcs in the wave-guide caused the decomposition of the polystyrene phase-shifters, and a general cleaning of the wave-guide and cavity-windows was necessary after several runs, because of a thick deposited layer of decomposition products.

After several tests of other dielectrics, halogen substituted hydrocarbons were finally found to be suitable in their microwave characteristics, and in their resistance to arcing. Therefore, the polystyrene phase-shifters were replaced by ones made from Teflon.

At the present time, our efforts are directed toward full remote control of the accelerator, in order to exclude all health hazards and toward continuation of the secondary emission experiments. Moreover, replacement of worn-out electronic equipment consisting of modified war surplus gear which has caused frequent failures and delays in operation has been started. In connection with these

modifications, the additional six cavities which will increase the output energy of the accelerator up to 4 Mev are being provided with water-cooling.

PUBLICATIONS

All of the work described in this Annual Report (appearing between dates of October 1, 1951 and September 30, 1952) will be published in suitable form in various scientific journals--primarily THE PHYSICAL REVIEW, REVIEW OF SCIENTIFIC INSTRUMENTS, or the JOURNAL OF THE FRANKLIN INSTITUTE.

Recently published works are:

"The Spectrograms of Some Ultraviolet Scintillators", by H. O. Albrecht and C. E. Mandeville, Rev. of Scient. Instru., Vol. 22, No. 11, 855-856, November, 1951

"Absence of a Detectable Diurnal Variation in the Frequency of Heavy Primaries and Nuclear Disintegrations at 80,000 Feet", by Gordon W. McClure and Martin A. Pomerantz, Phys. Rev., Vol. 84, No. 6, 1252-1253, December 15, 1951

"Trajectories in an Axial Focusing Double Lens Spectrometer", by S. C. Snowdon, Rev. of Scient. Instru., Vol. 22, No. 12, 875-885, December, 1951

"Neutrons from the Disintegration of the Separated Isotopes of Silicon by Deuterons", by C. E. Mandeville, C. P. Swann, and S. D. Chatterjee, Phys. Rev., Vol. 85, No. 2, 193-196, January 15, 1952

"Electron Velocities in Geiger Counter Gas Mixtures. Letter I", by Alden Stevenson, Rev. of Scient. Instru., Vol. 23, No. 2, 93, February, 1952

"Coincidence Time Delays in Geiger Counters. Letter II", by Alden Stevenson, Rev. of Scient. Instru., Vol. 23, No. 2, 93-94, February, 1952

"Short Double Coincidence Resolving Times for G-M Tubes. Letter III", by C. E. Mandeville, Rev. of Scient. Instru., Vol. 23, No. 2, 94, February, 1952

"General Observations on Discharge Lag in Counters. Letter IV" by W. E. Ramsey, Rev. of Scient. Instru., Vol. 23, No. 2, 95, February, 1952

PUBLICATIONS (Continued)

"Decay Times in G-M Counters. Letter V", by W. C. Porter and W. E. Ramsey, Rev. of Scient. Instrs., Vol. 23, No. 2, 95-96, February, 1952

"Radiations from Radioactive Rhodium (103)", by C. E. Mandeville and E. Shapiro, Jour. Frank. Inst., Vol. 253, No. 2, February, 1952

"The Primary Cosmic Radiation at High Latitudes", by Martin A. Pomerantz and Gordon W. McClure, Phys. Rev., Vol. 86, No. 4, 536-545, May 15, 1952

"Radiations from Nb^{97m}", by C. E. Mandeville, E. Shapiro, R. I. Mendenhall, E. R. Zucker and G. L. Conklin, Phys. Rev., Vol. 86, No. 5, 813, June 1, 1952

"A Circuit for the Limitation of Discharge in G-M Counters" by W. C. Porter and W. E. Ramsey, Jour. Frank. Inst., Vol. 254, No. 2, August, 1952

"A Multiple-Cavity Linear Electron Accelerator, by Bernard L. Miller, Rev. of Scient. Instru., Vol. 23, No. 8, 401-408, August, 1952

"Ionization by Cosmic-Ray Mesons in Argon", by G. W. McClure Phys. Rev., Vol. 87, No. 4, 680, August 15, 1952

"Neutrons from the Disintegration of Phosphorus by Deuterons" by S. C. Snowdon, Phys. Rev., Vol. 87, No. 6, 1022-1025, September 15, 1952

"A Radiofrequency Ion Source", by C. P. Swann and J. F. Swingle, Rev. of Scient. Instru., Vol. 23, No. 11, 636-638, November, 1952

A DETERMINATION OF μ MESOTRON REST LIFETIME AND A VERIFICATION OF THE RELATIVISTIC EXPRESSION FOR VARIATION OF LIFETIME WITH MOMENTUM*

by

David W. Seymour

and

W. F. G. Swann[1)]

Bartol Research Foundation of the Franklin Institute,

Swarthmore, Pennsylvania

INTRODUCTION

Determinations of mesotron mean life have been made by various methods with varied results. Some methods involve knowledge of the relation between the absorption powers of great thicknesses of material[2)]. Others have

---

* Assisted by the Joint Program of the ONR and the AEC.

1) The theory of the method was developed by the senior author, (W. F. G. Swann), and the apparatus was designed under his direction by the junior author (D. W. Seymour) who also took the initial observations at Shenandoah Park. The subsequent routine data were taken by Mr. Harvey C. Taylor.

2) T. H. Johnson and M. A. Pomerantz, Phys. Rev., 55, 104 (1939); also M. A. Pomerantz, Phys. Rev., 57, 3, (1940)

---

involved comparison of measurements made at different times at different altitudes and localities[3)]. Moreover, there are wide

---

3) B. Rossi, N. Hilberry and J. B. Hoag, Phys. Rev., 57, 461 (1940).

differences between the results of different observers[4].

4) W. M. Nielsen, C. M. Tyerman, L. W. Nordheim and K.Z.Morgan, Phys. Rev., 59, 547 (1941) give a value of 1.25 microseconds, while M. Ageno, G. Bernardini, N.B.Cacciapuoti, B. Ferretti and G. C. Wick, Phys. Rev., 57, 945 (1940) give values in excess of 4 microseconds.

In view of the foregoing situation, the authors have planned and carried out simultaneous measurements at different altitudes in the same locality. Moreover, it has been felt necessary to interpret the observations in terms of a more precise theory than seems to have been used heretofore. The desire was also to verify the variation of mean life with momentum since, relativistic arguments notwithstanding, there could be sense to a situation in which the variation in question did not follow the relativistic form[5].

5) The reasons for these considerations which are not primarily relevant to the present paper are given in a semi-classified report of limited circulation.

EXPERIMENTAL ARRANGEMENT

The general plan was to operate cosmic ray telescopes at two different altitudes, with various thicknesses of lead absorbers between the trays. It was necessary to compensate the momentum absorption of the additional air above the lower telescope by inserting an additional equivalent thickness of

lead in the upper telescope. The thickness of this "compensator" is determined by the following considerations. If L_1 is the thickness of the block of lead in the lower telescope, the total thickness L_2 in the upper telescope must be such that the momentum necessary to penetrate L_2 is equal to the momentum necessary to penetrate L_1 plus the air column between the upper and lower telescopes. If this conditiin is satisfied, then in discussing the penetration through the lead of thickness L_1, we have simply to consider that portion of the spectrum which, at the high altitude, would penetrate L_1 plus the air equivalent addition and attenuate it by mean life considerations in accordance with the calculations to be presented later. It will later be seen that the thickness of the compensator depends in principle upon L_1 as well as upon the mass of the air column. The dependence upon L_1 is, however, very slight, so that in practice, a single compensating thickness serves for all values of L_1 employed.

The compensator, which comprised 14 cms of lead, was placed within the telescope. Arguments have been given for placing the compensator above the telescope[3], these arguments being based on the fact that the air which is being compensated is also above the corresponding telescope. However, the real disturbing features, such as scattering, shower production, etc., play an entirely different role in the measurements for a thinly dispersed medium like air than they play for a dense medium. On the other hand, mesotron production in the lead itself[6] may be serious in the

---

6) M. Schein and V. C. Wilson, Phys. Rev., 54, 304 (1938).

located in a garage in Fern Royal, Virginia (elevation 490 feet). The horizontal distance between the two stations was about 8 miles.

THEORY OF THE EXPERIMENT

The Compensator

If L_1 is the thickness of lead (in mass per unit area units) in the lower telescope, $f_L(p)$ the loss in momentum (p) per unit (mass) thickness in lead, and if p_b is the momentum necessary for penetration of the lead of thickness L_1, then p_b is determined by

$$L_1 = \int_0^{p_b} \frac{dp}{f_L(p)} \qquad (1)$$

The thickness of the upper block L_2 must be such that

$$L_2 = \int_0^{p_b + p_{hb}} \frac{dp}{f_L(p)} \qquad (2)$$

where p_{hb} is the momentum loss of a ray which, on passing through the column of air of thickness h, ends up with momentum p_b, the quantity h being the mass per unit of area of the air between the two telescopes. If this condition is satisfied, and if $F_2(p)$ is the spectral distribution function for the higher altitude, the rays which penetrate the upper and lower

telescopes will be determined respectively by N_2 and N_1, where

$$N_2 = \int_{p_b + p_{hb}}^{\infty} F_2(p)\,dp \quad ; \qquad N_1 = \int_{p_b + p_{hb}}^{\infty} a_p\, F_2(p)\,dp$$

and where a_p is an attenuation factor determined entirely by mean life considerations.

If $f'_a(p)$ is the loss in momentum per unit (mass) thickness of the air, and p_h is the momentum, at entry, of a ray which, after passing through the mass thickness of air, has momentum p, we have

$$\int_{p}^{p_h} \frac{dp}{f'_a(p)} = h \qquad (3)$$

This determines p_h as a function of p and h, so that $p_{hb}(= p_h - p_b)$ is determined in terms of p_b and h. The values of $f'_\ell(p)$ and $f'_a(p)$ were obtained from the calculations of Rossi and Greisen[7]

---

7) B. Rossi and K. Greisen (Rev. Mod. Phys., 13, 240 (1941)). These authors give dE'/dx' as a function of momentum, where E' is in electron volts, momentum is in e.v/c units, and x' is in grams per cm^2. To convert E' to m_0c^2 units, we multiply by $e/300\ m_0c^2$. To convert momentum to m_0c units, we multiply by $e/300\ m_0c^2$, and to convert dx' to dx, as measured in cms, we utilize the data obtainable from the Government's publication "The U.S. Standard Atmosphere".

Now in ordinary units, the momentum loss per cm $-dp''/dx$ is related to the energy loss dE''/dx per cm by

$$\frac{dp''}{dx} = \frac{1}{\beta c}\,\frac{dE''}{dx}$$

If p and E refer to m_0c units and m_0c^2 units respectively,

$$-f_a(p) = \frac{dp}{dx} = \frac{1}{\beta m_0 c^2}\,\frac{dE''}{dx} = \frac{1}{\beta}\,\frac{dE}{dx}$$

The compensator thickness is, of course, $L_2 - L_1$; and in principle it depends upon p_b, but in practice the dependence is very slight[8].

8) It turns out that for thickness of lead ranging from 10 cms to 60 cms, the compensator thickness altered by only 4 per cent.

The Attenuation Through Mean Life Considerations.

If $\Delta n_2 (= F_2(p)dp)$ is the number of rays having momentum between p and p + dp at the higher altitude, then the group Δn_2 suffers attenuation due to decay on its journey through the atmosphere according to the law

$$\frac{d}{dx}(\Delta n) = \frac{-\Delta n}{v\tau} \tag{4}$$

where dx is an element of path in cms, v is the velocity of the rays at a point in the path, and τ is the mean life for the velocity v. The momentum p in m_0c units is given by

$$p = \frac{v/c}{(1-v^2/c^2)^{1/2}} \tag{5}$$

Hence

$$v = \frac{pc}{(1+p^2)^{1/2}} \tag{6}$$

If we assume the relativistic expression for τ,

$$\tau = \frac{\tau_0}{(1-v^2/c^2)^{1/2}} = \tau_0 (1+p^2)^{1/2}$$

where τ_0 is the rest mean life. Hence, from (4), (5) and (6), we have, on integrating over the path h, here expressed in cms,

$$\frac{\Delta n_2}{\Delta n_1} = Exp \int_0^h \frac{dx}{c\tau_0 p} \tag{7}$$

Since, with f(p) referring to the loss per cm of air,

$$-\frac{dp}{dx} = f_a(p) \tag{8}$$

we may write (7) in the form

$$\frac{\Delta n_2}{\Delta n_1} = Exp \frac{1}{\tau_0} \int_p^{p_h} \frac{d\xi}{c\xi f_a(\xi)} \tag{9}$$

where p is the momentum above the lower telescope of a ray which has momentum p_h at the level of the upper telescope, and where we have changed the variable from p to ξ in order to avoid confusion with the limits of the integral. Since p_h is a function of p and the altitude difference h, the entire integral in (9) is a definite and calculable function of p, which we shall call $\psi(p)$, so that

$$\psi(p) = \int_p^{p_h} \frac{d\xi}{c\xi f_a(\xi)} \tag{10}$$

and

$$\frac{\Delta n_2}{\Delta n_1} = Exp\left(\psi(p)/\tau_0\right.$$

$$\Delta n_1 = e^{-\psi(p)/\tau_0} F_2(p)\, dp$$

If N_2 is the number of rays which penetrate the upper telescope with compensator, and whose momentum for penetration is p_2

$$N_2 = \int_{p_2}^{\infty} F_2(p)\,dp \tag{11}$$

and if N_1 is the number of rays which penetrate the lower telescope

$$N_1 = \int_{p_2}^{\infty} \Delta n_1 = \int_{p_2}^{\infty} e^{-\psi(p)/\tau_0} F_2(p)\,dp \tag{12}$$

Let $\varphi_2(p)$ be some indefinite integral of $F_2(p)dp$. Then $\varphi_2(p)$ is undefined to the extent of a constant. However, for any choice of $\varphi_2(p)$

$$F_2(p) = \frac{d\varphi_2(p)}{dp}$$

and

$$N_2' = \varphi_2(\infty) - \varphi_2(p_2) \tag{13}$$

$$N_1 = \int_{p_2}^{\infty} e^{-\psi(p)/\tau_0} \frac{d\varphi_2(p)\,dp}{dp}$$

$$= \left| e^{-\psi(p)/\tau_0} \varphi_2(p) \right|_{p_2}^{\infty} + \frac{1}{\tau_0} \int_{p_2}^{\infty} \varphi_2(p) e^{-\psi(p)/\tau_0} \psi'(p)\,dp \tag{14}$$

Now although φ_2 is undefined to the extent of a constant, N_2 is obviously independent of the choice of the constant as may be seen from (13) or more fundamentally from (11). Now

equation (14) does not explicitly exhibit N_1 as independent of the constant, but we know that it must be from (12). Hence, we can choose any constant A we please in (14). We shall imagine the constant to be chosen so that $\varphi_2(\infty) = 0$. In this case, we have for any value of p as corresponding to the upper telescope, the value of N for that telescope as given by

$$N = \varphi_2(\infty) - \varphi_2(p) = -\varphi_2(p)$$

Thus (14) becomes

$$N_1 = e^{-\psi(p_2)/\tau_0} N_2 - \frac{1}{\tau_0}\int_{p_2}^{\infty} N e^{-\psi(p)/\tau_0}\psi'(p)\,dp \qquad (15)$$

where N in the integral refers to the number of rays which penetrate the upper telescope when the thickness of lead therein requires a momentum p for penetration.

Since the values of N are known over only a finite interval of p, the integral in (15) is unknown except between such limits p_{2a} and p_{2b} as those over which N is known. If, therefore, N_{1a} and N_{1b} refer to the numbers of rays which in the lower telescope penetrate two pieces of lead whose representatives in the upper telescope are penetrated by N_{2a} rays of momentum greater than p_{2a} and N_{2b} rays of momentum greater that p_{2b} respectively, then

$$N_{1a} - N_{1b} = e^{-\psi(p_{2a})/\tau_0} N_{2a} - e^{-\psi(p_{2b})/\tau_0} N_{2b} - \frac{1}{\tau_0}\int_{p_{2a}}^{p_{2b}} N e^{-\psi(p)/\tau_0}\psi'(p)\,dp \qquad (16)$$

where N, as already stated under the integral, refers to the upper telescope.

Assuming successive values of τ_0, equation (16) was tested, using graphical integration, until the τ_0 necessary to satisfy the equation was found.

An important feature of the above analysis lies in its allowance for the proper loss of momentum, and consequent variation of mean life during the passage of the mesotron through the air separating the altitudes of our telescopes. It can be shown that if the calculation had been made on the basis of an average momentum for any ray over the air journey, a significant change in the values of τ_0 calculated from the data would have resulted. In spite of the fact that an "integral method"[9] has been used in deducing the values of τ_0

9) D. J. X. Montgomery: Cosmic Ray Physics, Pages 210-211.

from experimental data, the method makes no assumption as to the form of the spectral distribution of the mesotrons. This distribution dictates the values of N, but those values themselves depend only upon measurements.

Results.

The measured absorption curves are shown in Fig. 2. The intensity is given in coincidences per minute and the absorber thickness in centimeters of lead. In the case of the upper telescope, the abscissa represents thickness in addition to the 14 cms

accompanying absorber.

TABLE I

p	p_b	τ_0
(m_0c units)	cms	(sec $\times 10^{-6}$)
2.33 - 6.28	10 - 40	2.4 ± 0.8
4.95 - 9.10	30 - 60	2.2 ± 0.8
2.33 - 9.10	10 - 60	2.3 ± 0.6

Table I shows various values of τ_0 computed for different regions of the absorption curve. These calculations are based on the value $m_0 = 196$ electron masses (1.00×10^8 e.v/c). We have chosen this value of m_0 because it is the value which has been used by most former observers with whose measurements it is of interest to compare our results.

It is easy to show that with this value of m_0 a 10 per cent increase in m_0 corresponds to a 7 per cent increase in the value of τ_0 which would be calculated from the data. Thus, if we take the value of m_0 more usually accepted at present, namely, $m_0 = 212$ electron masses, the values of τ_0 given in the Table would be increased by 5.6 per cent.

The consistency of the values in the Table for different portions of the absorption curve is interpreted as confirmation of the relativistic variation of τ with p, namely $\tau = \tau_0 (1 + p^2)^{1/2}$. If the lifetime varied by some other law, for example, $\tau = \tau_0 (1 + p^2)^{3/4}$, then it can easily be shown that the value of τ_0 for the higher values of p would be about twice the value for the lower values of p. Such differences in the values of τ_0 as exist for the different ranges of momentum are small, and well within the statistical uncertainty, yet they are in such a direction that if the variation is real, it can be attributed to the effect of a non-decaying component.

Comparison of Results with Those of Other Observers. Our results are in close agreement with the value $\tau_0 = 2 \times 10^{-6}$ sec. found by Rossi et al[3], using a similar method founded upon observations taken at two different altitudes widely separated, however, in position and time. They are, however, quite different from the result $\tau_0 = 1.25 \times 10^{-6}$ sec. obtained by Nielsen et al[4], again by a method involving measurements at different times in the same locality. Nielsen's calculations do not take account of the change of mean life resulting from the loss of momentum of the mesotrons as they pass through the air. However, we have recalculated a value of τ_0 from Nielsen's data as given, the calculation being made according to the theory outlined above, and while the value obtained differs appreciably from that calculated by Nielsen, and in the sense to make his results harmonize more closely with ours, there is still a wide discrepancy. Nielsen's result, as calculated by our method, is $\tau_0 = 1.7 \times 10^{-6}$ sec.

ACKNOWLEDGMENTS

We are indebted to Dr. Lyman J. Briggs, through whose good offices we secured the kind cooperation of Mr. Guy D. Edwards, Superintendent of the Shenandoah National Park, who put facilities, including the forest ranger's cabin, at our disposal. We are also indebted to Mr. R. G. Ovelman of the J. W. Meyers Company for the use of his Company's garage. The counters were constructed by Mr. A. G. Nester, and technical assistance was afforded by Mrs. F. J. Seymour, Mr. R. C. Pfeiffer and Mr. S. Berko.

CAPTIONS

Caption to Figure 1.

A COUNTER TELESCOPE

Counter trays 12 cm X 12 cm sensitive area. 27 cm between trays. Measured efficiency = 97%. A Rossi coincidence circuit operates a thyratron and mechanical recorder. Resolving time for accidentals = 5×10^{-5} sec; coincidence dead time = 5×10^{-3} sec.

Caption to Figure 2.

Absorption curves measured at the two altitudes. For the upper telescope the thicknesses of lead are in each case 14 cms greater than are recorded by the abscissae of the curves.

Caption to Photograph.

Photograph of one of the telescope units. There are four trays of counters; 17 counters in each tray, straddled in a manner to increase tray efficiency.

GAMMA RAYS FROM Sn^{125} [X]

C. E. Mandeville, E. Shapiro, R. L. Mendenhall, E. R. Zucker[*], and G. L. Conklin

Bartol Research Foundation of the Franklin Institute, Swarthmore, Pennsylvania

[X] Assisted by the joint program of the ONR and the AEC

[*] Frankford Arsenal

The ten-day activity in tin has been assigned[1] to Sn^{125}. Spectrometric measurements[2] have yielded maximum beta-ray energies of 2.3% ± 0.02 Mev and 0.40 ± 0.01 Mev. The spectrum of lower energy was estimated to contain five percent of the total beta radiation. A search was made for the gamma radiation which should accompany the beta rays of the inner group, but because of low intensity, none was detected by the spectrometric method. It was mentioned, however, that absorption measurements in lead indicated the "possible presence" of a gamma ray at 1.5 Mev.

During the past four years, four different quantities of metallic tin, two isotopically concentrated in Sn^{124} and two of naturally occurring tin, have been irradiated in the Oak Ridge pile[3]. The following chemical procedure has been followed. Irradiated metallic tin was dissolved in HCl and carrier, Sb and Te solutions were added. Metallic Te precipitated at once, and Sb was precipitated as a metal by addition of powdered Fe to the hot 6N - HCl solution. Sn and some Fe were precipitated from the filtrate by addition of metallic zinc. This precipitate was dissolved by HCl, oxidized with H_2O_2, and Sn and Fe were separated by addition of NaOH to excess to form soluble Na_2SnO_3 and insoluble $Fe(OH)_3$. The filtrate was acidified with HCl, then made slightly ammoniacal, precipitating $SnO_2 . xH_2O$ which was ignited to SnO_2.

A gamma ray at 1.7 Mev was noted in the tin fraction in 1948 but was dismissed as the intense hard gamma ray of Sb^{124}. More recently this gamma ray has been observed in a coincidence absorption counting arrangement, and the quantum energy has been measured as 1.67 ± 0.10 Mev. This coincidence absorption curve of the secondary electrons of the gamma ray was observed repeatedly for forty days, and the ordinate values were observed to decay with a half-life of ten days.

A source of the ten day tin was placed in a beta-gamma coincidence counting arrangement, and beta-gamma coincidences were measured as a function of aluminum absorber thickness before the beta-ray counter. The data are shown in Figure 1 where the beta-gamma coincidence rate is seen to decrease to zero at 180 mg/cm^2 of aluminum, indicating an inner beta-ray group at ~0.5 Mev. On calibration of the beta-gamma coincidence counting arrangement with the beta-gamma coincidence rate of Sc^{46}, the beta-gamma coincidence rate of Figure 1 indicated, on extrapolation to zero absorber thickness, that the gamma ray at 1.67 Mev is coincident with 10 ± 2 percent of the beta rays of the 10-day Sn^{125}.

Measurements by Boyd and associates[4] at Oak Ridge, employing a scintillation spectrometer, yield a quantum energy of ~1.9 Mev for this gamma ray.

References

1. J. C. Lee and M. L. Pool, Phys. Rev. 76, 505 (1949).

2. R. W. Hayward, Phys. Rev. 79, 409 (1950).

3. Isotopically concentrated Sn^{124} supplied by Y-12 Research Laboratory, Carbide and Carbon Chemicals Division, Union Carbide and Carbon Corporation, Oak Ridge, Tennessee.

4. Nuclear Data, Supplement 2 to NBS Circular 499.

Caption

Figure 1 - Beta-gamma coincidence rate of Sn^{125} as a function of the surface density of aluminum before the beta-ray counter.

Reprinted from THE REVIEW OF SCIENTIFIC INSTRUMENTS, Vol. 23, No. 11, 636-638, November, 1952
Printed in U. S. A.

A Radiofrequency Ion Source*

C. P. SWANN AND J. F. SWINGLE, JR. †
Bartol Research Foundation of the Franklin Institute, Swarthmore, Pennsylvania
(Received August 13, 1952)

An rf ion source with transverse magnetic field giving 50 μa of resolved protons with a gas flow of less than 1 cc per hour and with a power input of 150 w is described. The effect of magnetic field upon power requirements is discussed.

With increased gas flow resolved currents in excess of 100 μa of protons have been obtained.

IT was decided to undertake, for the Bartol Van de Graaff generators, the construction of an ion source which meets the following requirements: a proton current, continuously variable up to 40 μa; a gas flow of less than 1 cc of gas per hour as measured at atmospheric pressure; a reasonable efficiency; and a low power consumption. We have defined efficiency in this case as the ratio of proton current to total ion current in the resultant beam. Many ion sources are described in the literature,[1,2] but none of them incorporate all of these features.‡ An rf ion source using a probe-cathode scheme devised by D. Ralph[3] was decided upon. This ion source operated at 10 Mc/sec and produced about 100μa total ion current, but the gas flow was about 8 cc/hr and the power input to the oscillator was about 300 w, both of which we considered excessive for our needs.

It was observed during initial tests that a small transverse magnetic field produced by a magnetron type permanent magnet caused large increases in the magnitude of the arc discharge when the magnetic field was adjusted to the proper value. Axial magnetic fields have been employed in many sources.[1,2] However, at the frequencies and pressures we tried, we did not observe the effect for an axial field.

When the magnetic field is perpendicular to the axis of the source, the axial ac electric field, when of suitable frequency, cooperates with the magnetic field in such a way that an electron receives energy in both the upward and downward path of each cycle while it describes a spiral orbit in the plane containing the axis of the ion source. The necessary frequency, of course, corresponds to a cyclotron frequency as first recognized by Hall.[1] At the frequency now used of 25 Mc/sec, the value of B calculated for this cyclotron frequency is approximately 9 gauss which agrees well with the measured value.

Theory indicates that, for resonance at the cyclotron frequency and with neglect of damping, an electron starting from rest describes a spiral path whose radius vector from the origin is proportional to the electric field and inversely proportional to the square of the cyclotron frequency at any time in terms of the cyclotron period as the unit of time. If the electric field were given by the electric field of the rf coil operating in a vacuum, it would amount to about 100 v/cm, and with such a field the electrons in our apparatus would strike the glass vessel in a fraction of a cycle. However, the nature of the electric discharge in a gas is such as to result in a field which, in the main body of the gas, is much smaller than the average field and, indeed, of the order of 10 or 20 v/cm. With a field of 10 v/cm, we should expect that a mean free path of the order of 1 cm would be necessary to initiate ionization. Experiment showed that the discharge became initiated at a pressure of the order of 10^{-2} mm, at which pressure the mean free path of a gas molecule would be of the order of 1 cm and that of an electron somewhat greater. There is, thus, harmony between the magnitudes concerned and the fact that the discharge becomes initiated at about 10^{-2} mm, with an electric field of the order of 10 or 20 v/cm, which would permit the spiral path to develop within the confines of the tube to such an extent as to enhance the total ionization appreciably.

Experiment shows that when the pressure is reduced to the point at which the magnetic field is operative in increasing the total ionization, the amount of power necessary to produce an assigned amount of ionization is less than when the conditions are such that the magnetic field is not operative.

As has been mentioned, the magnetic field is obtained from a magnetron type permanent magnet, or from clusters of small magnets as pointed out later. The field strength was measured as a function of distance from the axis of the pole pieces. The magnet was then positioned for maximum intensity of the ion source discharge.

As the static magnetic field was increased from zero, a very definite change in color of the discharge was observed, namely, light blue to a bright red. Spectroscopic analysis of the discharge shows bright and clear Balmer lines with little band structure when the arc is red. The magnetic field could be varied through several gauss once the bright red discharge was initiated; however, a definite maximum of current was detected.

* Assisted by the joint program of the ONR and the AEC.
† Now at the University of Virginia.
[1] R. N. Hall, Rev. Sci. Instr. 19, 905 (1948).
[2] Bailey, Drulrey, and Oppenheimer, Rev. Sci. Instr. 20, 189 (1949).
‡ *Note added in proof:* A description of the high efficiency Oak Ridge ion source was recently published by Moak, Reese, and Good, *Nucleonics* 9, 18 (1951) shortly after completion of the source here discussed.
[3] D. Ralph, private communications.

Of course, the positive ions which result from the ionizing action of the electrons are carried down by a superimposed steady electric field, and their large mass prevents them from being affected by the magnetic field. This electric field is created by a probe inserted in the top of the glass vessel.

The total ionization current resulting from the action of the electrons was measured by means of the probe which was kept at a potential of 2 to 5 kv. It was of interest to compare this current with the power supplied to the rf oscillator. It was found, as was expected, that the ionization current increased with increase of power supplied to the oscillator, as reflected in a larger alternating electric field. However, for any given power supplied, the total ionization current was increased by the application of a magnetic field adjusted to the proper value. The results in this connection are shown in Fig. 1. The slope of the graph with the magnetic field is approximately 40 w/ma and without it approximately 100 w/ma, the graphs being linear.

Of course, we are really concerned with the currents which pass through the hole in the cathode. This current was measured in the following manner. The beam, after traveling along the axis of the apparatus, struck a plate. It was possible to deflect it by a magnetic field, and this resulted in a separation into its various components, the proton component being deflected to the greatest extent. Off the axis of the undeflected beam, there was a slit, and the magnetic field could be adjusted to deflect either the proton component or any of the others in such a manner as to pass through this slit and become measured by a suitable collecting electrode which was placed below it. The usual precautions to avoid measurement of secondaries were, of course, adopted.

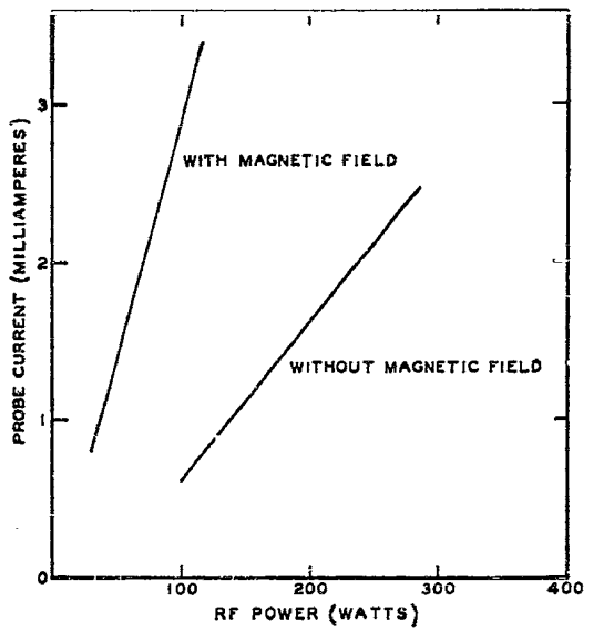

FIG. 1. Rf power as a function of probe current with and without transverse magnetic field.

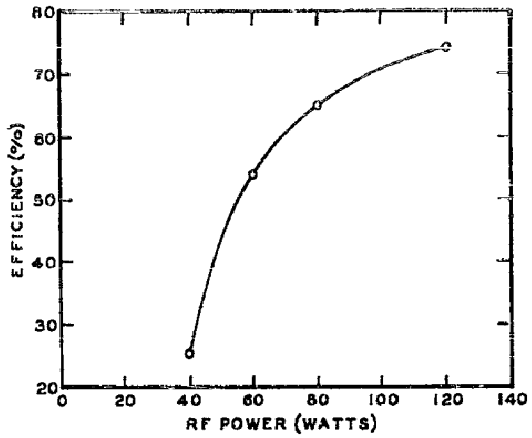

FIG. 2. Positive ion efficiency as a function of rf power with transverse magnetic field.

It was found that proton currents of over 100 μa were obtainable through an exit hole from the ion source having a diameter of 0.040 in. and a length of 0.120 in., the gas flow being about 8 cc/hr. Proton currents up to 50 μa were still obtainable through an exit hole having a diameter of 0.020 in. and a length of 0.120 in., the gas flow being reduced to between 0.4 cc and 1 cc/hr.

By the foregoing procedures, it was possible to measure what we have defined as the efficiency and to plot it against the rf power, the magnetic field adjusted to the cyclotron frequency being, of course, in operation. Figure 2 shows the results. It will be seen that when the power was 100 w, the efficiency was close to the extrapolated maximum.

The efficiency was found to vary with the surface temperature of the glass vessel in which the ionization occurred (decreased temperature, increased efficiency) and with the length of time run. This phenomenon may be concerned with the recombination of ions on the walls of the vessel. After several hours of operation, the efficiency rose to 80 percent at 100 w input.

The focusing of the beam was accomplished by the use of coaxial cylinders operating at potentials of 5 kv, 25 kv, and 50 kv, respectively, the intermediate voltage being the half voltage tap on the 50 kv supply. These cylinders focused the beam to a spot $\frac{1}{16}$ in. in diameter at a distance of 5 ft. The first focusing electrode collected 10 μa, the current to the remainder of the electrodes being negligible. Total power input to the unit including probe supply, oscillator supply, focusing supplies, and palladium leak was 500 w, the power being obtained from a 140-v, 400-cy generator.

DESIGN

The ion source and lens assembly are shown in Fig. 3. The cathode-shield scheme is much the same as is suggested by D. Ralph. The Lavite piece serves the following purpose. In the absence of this element, the positive ions generated in the upper chamber would be brought down by the field and deposited, for the most part, upon the metal parts at the lower end of this

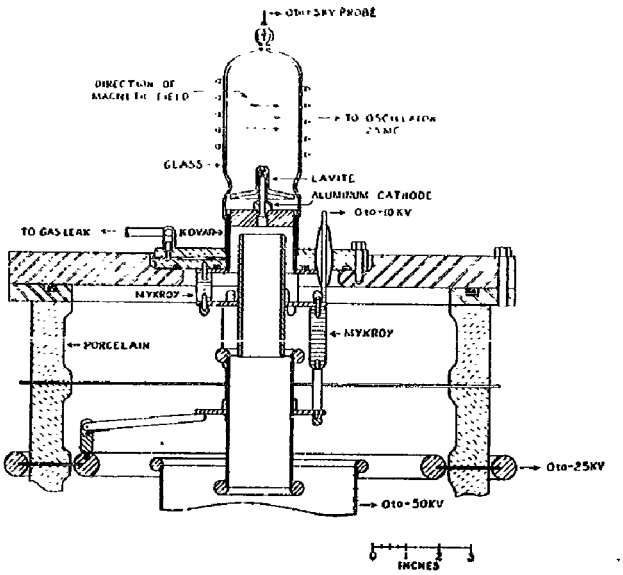

FIG. 3. Schematic diagram of the rf ion source and focusing electrodes. The direction of the magnetic field is shown by the arrows.

chamber. The Lavite, being an insulator, becomes charged by the arrival of the positive ions in such a manner as to discourage further arrival of these ions. As a result, more positive ions are rendered available for passage through the aperture at the center of the shield. The hole in this aperture is 0.120 in. in diameter, and its length is 0.120 in. The holes in both the shield and the anode should be concentric and straight. Furthermore, the probe supply must be current limited for, otherwise, surges are apt to take place which may crack the Lavite.

The magnet assembly is supported with its field perpendicular to the axis of the ion source. The support consists of a clamp which allows for vertical and horizontal positioning of the magnet. The source is then tuned by adjusting the position of the magnet to obtain maximum power as observed by noting the current drawn from the oscillator power supply.

The whole assembly was designed for ease of construction and assembly. Accurate glass blowing has been eliminated in favor of machined parts. Furthermore, any one component may be changed without necessarily affecting the other components; thus, anodes with different size holes may be used in the same source and damaged or worn out parts may be replaced. Since the focusing lenses are integral with the source itself, the matter of alignment and installation is a simple process. The whole unit can be tested on a bench set-up prior to installation in the generator.

The tests on this ion source were performed on a bench which consists of four porcelains which serve both to insulate the ion source, which was run hot, from ground and to provide a means for taking into the vacuum the intermediate focusing voltage. After passing the last electrode, the beam passed about four feet to the collector.

Following these tests a similar source was installed in the test section of the new Bartol Van de Graaff generator. The beam in this section passed through about seventeen feet, seven feet of which was the accelerating tube. Voltages up to about 2 Mev were reached to determine the effect with and without the beam.

The ion source arrangement used here was only slightly different from that described above. Two sets of three small permanent magnets were used instead of one magnetron type magnet, these magnets being placed 180° from each other around the ion source vessel. Also a steel cathode assembly replaced the aluminum assembly shown in Fig. 3. The former change was made because of space limitations; the latter change was made to withstand the tank pressure in case the ion source vessel broke and also to shield the beam of particles passing through the cathode from the magnetic field.

A total beam current of over 50 μa has been obtained from this source with about 0.5 cc of gas per hour and about 85 w input to the oscillator. The beam is well focused into a spot of about $\frac{1}{16}$ in. The focusing scheme is the same as that used on the bench set-up; that is, there are two supplies, one variable up to 10 kv, and the other variable up to 50 kv, the intermediate electrode potential being a half-voltage tap on the 50-kv supply. As yet the beam has not been analyzed to determine the proton efficiency. The beam current is reduced by reducing the power input, but, of course, this means lower efficiency as indicated in Fig. 2.

CONCLUSION

The bench test ion source assembly was operated for well over 100 hrs. During this time, one glass vessel cracked when the rf coil came in contact with the glass, causing local stresses due to heat, and two Lavite shields cracked, one as a result of not limiting the probe current, the other as a result of expansion. In other words, although the cathode should fit fairly well into the shield, the relative expansion of aluminum and Lavite should be considered. For high pressure machines the glass jar should be as round as possible and the glass thickness as great as possible to avoid collapsing. The source in the Van de Graaff generator has been operated for well over 50 hr without any failures. Further studies should be made in order to obtain beam currents of the order of one ma, and this can probably be done by revising the cathode-shield geometry.

The writers wish to acknowledge the continued interest of the Director of the Bartol Research Foundation, Dr. W. F. G. Swann.

Reprinted from JOURNAL OF THE FRANKLIN INSTITUTE,
Vol. 254, No. 2, August, 1952
Printed in U. S. A.

A CIRCUIT FOR THE LIMITATION OF DISCHARGE IN G-M COUNTERS *

BY

W. C. PORTER [1] AND W. E. RAMSEY [1]

ABSTRACT

A simple two tube feedback arrangement to limit the discharge in a counter to a small segment of its length subsequently restoring all but a small portion of the tube to full sensitivity in about a microsecond, has been achieved. The procedure results in a marked reduction in dead-time, and a correspondingly large increase in life. For example, a 20-cm. counter may be operated at a rate of 20,000 counts per second with a loss no greater than that normally encountered at 1000 counts per second. Counting rate data are given along with studies of the discharge distribution with and without the cut-off procedure. Alteration in the dead-time picture is illustrated by oscillograms.

INTRODUCTION

As conventionally used, the discharge in a G-M counter spreads, from one or more points, over the entire length of the wire. Subsequently, the tube remains unresponsive to radiation until such time as the positive ion sheath, in its motion toward the cathode, permits a restoration of the starting field. This "dead-time," which frequently is as long as one hundred microseconds, very seriously limits all applications wherein a counter must be used at high rates. The dead-time is particularly serious in coincidence operation where the large collecting surface of long counters is required but an intense background field is unavoidable. Following the fundamental work of Simpson (1)[2] numerous investigators (2–5) have succeeded in reducing this limitation. However, it continues to be one of the problems associated with this versatile instrument. The procedure to be discussed here greatly increases the rate at which a counter may be operated without loss and achieves an equally great increase in tube life. The increase in rate and life both depend upon tube length. Thus for a given percentage loss, a 40-cm. counter can be operated at forty times its usual rate, while a factor of twenty is possible with a 20-cm. tube.

Fortunately the circuit is quite simple. It can be made very compact and does not lead to geometrical complications as when a number of tubes are to be used in coincidence.

Studies were made with numerous counters at this laboratory and the circuit operated satisfactorily with all of them.

Although with a multiple tube circuit operating on the same prin-

* Assisted by the joint program of the ONR and the AEC.

[1] Bartol Research Foundation of The Franklin Institute, Swarthmore, Pa.

[2] The boldface numbers in parentheses refer to the references appended to this paper.

ciple much higher overvoltages are possible, simplicity is lost. The slight gain in efficiency with marked reduction of counter life hardly justifies a complexity which discourages use. Such a procedure after test was abandoned in favor of the simple arrangement discussed here.

THE CUT-OFF CIRCUIT

The main circuit shown in Fig. 1 is labeled Cut-Off Circuit. It is accompanied by two subsidiary circuits labeled, respectively, Viewing Circuit and Rate-Measuring Circuit. These subsidiary circuits serve the purpose of facilitating the study of the cut-off circuit. The cut-off circuit itself is coupled directly to the wire of the counter. Since the high potential is applied to the cylinder of the counter at the point A, the cut-off circuit is at normal voltage levels.

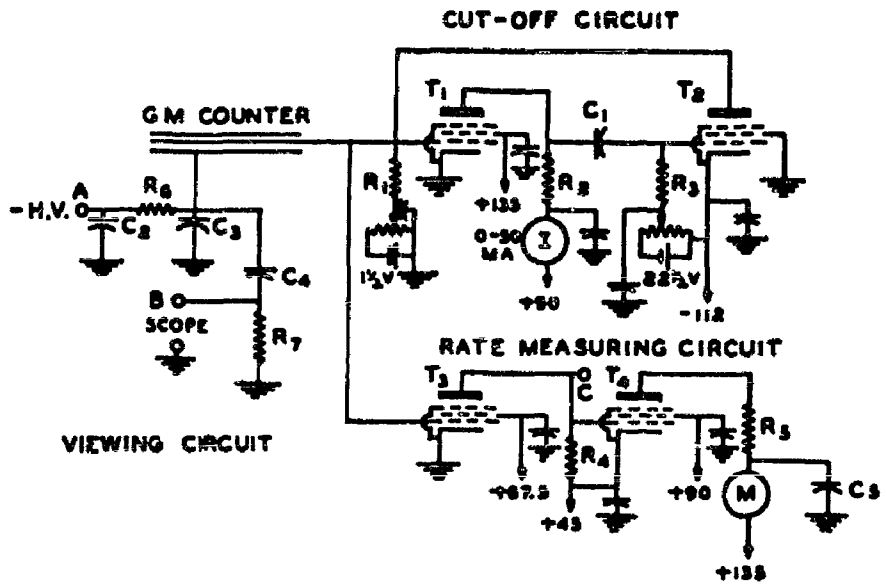

FIG. 1.

All tubes are 6AK5's and all unlabeled by-pass condensers are 0.0025 microfarads.

C_1 = 50$\mu\mu f$ C_2 = 0.1μf C_3 = 400$\mu\mu f$ C_4 = 4000$\mu\mu f$ C_5 = 1.0μf R_1 = 1800
R_2 = 2700 R_3 = 2200 R_4 = 1000 R_5 = 3300 R_6 = 47,000 R_7 = 100,000

When an ionizing particle passes through the counter, it starts the normal spreading process down the wire from which we obtain the "electron component" (6, 7) necessary to actuate the circuit. When the voltage pulse appearing across R_1 is approximately 0.2 volts, it is amplified enough in T_1 to cause the grid of T_2 to come from below cut-off bias; hence, the plate current of T_2 adds to the voltage drop of R_1—a cumulative action which proceeds until T_1 is cut off. The grid of T_2 starts to recover rapidly by virtue of the short time constant determined by C_1, R_2, R_3 and the input impedance of T_2. As the grid of T_2 recovers, the plate current of T_2 decreases until the voltage drop across R_1 is less than the cut-off bias of T_1. The resulting negative pulse on the plate of T_1 abruptly returns the grid of T_2 below its cut-off value. The time required for an entire cycle of the circuit operation is approximately

1.5 microseconds: after this period the circuit is again ready to accept a new pulse.

In order to make the circuit operate as rapidly as possible, the stray capacitance must be kept at a minimum. Tubes T_1 and T_2 (Western Electric 6AK5's) were mounted adjacent to each other and

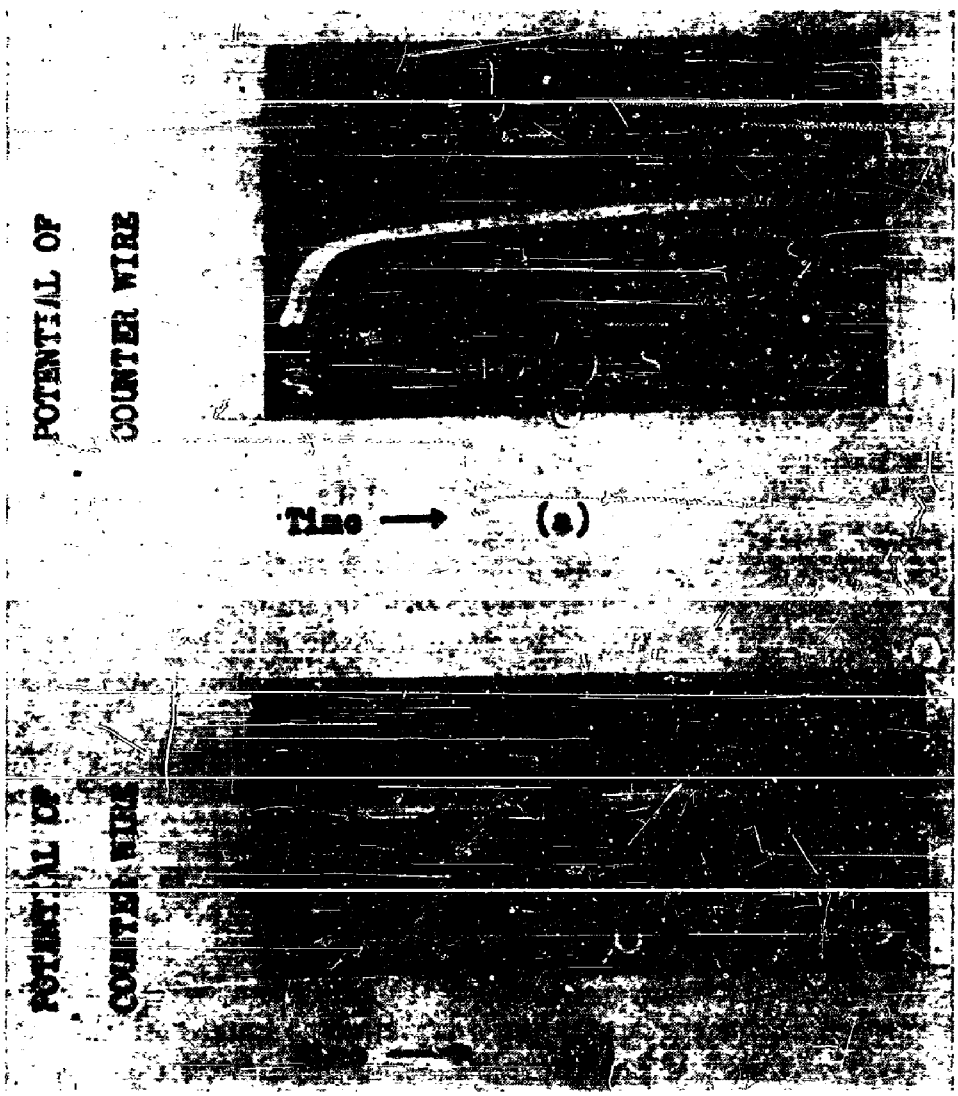

FIG. 2.—Presentation of dead-times.

(a) Normal counter discharge.
(b) Same counter discharge with cut-off circuit operating. Only saturated pulse bottoms are visible in (b).

connections were soldered directly to the tube pins. T_1 and T_2 were chosen so that with plate voltage = 45V, screen grid voltage = 67.5V, and control grid voltage = − 5.0V, the plate current was less than 0.2 μa. However, in the actual circuit, these values were increased.

The circuit output pulses were found to be uniform in shape and amplitude up to the highest rates encountered—2×10^5 counts per second. However, at very high rates of counting, resistor R_6 should be short-circuited so that the potential across the counter remains

constant. No alteration in size or shape of the pulses was observed over the operating range of counter voltages used from six to thirty volts above the starting potential. In virtue of this fact, the pulses appearing across R_1 may be applied to a rate measuring circuit consisting of T_3 and T_4. The current through meter M served as a rate indicator. Obviously, at the higher rates, the fluctuations in M were quite small. The resistor R_8 was added so that the plate pulse of T_4 would trigger a scaler directly for calibrating purposes.

Figure 2 shows the results of the method used to find the dead-time. The method, due to Stever (8), consists of triggering an oscilloscope sweep by a counter pulse, delaying the pulse so that it can be seen at a fixed position near the beginning of the sweep, and observing any other pulses which occur in the interval of the time base. A triggered oscilloscope connected at point C (Fig. 1) was used for these presentations. Photons were used to initiate the pulses. It should be noted that these photographs are time exposures so that a large number of triggering pulses are superposed at the left end of the time base; whereas subsequent individual pulses occur at random and appear less intense in the photograph. The same counter was used for both presentations of Fig. 2.

In the upper photograph no pulses appear until after approximately 45 microseconds have elapsed[3] since the beginning of the triggering pulse. After this time, the pulse height is dependent upon the time since the triggering pulse has occurred. The manner of build-up of pulse sizes in this region can be correlated to the motion of the positive ion sheath in the counter after the discharge. Although the potential of the wire is returned to normal in a short time, the electric field is still being partially controlled by the ion sheath.

The case of Fig. 2*b* is different. With the circuit in operation, no pulses were observed in the first 1.5 microsecond interval. After this time pulses appear, and any pulse appearing on the time base is identical in size and shape with the pulse which triggered the sweep.[4] Since the cut-off circuit limits the spreading to a short segment of the counter length, positive ions are present only in the vicinity of this discharged region. When the circuit returns the potential of the counter to its normal value, the electric field near the wire is returned to normal also, except for the short segment used in the previous discharge.

The auxiliary viewing circuit connected to the counter cathode is designed in such a way that the pulses at point B (Fig. 1) are proportional to the number of positive ions evolved in the counter discharge. The ratio of the pulse heights observed at B with and without the

[3] The vertical descents of the pulse traces are invisible on the photograph on account of the rapidity of the sweep.

[4] Again, on account of the rapidity of the sweep, only the lower parts of the pulses are represented. They correspond to the thickenings on the faint, approximately horizontal line.

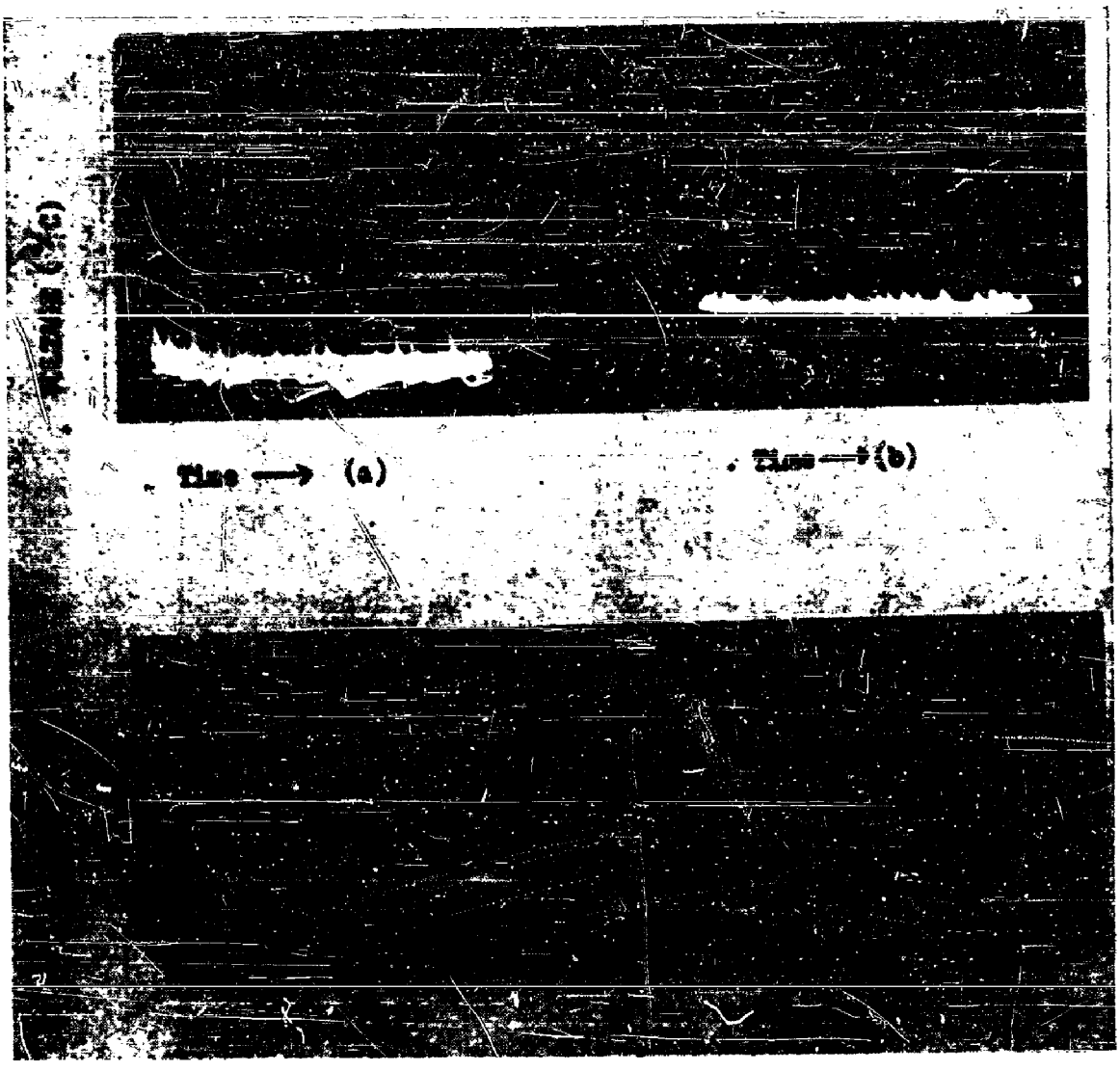

FIG. 3.—Observations from cylinder of counter.

(*a*) Normal discharge from photons.
(*b*) Discharge from photons with cut-off circuit operating.
(*c*) Discharge from β-rays at side window of counter with cut-off circuit operating.
(*d*) Discharge from β-rays at end of counter with cut-off circuit operating.

circuit in operation (Fig. 3*a*, *b*) indicates that the circuit limited the spreading of the discharge to 1/20 of the length of the counter or approximately 1 cm. If two centers separated by more than 1 cm. are formed by an ionizing particle, a pulse larger than a single center pulse may be produced. In Fig. 3*c*, β-rays were sent in through a side window in the counter and scattered β-rays produced some of these multiple centers. The effect of more starting centers (or multiple centers) is shown more clearly in Fig. 3*d*, where the β-rays were admitted through an end window.

INVESTIGATION OF EXTENT OF SPREADING

In order to check the previous assumption that the spreading process was limited to approximately 1 cm. of length, a special counter with the cathode split into a number of individual cylindrical segments was

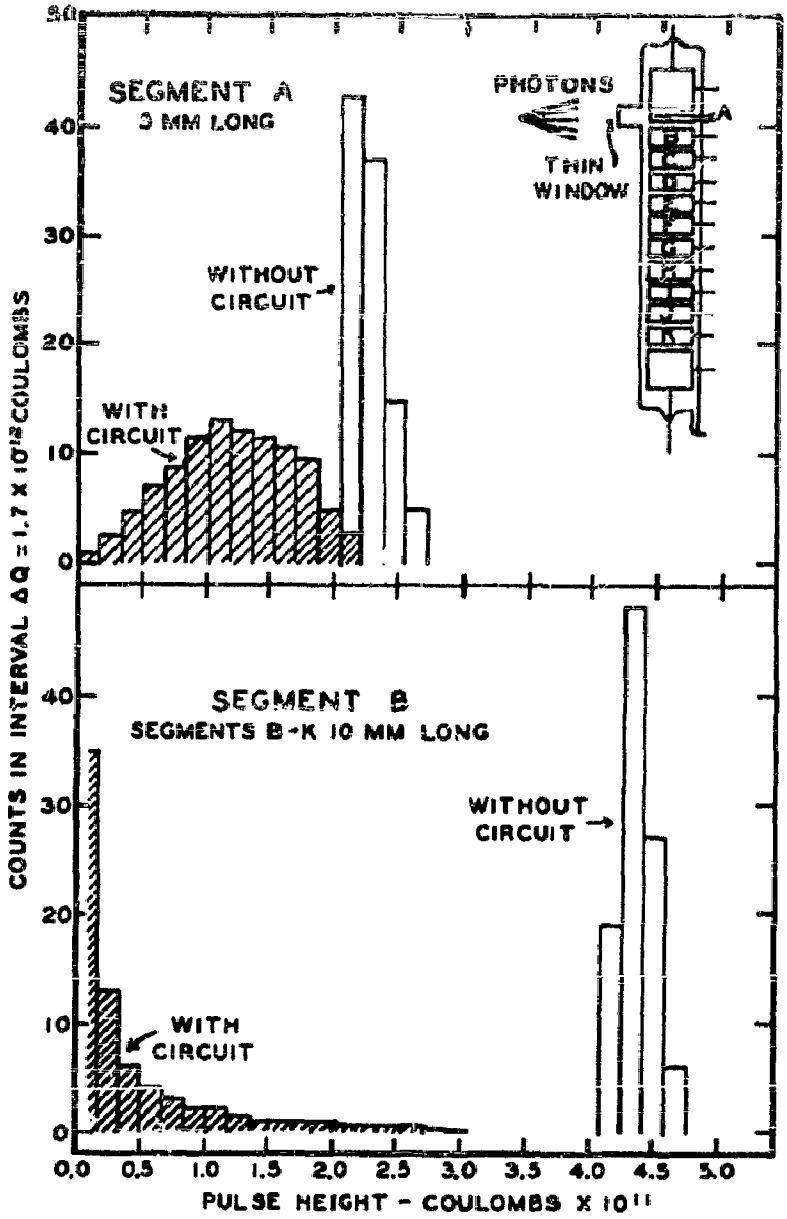

FIG. 4.—Pulse height distributions from cathode segments along the counter length showing the effect of the cut-off circuit.

used (Fig. 4). Opposite to segment *A* was a thin window which admitted photons so that a single-centered discharge always started in the vicinity of segment *A;* hence, the spreading started from this region. The experiment consisted of measuring the distribution of pulse heights on different segments under two conditions: with and without the cut-off circuit. The results of these tests are shown in Fig. 4. Without the circuit, the pulses appearing on segment *B* are about twice as large as those on segment *A*, as may be seen from the plain block pulse height distribution. This is to be expected fro n the relative lengths of the two segments (10 mm. and 5 mm., respectively).

Segments C through K had distribution curves, without the circuit operating, similar to that shown for segment B.

With the circuit in operation, the pulse-height distributions on all segments of the counter are markedly changed. While the counting rate of segment A remained unchanged, that of segment B was reduced by approximately 25 per cent and that of segment C by more than 99 per cent of the "no-circuit" rate. This constitutes evidence that the circuit limits the spreading to not more than 1 cm. from the point of origin of the discharge.

The rather broad pulse-height distribution observed on segments A and B is believed to result mainly from poor collimation of the photon beam rather than statistical fluctuations in the spreading process or in the cut-off time of the circuit. Comparison of the shaded pulse-height distributions observed on segments A and B (Fig. 4) indicates that the average charge developed along the length of segment B is much less than in A with the circuit in operation.

COUNTING RATES

If N' is the number of impulses which should be counted per unit time, and N is the number actually counted per unit time, the relation between N and N' is

$$N = \frac{N'}{1 + N'\sigma},$$

where σ is the dead-time. The formula is based upon the assumption that the counter and associated circuit are completely incapable of registering a count during a time interval σ following each count, and that full efficiency is restored abruptly at the end of the interval σ.

In order to obtain equally spaced values of N', five radioactive sources A, B, C, D, E were used. The plan was first to find positions for these sources in which each individually gave the same value for N. We are then assured that the use of A, followed by the use of A plus B, followed by the use of A plus B plus C, etc., provides successively equal increments of N'. If we set $N' = \alpha n$ where n is the number of sources irradiating the counter, we have

$$N = \frac{N'}{1 + N'\sigma} = \frac{\alpha n}{1 + \alpha n \sigma}. \qquad (1)$$

Now with source A alone in position, it was found that $N = 10^4$ cps. Hence

$$10^4 = \frac{\alpha}{1 + \alpha\sigma}$$

$$\alpha = \frac{1}{10^{-4} - \sigma}.$$ **

** It may be remarked that 10^{-4} seconds is the greatest value for σ consistent with the measurement of 10^4 counts per second.

Now Eq. 1 yields

$$N = \frac{\left(\frac{1}{10^{-4} - \sigma}\right) n}{1 + \left(\frac{\sigma}{10^{-4} - \sigma}\right) n} = \frac{n}{\sigma(n-1) + 10^{-4}}. \qquad (2)$$

Substitution of the values $\sigma = 1$, 10 and 90 μ-sec. into Eq. 2 yields the set of dashed curves shown in Fig. 5. As the theoretical curves are

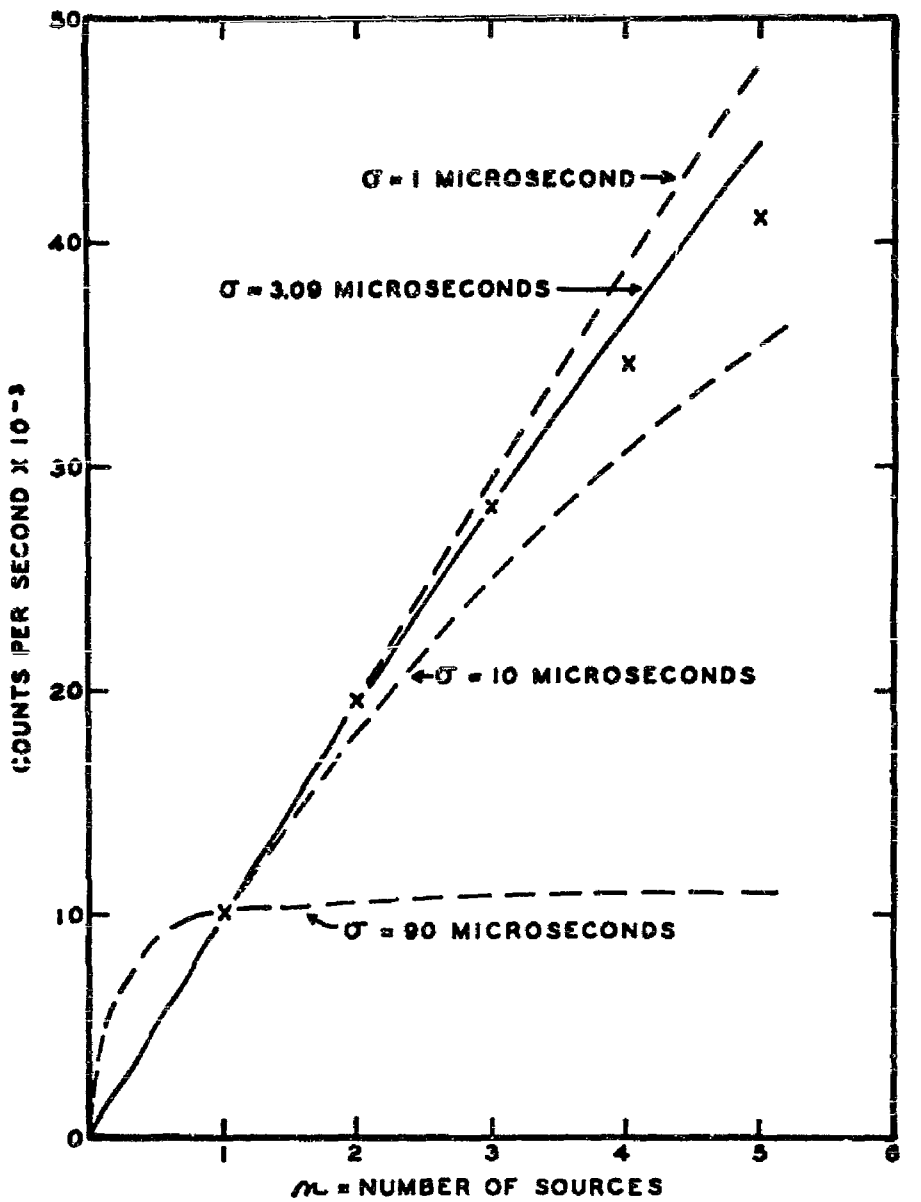

FIG. 5.—Counting rate for counters of various dead-times as a function of source strength. A unit of source strength is defined as that strength required to give 10^4 counts per second. This unit of source strength is given by $\alpha = \frac{1}{10^{-4} - \sigma}$. The X's are experimental points obtained with the cut-off circuit operating.

plotted in Fig. 5 it might appear that at low source intensities the counter would count faster with a 90 μ-sec. dead-time than with a 1 μ-sec. dead-time. This apparent absurdity arises from the fact that the method used to normalize the theoretical curves to the experimental data yields a different value of α for each dashed curve. The solid curve, which fits the experimental data for $n = 1$, 2, and 3 within the statistical errors, is obtained by setting $\sigma = 3.09$ μ-sec. The agreement of the solid curve with the experimental data is as good as might be expected[5] in view of the limited extent to which Eq. 1 is applicable to the experimental conditions.

EFFICIENCY AT LOW OVERVOLTAGE

Because it has been generally believed that the efficiency of G-M counters is low near the starting voltage,[6] and since the present experiments were carried out at relatively low overvoltages, a measurement

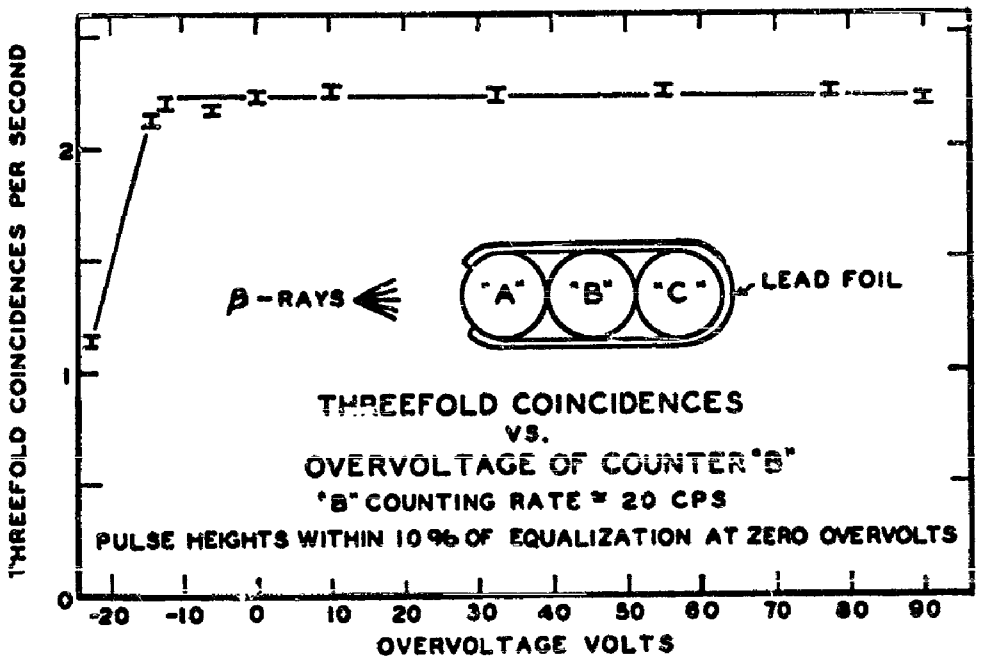

FIG. 6.—Relative efficiency of counter *vs.* overvoltage.

of the relative efficiency of the counter as a function of overvoltage was made in a triple coincidence arrangement. The results shown in Fig. 6 indicate no loss of efficiency at the voltages used in these experiments.

COUNTER DESCRIPTIONS

While most of the work reported here was done with tubes 20 cm. long and 1 cm. in diameter, studies included the use of counters varying

[5] This value of σ calculated from the experimental observations is too large. The reason for this is that the first source was very near to the counter, saturating that portion immediately adjacent to it and decreasing the effective length of the counter for counting the radiations from the remaining sources which were placed at successively greater distances.

[6] The ambiguities associated with the definition of starting voltage in self-quenching mixtures are now under investigation.

in length from 8 to 40 cm. and in diameter from 0.9 cm. to 3 cm., all equipped with central wires 0.003 in. in diameter. Cylinders were either of copper 0.005 in. thick, or, where thin walls were desired, of Aquadag painted internally on glass walls of thickness 0.006 in. Thin windows were provided for the transmission of light where single centered discharges were essential. Gas mixtures were either argon-ether (6.5:1) at 5.5 cm. Hg pressure or argon-butane (6:1) at 8.5 cm. Hg pressure. The circuit operated effectively with all of the above counters without alteration.

SUMMARY

A two tube feed-back circuit, triggered about 10^{-8} seconds after the initiation of the discharge, interrupts the spreading process in a few hundredths of a microsecond by field reduction at the wire. The control circuit recovers, restoring normal operating field conditions except over a small segment near the point where the discharge started. Thus in about a microsecond most of the counter is resensitized, resulting in a very short dead-time. The voltage pulse on the wire, although triggered by the initial counter current, has a shape determined predominately by the parameters of the cut-off circuit and hence all pulses are equalized.

Since the circuit limits the spreading of discharge, the number of ion pairs formed in a discharge is decreased, consequently the life of the counter is greatly increased (9). Life is further increased by operating at low overvoltages for a similar reason. It should also be remembered that the velocity of propagation of discharge along the counter wire increases with overvoltage and hence a faster operating circuit capable of giving a larger reduction of field at the wire of the counter would be required if higher overvoltages are desired. However, efficiency measurements indicate that little is to be gained at higher overvoltage.

The single and multiple center effects observed suggest that with simple additional circuitry a counter may be rendered a directional radiation detector, and may also become capable of discriminating between various types of radiation.

Rates up to 200,000 counts per second with uniform pulse output have been achieved.

Acknowledgment

It is a pleasure to thank Dr. W. F. G. Swann, Director of the Bartol Research Foundation, Dr. G. W. McClure and Dr. C. E. Mandeville for their aid and assistance throughout this investigation.

REFERENCES

(1) J. A. SIMPSON, JR., "Reduction of the Natural Insensitive Time in G-M Counters," *Phys. Rev.*, Vol. 66, p. 39 (1944).
(2) A. L. HODSON, "Reduction of 'Insensitive Time' in Geiger-Muller Counters," *J. Sci. Inst.*, Vol. 25, p. 11 (1948).
(3) P. B. SMITH, "Dead-Time Reduction in Self-Quenching Counters," *Rev. Sci. Inst.*, Vol. 19, p. 453 (1948).
(4) B. COLLINGE, "Dead-Times of Self-Quenching Counters," *Proc. Phys. Soc. London*, Vol. 63B, p. 15 (1950).
(5) H. DEN HARTOG AND F. A. MULLER, "Dead-Time Theory and Technique," *Physica*, Vol. XVI, p. 17 (1950).
(6) G. G. KELLEY, W. H. JORDAN AND P. R. BELL, "Electron Component in Geiger Discharge," *Rev. Sci. Inst.*, Vol. 21, p. 330, (1950).
(7) W. E. RAMSEY, "Current Time Relationships for Single and Multiple Centered Geiger Counter Pulses," *Phys. Rev.*, Vol. 83, p. 242 (1951).
(8) H. G. STEVER, "The Discharge Mechanism of Fast G-M Counters from the Deadtime Experiment," *Phys. Rev.*, Vol. 61, p. 38 (1942).
(9) H. ELLIOT, "The Effect of External Quenching on the Life of Argon-Alcohol Counters," *Proc. Phys. Soc. London*, Vol. 62, p. 369 (1949).

Reprinted from THE PHYSICAL REVIEW, Vol. 86, No. 5, 813, June 1, 1952
Printed in U. S. A.

Radiations from Nb^{97}†

C. E. MANDEVILLE, E. SHAPIRO, R. I. MENDENHALL, E. R. ZUCKER,* AND G. L. CONKLIN
Bartol Research Foundation of the Franklin Institute, Swarthmore, Pennsylvania
(Received January 14, 1952)

THE properties of the 17-hr Zr^{97} and of its daughter element, the 70-minute Nb^{97}, have been the subject of considerable investigation.[1–5] Spectrometric measurements[5] have yielded beta-ray energies of 1.91±0.02 Mev and 1.267±0.02 Mev, and gamma-ray energies of 0.747±0.005 Mev for Zr^{97} and 0.665±0.005 Mev for Nb^{97}. The gamma-ray at 0.747±0.005 Mev was shown to be emitted from an isomeric level in Nb^{97} of half-period 60 sec.

In the present investigation $Zr^{96}O_2$ (isotopic concentration 90 percent in Zr^{96}), obtained from the *Y*-12 plant, Carbide and Carbon Chemicals Division, Union Carbide and Carbon Corporation, Oak Ridge, Tennessee, was irradiated by slow neutrons in the Oak Ridge pile. The radioactive materials were received within twenty-four hours after cessation of irradiation and chemical separations were immediately commenced. The slow neutron irradiated zirconium dioxide was dissolved by potassium pyrosulfate fusion, and the separation of the niobium daughter activity from zirconium was effected by the use of Steinberg's "oxalate" procedure.[6]

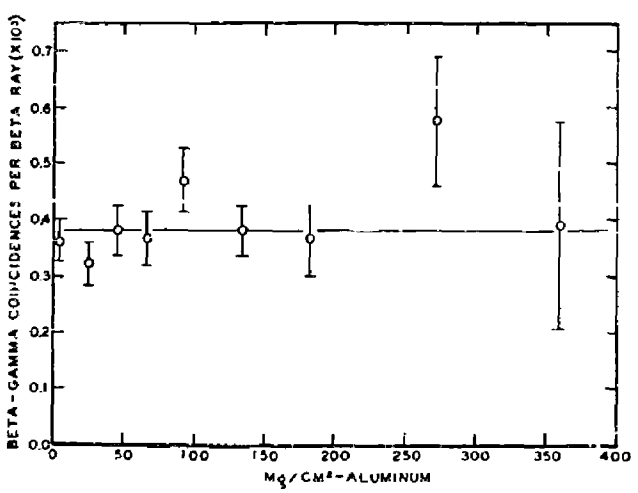

FIG. 1. Beta-gamma coincidence rate of Nb^{97} as a function of the surface density of aluminum placed before the beta-ray counter.

The decay of Nb^{97}, freshly separated from its parent element, was followed for ten half-periods, and the half-period, taken from the slope of the decay curve was found to be 72.1±0.7 minutes. This value is to be compared with previously reported values of 68 minutes[7] and 75 minutes.[8] The decay of Zr^{97} was followed for 200 hours, and the resulting half-period was calculated to be 17.0±0.2 hours, in agreement with the earlier measurements.

The beta-rays of Nb^{97}, freshly separated from its parent element, were absorbed in aluminum, and a Feather[8] plot of the data gave a maximum beta-ray energy of 1.40 Mev.

The beta-gamma coincidence rate of the 72-minute Nb^{97} is shown as a function of absorber thickness before the beta-ray counter in Fig. 1. It is seen to be constant, independent of the beta-ray energy, suggesting that the beta-ray spectrum of Nb^{97} is simple. Calibration of the beta-gamma coincidence counting arrangement by the beta-gamma coincidence rate of Sc^{46} showed that each beta-ray of Nb^{97} is followed, on the average, by 0.7 Mev of gamma-ray energy. Each point of Fig. 1 was, of course, properly corrected for decay of the source.

† Assisted by the joint program of the ONR and AEC.
* Frankford Arsenal, Philadelphia, Pennsylvania.
[1] Sagane, Kojima, Mijamoto, and Ikawa, Phys. Rev. 57, 1179 (1940).
[2] A. V. Grosse and E. T. Booth, Phys. Rev. 57, 664 (1940).
[3] S. Katcoff and B. Finkle, *Radiochemical Studies: The Fission Products* (McGraw-Hill Book Company, Inc., New York, 1951), Paper No. 83, National Nuclear Energy Series, Plutonium Project Record, Vol. 9, Div. IV.
[4] O. Hahn and F. Strassman, Naturwiss. 29, 285 (1941).
[5] Burgus, Knight, and Prestwood, Phys. Rev. 79, 104 (1950).
[6] E. P. Steinberg, *Radiochemical Studies: The Fission Products* (McGraw-Hill Book Company, Inc., New York, 1951), Paper No. 243, National Nuclear Energy Series, Plutonium Project Record, Vol. 9, Div. IV.
[7] G. E. Boyd, communication to G. T. Seaborg and I. Perlman, Revs. Modern Phys. 20, 585 (1948).
[8] N. Feather, Proc. Cambridge Phil. Soc. 30, 599 (1938).

Reprinted from THE PHYSICAL REVIEW, Vol. 86, No. 4, 536-545, May 15, 1952
Printed in U. S. A.

The Primary Cosmic Radiation at High Latitudes*

MARTIN A. POMERANTZ AND GORDON W. MCCLURE
Bartol Research Foundation of the Franklin Institute, Swarthmore, Pennsylvania
(Received December 14, 1951)

Various properties of the new group of low energy primary cosmic-ray particles ($E<1.6$ Bev for protons) which enter the top of the atmosphere at geomagnetic latitudes north of 52° were investigated during the summer of 1950. Measurements at both 52°N (Swarthmore, Pennsylvania) and 69°N (Fort Churchill, Manitoba) were obtained with the same quadruple-coincidence counter trains used previously, oriented either horizontally or vertically, and with pulsed ionization chambers biased to detect bursts exceeding 1.0 Po-α.

No diurnal or temporal variations in the cosmic-ray intensity were detected, and no change between 1949 and 1950 was indicated.

Flights were conducted with counter trains containing various thicknesses of interposed Pb absorber.

In contrast with the 46 percent increase in the vertical intensity between the two stations, no latitude effect was revealed either in the flux of cosmic rays traveling in the horizontal direction or in the frequency of bursts detected by the ionization chambers, at the highest altitudes attained (~9 mm of Hg).

The data permit conclusions to be drawn regarding the horizontal component, the solar dipole-moment, the nature of the low energy spectrum, as well as nuclear disintegrations and primary heavy nuclei.

I. INTRODUCTION

EXPERIMENTS which have revealed the presence in the primary cosmic radiation of particles having momenta below that required for entrance at geomagnetic latitude 50°N have been described previously.[1] The original conclusions were based upon a direct comparison, by identical instruments, of the vertical cosmic-ray intensity near the "top of the atmosphere" at Fort Churchill, Manitoba (geomagnetic latitude 69°N), during the summer of 1949 with that at Swarthmore, Pa. (geomagnetic latitude 52°N).

After it had thus been established that a new group of particles was reaching the earth north of the previously-assumed knee of the latitude effect which had heretofore been attributed to a cut off imposed by the magnetic field of the sun, it was of interest further to investigate certain other features of these particles. In particular, it was considered desirable:

(a) to determine whether any change of conditions such as might be produced by a variable solar magnetic dipole-moment had occurred subsequent to the initial observations;

(b) to conduct additional attempts to detect either diurnal variations or short-time temporal variations (over a period of weeks);

(c) to obtain measurements of the intensity *vs* altitude curves with an interposed absorber of thickness intermediate between those utilized previously (4 cm of Pb);

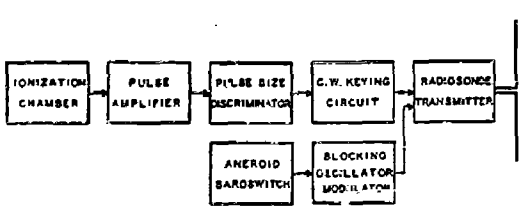

FIG. 1. Block diagram of circuits associated with ionization chamber.

(d) to compare the intensity in the horizontal direction at 69°N with that at 52°N in order to secure additional information regarding the nature of the new group of primary particles entering at the higher latitude;

(e) to observe the effect of the new low energy group of primaries upon the rate of bursts produced within the walls of an ionization chamber at high altitudes.

Under the sponsorship of the National Geographic Society, a second expedition to Fort Churchill, Manitoba, was therefore conducted during the summer of 1950. Two types of instruments, a burst-detecting ionization chamber and a quadruple coincidence counter train, were utilized to accomplish the aforementioned objectives.

II. EXPERIMENTAL PROCEDURE

A. Ionization Chamber Apparatus

A block diagram of the ionization chamber and associated circuitry is shown in Fig. 1. The instrument functions as follows: Voltage pulses produced in the ionization chamber (mainly by primary heavy nuclei and by nuclear disintegrations occurring in the chamber walls) are amplified by a linear pulse-amplifier and fed into a pulse-height discriminator. The latter permits the passage only of those pulses having amplitudes exceeding a predetermined size. Each discriminator output pulse triggers a keying univibrator, thereby causing the transmitter to emit a 75 megacycle C. W. signal for a period of 0.06 sec.

The telemetering system as well as the method for the determination of atmospheric pressure and temperature within the gondola during the balloon flights have already been described in detail elsewhere.[2]

The ionization chamber (Fig. 2) is composed essentially of an outer cylindrical pressure vessel, a concentric cylindrical cathode, and a central electron-collecting wire. The cathode, which operates at a potential of

* Assisted by the joint program of the ONR and AEC.
[1] M. A. Pomerantz, Phys. Rev. 77, 830 (1950).
[2] M. A. Pomerantz, Electronics 24, 88 (1951).

−300 v relative to the wire, is closed at the ends by copper guard disks having ½-inch center holes to pass the collector wire. The collector connects directly to the first grid of the linear amplifier and is maintained at dc ground potential by means of a 10^8-ohm grid-leak resistance. To eliminate the possibility of leakage from the high voltage cathode to the collector wire, the insulators supporting the wire are mounted on the grounded outer case.

In all measurements made to date, the chambers have been filled with 5 atmospheres of tank argon rated 99.9 percent pure. Before assembly, the internal parts are cleaned with an acid rinse, and immediately after the soldering operation, the chambers are evacuated for 24 hours while being maintained by an oven at a temperature of 125°C. The outgassing and filling procedures are accomplished on a special pressure-vacuum system, which permits both operations to be performed without the intervening admission of air into the chamber. A pressure gauge mounted permanently on each ion chamber permits the detection of leaks which might develop subsequent to sealing-off the unit.

For the purpose of calibration, each chamber contains a Po-α source plated onto an insulated silver electrode. The source protrudes slightly through a hole in the cathode and is "turned on or off" by connecting the probe to the cathode supply (−300 v) or to ground, respectively. In the "off" state, the α-particle ionization electrons are collected on the grounded source probe and are thus not permitted to reach the central wire.

The Po-α pulses reach voltage saturation at a cathode potential of −200 v immediately after a chamber is filled. However, the saturation voltage drops to an equilibrium value some 50 volts lower in the course of a few days. This tendency, which is probably caused by the "getter" action of the clean copper walls, insures that the normal operating potential of −300 v is adequate for saturation even long after the chambers are filled. The calibration source is used only for setting the discriminator and checking the over-all stability of the instrument in preflight tests. During flight the source is turned off so as not to interfere with the detection of cosmic-ray bursts. In the case of every instrument which has been recovered immediately after landing, postflight checks have revealed no detectable change in calibration.

The linear amplifier comprises three stages of amplification with 0.015 percent inverse feedback and has an over-all gain of 5×10^3. This amount of feedback, although not large, is sufficient to reduce to 2 percent the change in amplifier gain resulting from battery voltage drops during the normal (five hour) flight duration. The interstage coupling components of the amplifier are chosen to give a rise time (5 μsec) comparable to the electron collection time of the ionization chamber, and a decay time (100 μsec) sufficiently small that the inductive effect of positive ion motion is not amplified. Through careful selection of vacuum tubes, the amplifier output noise level is approximately 0.2 v, which is 5 percent of the amplitude of the smallest pulses allowed past the discriminator in the measurements reported here.

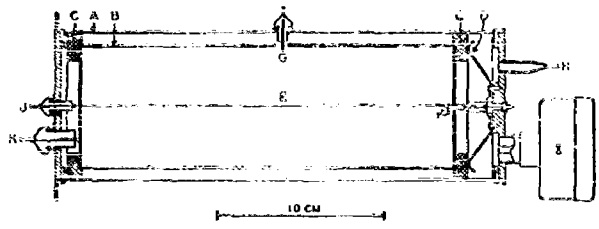

FIG. 2. Constructional details of ionization chamber. **A**, pressure vessel (0.032-in. Cu); **B**, cathode (0.032-in. Cu); **C**, cathode insulating rings (Mykroy); **D**, retaining spring; **E**, electron collector (0.010-in. Kovar); **F**, glass insulator; **G**, Po-α source electrode; **H**, pinch seal; **I**, 0–100 lb/in.^{2} pressure gauge; **J**, connection to amplifier; **K**, −300 v cathode connection.

The discriminator stage is a triode biased beyond cut off by a variable potentiometer adjustment. The (positive) amplifier output pulses reach the discriminator plate circuit (and thence trigger the subsequent keying univibrator) only when their amplitudes exceed the difference between the negative bias potential and the triode cut off potential. For all of the flights reported in the present paper, the discriminator was adjusted so that only bursts >1.0 Po-α were relayed to the ground station.

B. Quadrupole Coincidence Counter Train

The counter trains utilized in measurements of the intensity both in the vertical and horizontal directions were identical with those used in 1949[1] and previously.[3] The complete balloon-borne apparatus, as well as the ground receiving station, have also been described in detail.[2]

III. RESULTS

A. Search for Diurnal and Temporal Variations

The detection of a small diurnal variation had not been specifically attempted in 1949, although the data obtained in flights conducted at different times of the day revealed no indication of any marked differences which could be attributed to a diurnal effect. If the sun possesses a permanent dipole-moment of the magnitude which had previously been assumed, a diurnal variation of the intensity of the primary cosmic radiation must necessarily occur, for reasons which have already been discussed.[1] Observations conducted at a high northern latitude are optimum from the point of view of the magnitude of the change expected during the course of a day, since the variation is maximum at locations appreciably north of the previously-assumed knee of the latitude effect. Furthermore, the extreme change expected at high latitudes occurs during daylight hours,

[3] For details regarding geometry, see M. A. Pomerantz, Phys Rev. 75, 1721 (1949).

TABLE I. Summary of balloon flights.

Geomag. lat.	Flight date	Instrumental arrangement	Ceiling altitude, feet	Time of arrival at ceiling altitude, local solar time
69°N	8- 6-49	Vertical counter train containing 7.5 cm of interposed Pb absorber.	96,000	10:32 A.M.
	8- 9-49		85,500	8:40 A.M.
	8-11-49		74,000	4:24 P.M.
	8-16-49		81,000	10:17 A.M.
	8-21-49		73,500	10:13 A.M.
	7-24-50		67,000	8:31 A.M.
	7-25-50		100,500	9:07 A.M.
	7-26-50		76,000	10:18 A.M.
	7-31-50		74,800	9:04 A.M.
	8- 5-50		84,500	1:37 P.M.
	8-12-50		97,000	12:43 P.M.
52°N	7-26-47		89,000	6:39 A.M.
	7-20-49		83,000	8:33 A.M.
	9-27-49		112,000	10:52 A.M.
	5-25-50		94,000	8:52 A.M.
69°N	8- 2-50	Vertical counter train containing 4.0 cm of interposed Pb absorber.	91,000	8:17 A.M.
	8- 5-50		81,800	8:15 A.M.
	8-29-50		74,500	4:16 P.M.
	8-30-50		100,000	9:43 A.M.
52°N	6-24-48		95,000	8:24 A.M.
	10- 6-49		68,000	10:26 A.M.
	10-14-49		81,500	10:33 A.M.
69°N	8-18-50	Horizontal counter train containing no interposed Pb absorber.	80,000	6:14 P.M.
	8-19-50		97,000	2:28 P.M.
	8-24-50		83,000	10:00 A.M.
52°N	7- 7-50		105,000	9:37 A.M.
	10-17-50		102,200	10:43 A.M.
	10-27-50		104,200	11:13 A.M.
	11- 7-50		108,000	3:22 P.M.
52°N	7- 9-48	Horizontal counter train containing 1.0 cm of interposed Pb absorber.	109,500	9:51 A.M.
	10- 7-48		109,000	11:18 A.M.
	10-28-49		117,500	11:02 A.M.
69°N	8- 9-50	Horizontal counter train containing 7.5 cm of interposed Pb absorber.	83,000	9:26 A.M.
	8-16-50		72,500	10:25 A.M.
	8-18-50		87,500	9:14 A.M.
	8-29-50		85,400	9:29 A.M.
52°N	7- 7-48		104,000	8:24 A.M.
	10-29-48		102,000	11:03 A.M.
	11-23-48		115,000	10:59 A.M.
69°N	9- 2-50	Ionization chamber biased to record events exceeding 1 Po-α.	78,500	6:01 P.M.
	9- 3-50		91,500	4:59 P.M.
	9- 4-50		110,500	10:46 A.M.
52°N	4-30-50		83,000	9:50 A.M.
	6- 2-50		103,500	9:00 A.M.
	6- 9-50		94,000	8:25 A.M.
	3- 7-51		80,000	12:35 P.M.

to which the present flights were necessarily confined owing to technical limitations imposed by the absence of heating by solar radiation at night. Finally, and most important of all, the intensity at the higher latitude should actually be lower than that at Swarthmore in the early morning, and equal in the late afternoon, according to Dwight's calculations.[4]

Therefore, the flights in 1950 were released over a wider range of times to broaden the scope of this important phase of the investigation. For reasons cited earlier,[1] measurements were obtained principally with counter trains containing 7.5 cm of interposed lead absorber. Table I contains a summary of the 1950 series at Fort Churchill, and as may be seen in Figs. 3 and 4, there is no detectable dependence of the results upon the time of day.

Furthermore, it is apparent in Fig. 3 that the present measurements have quantitatively confirmed the earlier data, thus indicating no observable difference in the conditions existing during the summers of 1949 and 1950. Finally, it is to be noted that, during the course of continuous observations extending over a period of more than a month, no changes sufficient to be detected by the instruments utilized in these investigations are manifested.

B. Intensity *vs* Altitude Curve with 4 cm Pb

The nature of the dependence of the intensity upon altitude at 69°N in the case of particles capable of penetrating 4 cm of Pb is of particular interest. The fact that a definite maximum in the curve is observed at 52°N for 4 cm but not 6 cm provided a basis for the prediction that the maximum with 4 cm would disappear at the higher latitude. Low energy primaries, such as were presumably entering at Fort Churchill, were expected, through their progeny, to contribute appreciably to the intensity only near the top of the atmosphere.

This hypothesis is supported by the results plotted in Fig. 4. It is observed that, at Fort Churchill, the intensity of particles having a residual range of 4 cm of Pb is essentially constant throughout the upper seven percent of the atmosphere.

This latitude dependence of the critical thickness of interposed absorber for which the maximum in the intensity *vs* altitude curve disappears, arising from the change in the minimum allowed primary energy, would result in the appearance of a maximum at low latitudes even for thick absorbers. Thus, Rao *et al.*,[4a] at 3°N, have observed a distinct peak in the vertical intensity of cosmic radiation penetrating 10 cm of Pb, at a pressure of 90 mm of Hg. This is entirely in accord with expectations on the basis of the present considerations. Furthermore, as a consequence of this effect, the atmospheric pressure at which the maximum occurs for any particular amount of absorber would increase as the latitude is decreased.

C. Intensity in the Horizontal Direction

Investigations[6-7] of the cosmic-ray intensity at various zenith angles have revealed an appreciable

[4] K. Dwight, Phys. Rev. 78, 40 (1950).

[4a] Rao, Balasubrahmanyam, Gokhale, and Pereira, Phys. Rev. 83, 173 (1951).

[6] Swann, Locher, and Danforth, Natl. Geographic Soc. Contributed Tech. Papers, Stratosphere Series 2, 13 (1936).

[6] M. A. Pomerantz, Phys. Rev. 75, 1335 (1948).

[7] Winckler, Stroud, and Shanley, Phys. Rev. 76, 1012 (1949).

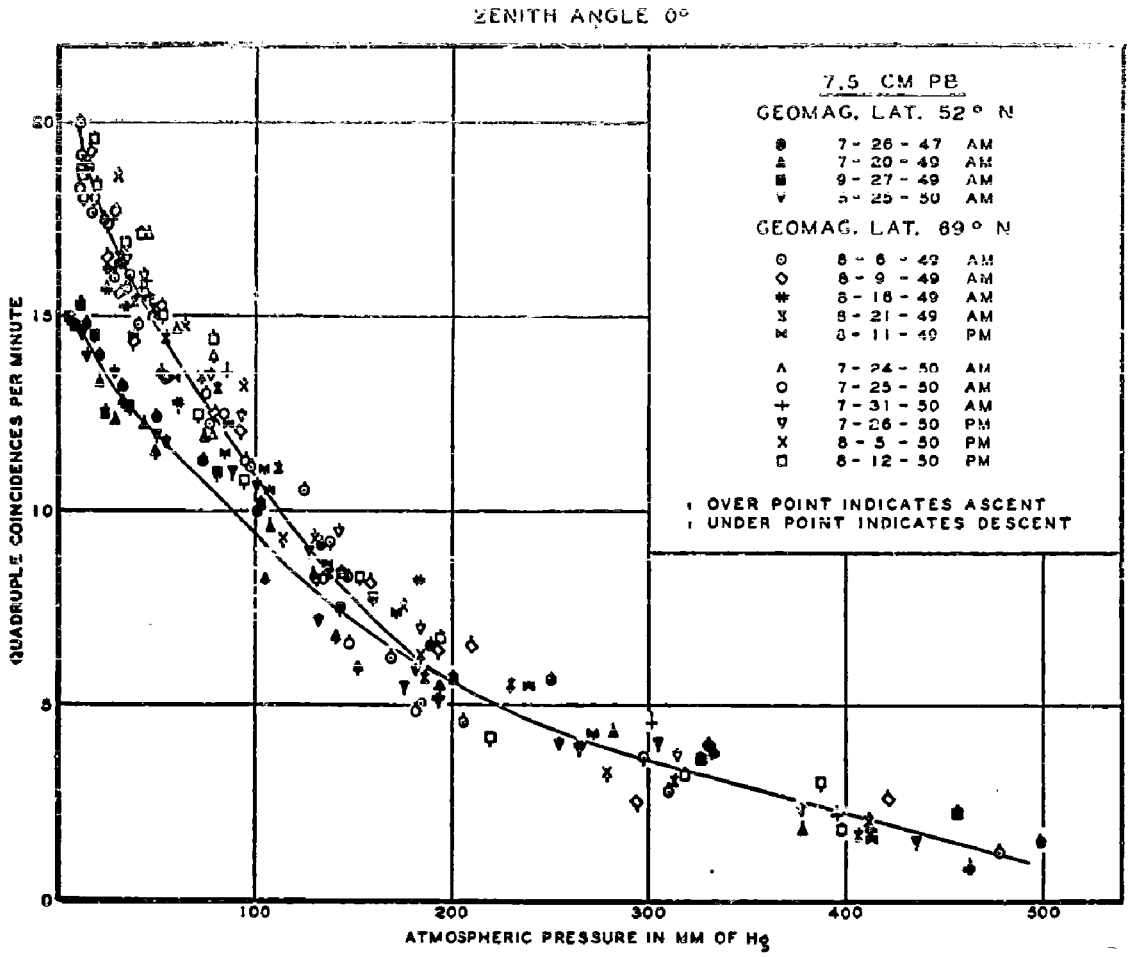

FIG. 3. Intensity *vs* altitude curves for cosmic rays arriving vertically, and penetrating 7.5 cm of Pb at $\lambda = 52°$N (Swarthmore, Pennsylvania) and $\lambda = 69°$N (Fort Churchill, Manitoba). Note the absence of detectable diurnal or temporal variations.

component at large angles. The observed horizontal intensity at very high altitudes appreciably exceeds that at the terminus of a corresponding effective atmospheric path in the vertical direction, and must consist predominantly of secondary particles emitted in acts in which the initial direction is not propagated. It was of interest to ascertain whether the new group of low energy primary particles entering at Fort Churchill would enhance the horizontal intensity at that station. Therefore, a direct comparison of the horizontal intensities at the two latitudes was conducted.

The measurements were obtained with the same counter trains used in the other phases of these experiments. When the instruments are oriented horizontally, the maximum aperture between the extreme ray and the horizontal plane is 4.5°. Telescopic observations of the swinging of the instruments during flight revealed that the maximum excursion was usually less than 2° from the vertical even during the more turbulent initial portions of the ascent.

In some of the flights, a 7.5 cm Pb absorber was interposed in the counter train. In others, no absorber was present other than the counter walls. In this case all particles capable of penetrating 4.4 g/cm² were detected. This corresponds to a minimum energy for mesons of approximately 20 Mev.

A detailed statistical analysis of flights under the latter condition is summarized in Table II. These

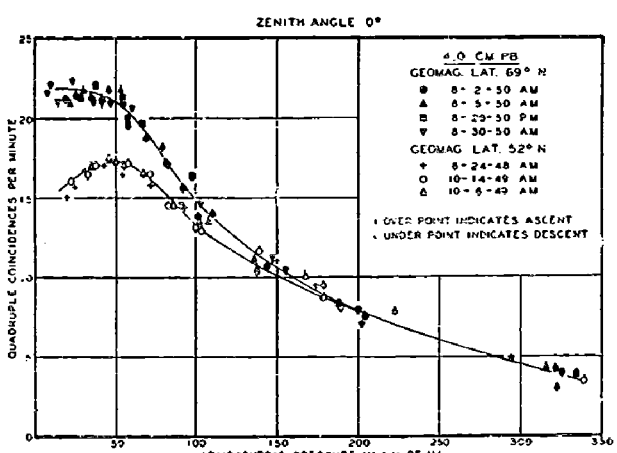

FIG. 4. Intensity *vs* altitude curves, obtained with concidence-counter trains containing 4 cm of Pb, for cosmic rays arriving vertically at $\lambda = 52°$N and $\lambda = 69°$N. The maximum disappears at the more northern station.

TABLE II. Summary of data obtained with horizontal quadruple-coincidence counter trains containing no interposed Pb absorber. Within the statistical uncertainties, no dependence upon latitude between 52°N and 69°N is indicated.

Geomag. lat.	Flight date	Average counting rates, counts per minute, in indicated pressure interval			
		54–33 mm of Hg	33–21 mm of Hg	21–13 mm of Hg	13–8 mm of Hg
69°N	8-18-50	19.3±0.8	25.4±1.1		
69°N	8-19-50	18.1±1.0	25.0±1.9	31.0±0.9	33.3±1.1
69°N	8-24-50	17.9±0.9	28.1±1.1		
69°N	Average	18.5±0.5	26.3±0.6	31.0±0.9	33.3±1.1
52°N	7- 7-50	17.7±1.1	25.8±1.1	29.5±1.0	
52°N	10-17-50	17.2±0.9	27.1±1.9	28.8±1.1	
52°N	10-27-50	18.0±0.8	23.1±1.2	29.7±1.2	32.1±1.0
52°N	11- 7-50	18.1±0.9	29.0±2.1	33.6±1.2	34.5±1.1
52°N	Average	17.8±0.5	25.7±0.7	30.9±0.6	32.5±0.6

experiments have indicated, as may be seen also in Fig. 5, that, unlike the situation in the vertical direction, even at the highest altitudes attained the horizontal intensity is not dependent upon latitude north of 52°.

Data obtained at 52°N with 1.0 cm of absorber are also included in Fig. 5 because these constitute a self-consistent set of measurements, with good resolution in zenith, of the intensity and the rate of absorption of the horizontal component of the cosmic radiation.

D. Ionization Chamber Bursts

The data obtained in four ionization chamber flights at Swarthmore, Pennsylvania (52°N geomagnetic latitude) and in three flights at Fort Churchill (69°N geomagnetic latitude) are plotted in Fig. 6. Statistical errors (not shown in the figure) are approximately ±10 percent for points near the top of the atmosphere and ±20 percent for the lower points. A statistical analysis of the data from the seven separate flights at the two locations (Table III) shows that all individual flights agree within statistical expectation. Similarly, the combined average counting rates of the Fort Churchill flights agree with the combined average rates obtained at Swarthmore. Within the statistical uncertainties indicated in Table III the burst rates at the two locations are the same at all altitudes.

IV. DISCUSSIONS

A. Horizontal Intensity

The maximum residual range in air of the new particles which enter the top of the atmosphere at 69°N is approximately 150 g/cm². This is indicated by the fact that, as is shown in Figs. 3 and 4, no observable difference in the intensity at the two locations arises until the atmospheric pressure is somewhat less than 120 mm of Hg.

The ratio of the minimum amount of matter which a particle would have traversed through the spherical atmosphere before entering the geometrical arrangement utilized in these experiments in the horizontal direction to that in the vertical is 12. Thus, on the basis of mass-absorption alone, it is evident that none of the particles in this new group, which must have energies below 1.6 Bev, could be expected to penetrate to a horizontal detecting device of the present dimensions at an altitude lower than that corresponding to a maximum pressure of 120/12=10 mm of Hg. In view of the fact that the particles observed at the greatest depths in the vertical direction may be mesons rather than primary nucleons, the effects of decay would make the situation even more drastic.

The particles which constitute the horizontal intensity are principally secondaries produced at wide angles from the forward direction by primaries moving essentially downward through the atmosphere. This is immediately evident from the comparison of the counting rates recorded at high altitudes in the horizontal direction with those predicted on the basis of measurements obtained with an identical instrument oriented vertically. The expected counting rate $I_H(p_0)$ of a horizontal train at pressure p_0 can be computed on the basis of the assumption that the contribution at angle ζ is $I_\zeta(p_0)=I_0(p_0 f_\zeta)$, where f_ζ would be $\sec\zeta$ for a flat atmosphere of infinite extent. $I_0(p_0 f_\zeta)$ is obtained from the corresponding vertical intensity *vs* altitude

TABLE III. Summary of data obtained with ionization chambers biased to record pulse of height exceeding 1 Po-α. Within the statistical uncertainties, no dependence upon latitude between 52°N and 69°N is indicated.

Geomag. lat.	Flight date	Average counting rates, counts per minute, in indicated pressure interval						
		200–87 mm of Hg	87–54 mm of Hg	54–33 mm of Hg	33–21 mm of Hg	21–13 mm of Hg	13–8 mm of Hg	8–5 mm of Hg
69°N	9- 2-50	4.9±0.5	6.5±0.5	10.0±0.7	12.8±0.5			
69°N	9- 3-50	4.0±0.7	7.3±0.9	8.1±0.8	12.6±0.8	17.1±0.8		
69°N	9- 4-50	3.5±0.4	7.3±0.5	11.2±0.6		15.6±0.6	19.1±0.6	21.2±0.8
69°N	Average	4.1±0.3	7.0±0.3	10.2±0.4	12.7±0.4	16.3±0.5	19.1±0.6	21.2±0.8
52°N	4-30-50	5.0±0.3	6.8±0.6	10.0±0.6		17.0±1.0		
52°N	6- 2-50	4.5±0.3	8.5±0.7	10.4±0.7	13.1±1.0	15.6±0.8	19.0±0.8	20.8±1.4
52°N	6- 9-50	5.2±0.3	7.2±0.5	10.7±0.7	13.8±0.9	15.8±0.8	19.5±1.3	
52°N	3- 7-51	5.6±0.4	9.1±0.6	12.4±0.8	13.2±1.2			
52°N	Average	5.0±0.2	8.0±0.3	10.8±0.4	13.4±0.6	16.0±0.5	19.2±0.7	20.8±1.4

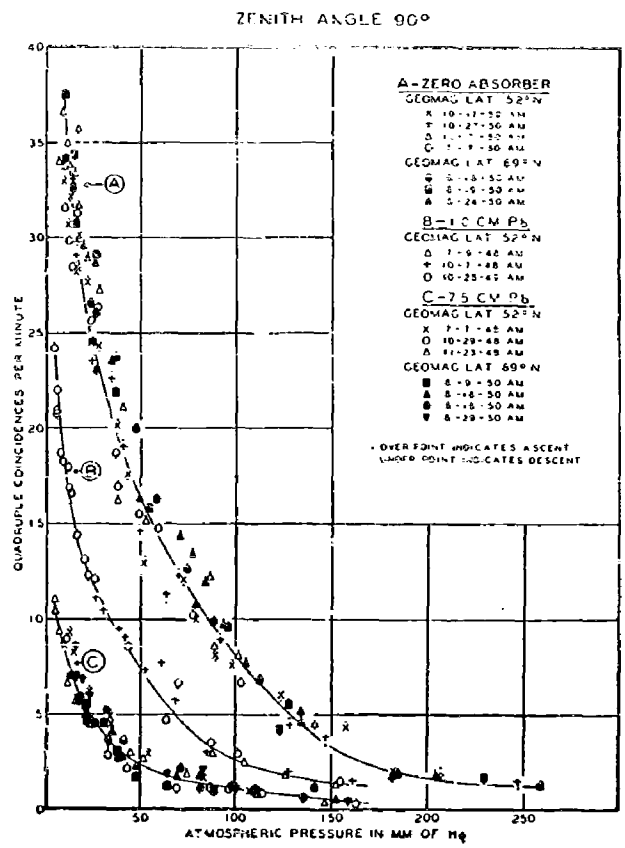

FIG. 5. Data obtained with counter trains oriented horizontally. No dependence upon latitude north of $\lambda = 52°$ is indicated.

curve. In the case of a spherical atmosphere, although $\int_t$ remains finite at 90°, the calculated counting rates are far less than the observed even if the attenuation introduced by meson decay is not taken into consideration. For example, at $p_0 = 30$ mm of Hg, the maximum expected counting rate with the geometry utilized in these experiments is 2 counts per minute as compared with 24 counts per minute observed with no interposed absorber. Meson decay should reduce this expected rate by a factor of at least 1000, depending upon the assumptions made regarding the production of mesons. This general situation (becoming even more drastic at lower altitudes), prevails for all thicknesses of absorber for which data are available up to the highest altitudes attained, although the disparity between the expected and observed intensities with 7.5 cm of Pb is considerably reduced at 5 mm of Hg. Thus, the horizontal intensity is far in excess of that expected for rectilinear propagation of an isotropic primary beam incident at the top of the atmosphere.

It might have been expected that low energy primaries would be most productive of wide-angle events, principally through the formation of low energy mesons. Furthermore, the spectrum is richest at the low end, and intensity considerations seemed to favor the primaries having energies near the geomagnetic cutoff at 52°N as the source of the horizontal component.

The absence of an increase in the horizontal intensity

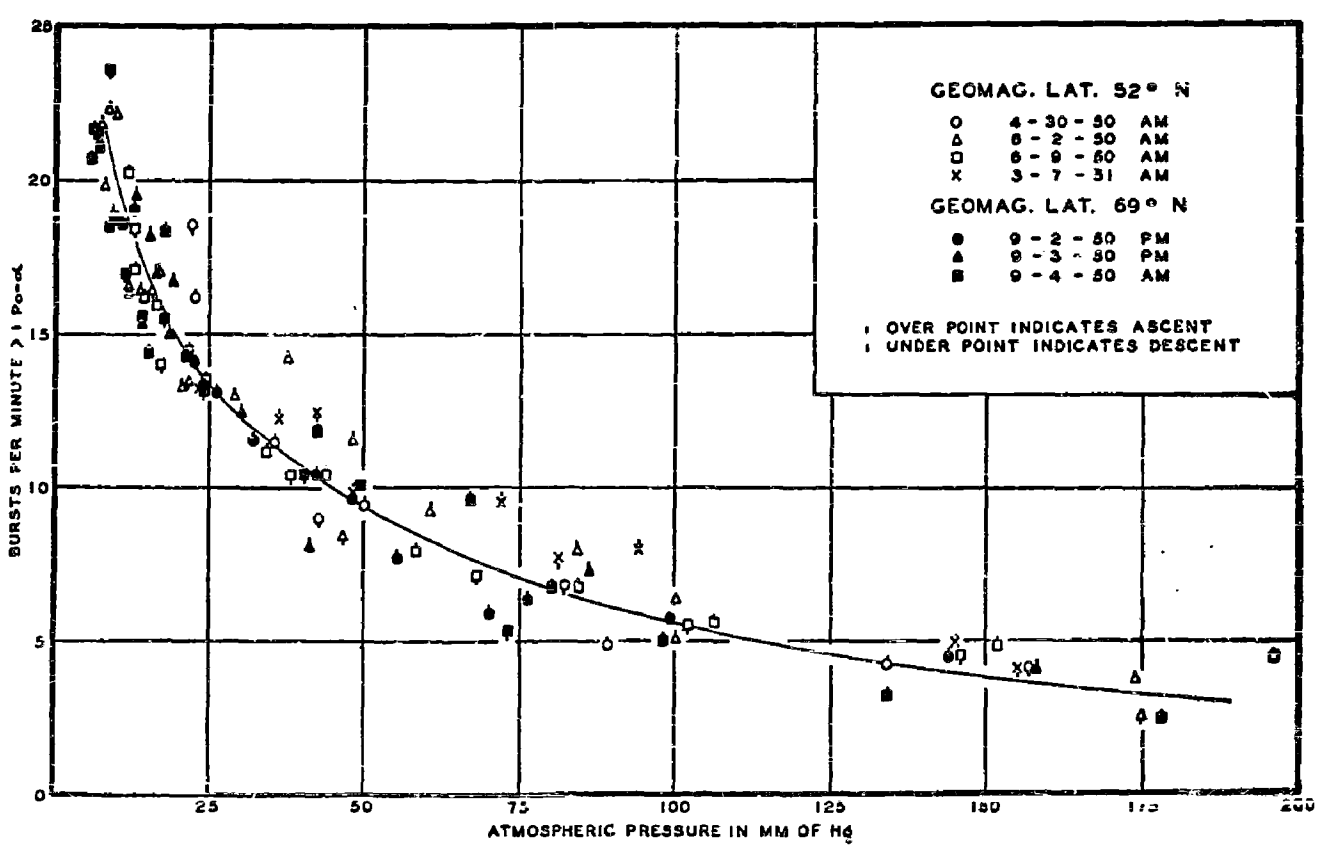

FIG. 6. Dependence of burst-rate upon altitude, as measured by ionization chambers biased to record events > 1.0 Po-α. No variation with latitude north of $\lambda = 52°$ is revealed.

at the highest altitude attained, corresponding to about 9 mm of Hg, is not consistent with this hypothesis. On the contrary, the results indicate that the secondary particles which constitute the horizontal component do not arise from primaries having energies near the minimum permitted at 52°N. Hence, they must be the progeny of the less numerous high energy primaries. The latter are particularly effective in contributing to the counting rate of a counter train inclined at a zenith angle of 90° because the total flux of vertically-directed particles which can produce wide-angle secondaries capable of actuating the horizontal instrument is, of course, much larger than the total flux through the same counter train oriented vertically.

B. Solar Dipole-Moment

The original conclusion[8] that the maximum value of the solar dipole-moment does not exceed 6×10^{32} gauss-cm^3 remains unchanged. It must be emphasized that this deduction from the present experimental results presupposes an infinitely distant source for most of the cosmic radiation reaching the earth. The concept of a solar allowed-cone created at the earth by a permanent magnetic field of the sun certainly does not apply to particles produced at that body and proceeding more or less directly to the earth. Hence, if it had been independently demonstrated that the sun did possess a dipole-moment of the previously assigned magnitude during the period when these experiments were performed, the present results would have constituted direct evidence for a solar origin of a large fraction of the primary intensity. However, the most recent astrophysical determinations of the solar field by Thiessen[9] and von Klüber[10] using vastly improved methods have yielded values no higher than 1–2 gauss.

The observed isotropy of the high energy nonfield-sensitive radiation ($>10^{13}$ ev) reveals that the entire galaxy must be the source of such particles, as has been demonstrated by Cocconi.[11] On the other hand, the low energy portion of the spectrum ($<10^{10}$ ev) must have a local origin in order to avoid the necessity of traversing an excessive mass of matter, as a consequence of the action of the galactic magnetic field, during the journey through the galaxy to this planet. The isotropy of the total incoming radiation, as revealed by measurements of the zenith[6] and azimuthal distributions[7] at high altitudes as well as by the absence of a detectable diurnal variation as reported herewith, indicates that the particles of solar origin do not in general proceed directly from the sun to the earth Hence, after they are emitted from the sun, the particles must subsequently follow complicated trajectories as a consequence of which the intensity ultimately becomes isotropic. Thus, the primaries reaching the earth appear to arrive from a distant (virtual) source uniformly distributed about the earth.

This is evidently accomplished by interactions with magnetic fields within the solar system. The particles which are observed to come more or less directly from the sun,[12] in contrast with the isotropically-distributed radiation, can be consequently accounted for only by a tunneling through the trapping field resulting from a sort of degaussing effect produced by transient local magnetic fields, such as was first proposed by Forbush, Gill, and Vallarta.[13]

C. Low Energy Spectrum

General considerations relating to the determination of the nature of the primary spectral distribution from the present results were discussed in reference 1. The exact value of γ in a differential energy distribution law of the form $i(E)dE=kE^{-\gamma}dE$ cannot be deduced in the usual manner from the geomagnetic cut-off energies and the observed ratio of the intensities at the two latitudes in this case. At high latitudes, atmospheric absorption rather than the terrestrial magnetic field determines the minimum energy which a primary particle must possess in order to reach the detecting apparatus. This lower limit $\epsilon_n(l, \lambda)$, required by a primary particle (or its progeny) to penetrate the thickness l of atmosphere above the detecting apparatus plus the counter walls, cannot be assigned a precise value.

Winckler, *et al.*,[14] have determined from measurements at low latitudes that the value of γ is 1.9 for primary protons having energies between 4 and 14 Bev. If the power law with the same exponent still prevailed at latitudes north of 52°, the observed ratio of intensities $I_{69°}/I_{52°}=1.46$ would correspond to an absorption cut-off energy $\epsilon_n(l, 69°)$ of 1.1 Bev for primary protons at 69°N.

The maximum depth of penetration of particles having energies just below the geomagnetic cutoff at 52°N ($\approx$1.6 Bev) is approximately 150 g/cm^2 of air (see Sec. IVA). Previous absorption measurements[15] have also revealed that 1.6-Bev particles are first absorbed[16] by something like the same amount of lead. Furthermore, from the location of the sea-level knee of the latitude effect, it is known that approximately 3 Bev are required for penetration of 1000 g/cm^2 of air. Although the effective range is falling off faster than directly proportional to the energy, it is inconceivable that primaries having an energy of 1.1 Bev would have a range $l\leq20$ g/cm^2. In any event, after the particle

[8] M. A. Pomerantz and M. S. Vallarta, Phys. Rev 76, 1889 (1949).
[9] G. Thiessen (private communication).
[10] H. von Klüber, Proc. Roy. Ast. Soc. 111, 8 (1951).
[11] G. Cocconi, Phys. Rev. 83, 1193 (1951).
[12] M. A. Pomerantz, Phys. Rev. 81, 731 (1951).
[13] Forbush, Gill, and Vallarta, Revs. Modern Phys. 21, 44 (1949).
[14] Winckler, Stix, Dwight, and Sabin, Phys. Rev. 79, 656 (1950).
[15] M. A. Pomerantz, Phys. Rev. 83, 459 (1951).
[16] Absorption is defined here as the reduction below unity of the probability that each primary, or at least one of its progeny created in the lead, always has sufficient residual range and is propagated in the proper direction to actuate the coincidence train.

has been slowed down to a velocity such that nuclear interactions are relatively improbable and ionization becomes the predominant mode of energy degradation, the residual range appreciably exceeds this amount. For example, the experimentally observed range of 340-Mev protons is 70 g/cm² in carbon.[17]

It is, therefore, necessary to conclude that the power-law spectrum observed for the primaries of higher energies does not apply at the low end. In fact, the differential spectrum may exhibit a maximum even south of 52°, followed by a rapid decrease toward the low energies which are permitted north of this latitude. This would not be inconsistent with either Winckler's results[14] or with those of Van Allen and Singer.[18]

A spectrum of this shape, poor in the low energy portion, would be expected if the regions where cosmic rays are being produced on the sun were distributed statistically uniformly over the surface. The low energy particles could, in general, move off toward infinity only near the poles, owing to the presence of the one gauss field, and the contribution from the polar regions would be a small part of the total. On the other hand, high energy particles, if indeed any are produced, would not be subject to trapping fields and could move off to infinity. The observed spectrum would, therefore, result from a combination of effects involving both the production and acceleration processes and the solar geomagnetic effects.

D. Nuclear Disintegrations and Primary Heavy Nuclei

When biased as in the present experiments, the ionization chamber instrument responds to: (1) relativistic heavy nuclei of atomic number $Z>8$; (2) single slow protons and α-particles; (3) nuclear disintegrations produced in the walls by fast protons and neutrons; (4) air showers in which at least 60 electrons traverse the chamber.

Of the above-listed events, air showers probably contribute the least to the observed counting rates. Chambers similar to those used in the present investigation have been operated in twofold coincidence as detectors of dense showers at mountain altitudes.[19] The results indicate that only a few percent of the bursts at these heights are produced by electron showers. Furthermore, the measurements of Kraybill and Ovrebo[20] show an altitude increase in the frequency of showers which is considerably less rapid than the observed altitude increase in the rate of ion chamber bursts.

In photographic emulsions exposed at atmospheric depths of 10 and 16 g/cm² at $\lambda=55°$, Bradt and Peters[21] have measured the collision mean free paths of heavy nuclei as a function of atomic number Z, and have calculated that the primary intensity of nuclei of $Z\geq 6$ is 1.4×10^{-3}/cm²/sec/sterad. The computation takes into account the absorption by nuclear collisions, but neglects a small fraction of the primary flux which is stopped as a consequence of ionization loss before reaching the depth at which the plates were exposed. On the basis of the above primary intensity value, and the Z-spectrum obtained by the same authors, the ionization chamber used in the present experiments should record 30 heavy nucleus counts per minute at the top of the atmosphere. In arriving at this result, isotropic incidence was assumed, and full account was taken of the rather complicated geometry of the chamber.

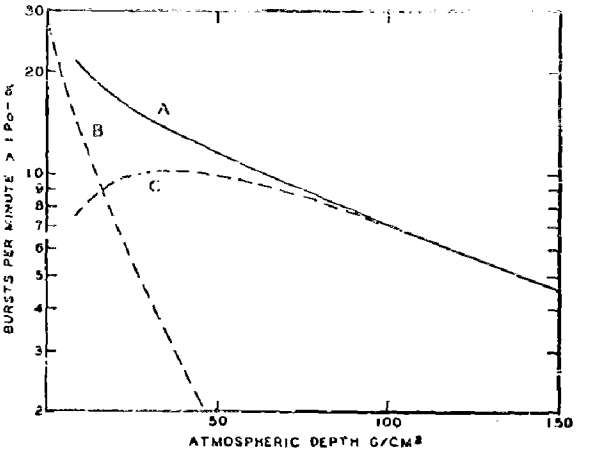

FIG. 7. Resolution of observed burst-rate, A, into the contributions by heavy primaries, B, and nuclear disintegrations, C.

If the emulsion observations[21] of the spectrum and the collision mean free paths of heavy nuclei are combined with a computation of the sensitivity of the ion chamber as a function of Z, the average collision mean free path in air for nuclei recorded by the chamber can be estimated as 30 g/cm². On the basis of this value for the absorption mean free path of the heavy primaries, and on the assumption of isotropic incidence above the atmosphere, the approximate heavy nucleus counting rate *vs* atmospheric depth curve labeled B in Fig. 7 is deduced. Inasmuch as the same absorption mean free paths used by Bradt and Peters in calculating the primary flux from observations at about 15 g/cm² were used in obtaining curve B, the counting rate given by the latter at 15 g/cm² is probably quite accurate. At atmospheric depths exceeding 15 g/cm² the computed curve may be somewhat high because of the neglect of ionization loss. However, this effect is partially compensated by the assumption of an absorption mean free path equal to the collision mean free path, although actually some of the heavy nuclei are not completely broken up into fragments too small to be counted by the ionization chamber in their first collision.

Curve C in Fig. 7 represents the difference between

[17] R. Mather and E. Segrè, Phys. Rev. 84, 191 (1951).
[18] J. A. Van Allen and S. F. Singer, Phys. Rev. 78, 818 (1950).
[19] C. G. Montgomery and D. D. Montgomery, Phys. Rev. 76, 1482 (1949).
[20] H. L. Kraybill and P. J. Ovrebo, Phys. Rev. 72, 351 (1947).
[21] H. L. Bradt and B. Peters, Phys. Rev. 77, 54 (1949).

the calculated heavy nucleus counting rate and the experimental curve A. Within the uncertainties in the heavy nucleus rates, curve C represents the variation with altitude of the total flux of protons, neutrons, and other particles capable of producing nuclear disintegrations in the chamber walls.

The maximum in curve C at a depth of 35 g/cm² is indicative of the cascade multiplication of the nucleonic component and agrees in position with the maximum obtained by Whyte[22] in the analysis of Coor's[23] burst data for $\lambda=52°$. Photographic emulsion studies of the development of the nucleonic cascade as manifested in the rate of star production *vs* atmospheric depth seem to conflict with one another regarding the existence of a maximum in the flux of star-producing particles. Freier *et al.*[24] report evidence of strong maxima below 45 g/cm² in the production rates of stars of all sizes up to and including those with more than 10 prongs. On the other hand, Lord[25] finds that the frequencies of stars of all sizes from 3 to more than 16 prongs decrease monotonically at atmospheric depths greater than 15 g/cm². The present results are qualitatively in accord with the former, whereas there appears to be a definite inconsistency with the latter which is not as yet understood.

The absorption mean free path of the burst-producing radiation as determined by the best exponential representation of the counting rate *vs* altitude curve between 60 and 200 mm of Hg is $L=165$ g/cm². This is in reasonable agreement with the value $L=160$ g/cm² derived from Coor's ionization chamber data in the same altitude range. In a similar manner, the star production *vs* altitude curves of Lord between 60 and 200 mm of Hg yield absorption mean free paths $L=165$, 120 and 110 g/cm² for the radiations producing stars with 3, 4, 5 prongs, 6, 7, 8, 9 prongs and more than 9 prongs, respectively. It seems reasonable to expect that the L value obtained from the ionization chamber results should lie somewhere within the above limits. However an exact comparison between ion chamber and emulsion data is precluded by inadequate knowledge of (1) the relative cross sections in Cu and emulsion for the production of stars of given size and (2) the burst-producing efficiency of stars as a function of size for the particular ion chamber geometry involved.

According to the emulsion work of Camerini, *et al.*[26] the integral cross section for production by neutrons and protons of stars with more than 2 prongs closely approximates the geometrical nuclear cross section. Assuming this to hold for primary cosmic rays incident upon copper, and using the value 0.17 particle/cm²/sec/sterad as the primary intensity[3] at $\lambda=52°$, we find that stars with more than 2 prongs should occur in the ion chamber walls at the rate of 240 per minute at the top of the atmosphere. Comparison of this rate with any reasonable extrapolation of curve C, Fig. 7, to zero g/cm² shows that at most 3 percent of the stars produced in the wall by primaries give rise to bursts >1.0 Bev. Some knowledge of the extent to which this surprisingly small efficiency can be attributed to the absorption of low energy star fragments before their entry into the gas could be obtained by employing chambers with various wall thicknesses in future flights.

According to the curves B and C in Fig. 7, the heavy nuclei and nuclear disintegrations contribute 13 counts per minute and 8 counts per minute, respectively, at a depth of 10 g/cm² at geomagnetic latitude 52°N. The latitude effect between 52°N and 69°N at 10 g/cm² is 0±5 percent. Considering the extreme case of a possible 5 percent increase (1.0 std. dev.) assignable solely to heavy nuclei, the increase in the latter at 10 g/cm² would be 8 percent. On the other hand, if the heavy nucleus flux were assumed to be unchanged, the corresponding increase in the nuclear disintegration rate would be 13 percent.

Extrapolation of the curves of Figs. 3 and 4 to the top of the atmosphere yields a lower limit of 45 percent for the increase in the vertical primary intensity between $\lambda=52°$ and $\lambda=69°$. Comparison of this result with the aforementioned 0±13 percent latitude effect shows that primaries of energy below the geomagnetic cutoff at $\lambda=52°$ yield at a depth of 10 g/cm² less than one-third as many nuclear bursts per primary particle as the primaries entering at $\lambda=52°$.

It should be noted that the nuclear disintegration latitude effect deduced from the present measurements at 10 g/cm² does not necessarily apply at higher altitudes, for a considerable portion of the nuclear bursts at 10 g/cm² is produced by secondaries. (Note the shape of curve C, Fig. 7.) In addition, the primaries undergo some energy loss by ionization and nuclear collisions in the residual atmosphere. The magnitudes of these effects are undoubtedly quite different for the primary protons of energy $E>1.6$ Bev entering at $\lambda=52°$ and for those of energy $E<1.6$ Bev which comprise the additional proton intensity at $\lambda=69°$.

If the multiplicity of secondary nucleon production increases with the energy of the primary, and the probability of burst production in the chamber wall increases with the energy of the incident particles, a latitude effect should become apparent above 10 g/cm². In this case the low energy primaries at $\lambda=69°$ as they exist above the atmosphere could have a considerably higher burst-producing efficiency relative to the primaries at $\lambda=52°$ than the data at 10 g/cm² indicate.

It is not possible to deduce from the present measurements any quantitative information regarding the low energy portion of the heavy primary spectrum because a substantial fraction of the particles of atomic number $Z>8$ in the band of energies admitted between $\lambda=52°$

[22] G. N. Whyte, Phys. Rev. **82**, 204 (1951).
[23] T. Coor, Phys. Rev. **82**, 478 (1951).
[24] Freier, Ney, and Oppenheimer, Phys. Rev. **75**, 1451 (1949).
[25] J. J. Lord, Phys. Rev. **81**, 901 (1951).
[26] Camerini, Fowler, Lock, and Muirhead, Phil. Mag. **41**, 413 (1950).

and $\lambda = 69°$ (where the vertical cut-off energies are 0.57 Bev per nucleon and 0.025 Bev per nucleon, respectively) are absorbed as a result of energy loss by ionization in the 10 g/cm² residual atmosphere above the apparatus.

V. ACKNOWLEDGMENTS

The continued support of the National Geographic Society, sponsor of the Expeditions to Hudson Bay, and the constant encouragement of Dr. Lyman J. Briggs, Chairman of the Committee on Research, are gratefully acknowledged. Appreciation is expressed for the kind cooperation of the Canadian government, particularly to the Defence Research Board for making its facilities at Fort Churchill available; individual thanks are especially due Dr. Kenneth Fisher, Superintendent, and Mr. A. V. Hannam, Administrative Officer of Defence Research Northern Laboratories; and Mr. G. W. Rowley of D. R. B. Arctic Division. E. R. Swoffer provided valuable technical assistance. Finally, the authors are grateful to Dr. W. F. G. Swann for his constant interest in this work.

Reprinted from JOURNAL OF THE FRANKLIN INSTITUTE,
Vol. 253, No. 2, February, 1952
Printed in U. S. A.

RADIATIONS FROM RADIOACTIVE RHODIUM (105) *

BY

C. E. MANDEVILLE [1] AND E. SHAPIRO [1]

ABSTRACT

The characteristic radiations of the 36-hr. rhodium (105) have been investigated with the use of conventional absorption and coincidence methods. The beta rays were found to have a maximum energy of 0.55 Mev., and the gamma rays a quantum energy of ~0.3 Mev. The beta-gamma coincidence rate of Rh^{105} indicated that less than 8 per cent of the beta rays are coupled with the gamma ray.

INTRODUCTION

When ruthenium is irradiated by slow neutrons, two radioactive isotopes of ruthenium are formed, the 42-day Ru^{103} and the 4.5-hr. Ru^{105}. The 42-day activity decays to stable Rh^{103}, but the 4.5-hr. period forms as its daughter element, the 36-hr. Rh^{105} which in turn decays to stable Pd^{105}. The radiations of the 36-hr. Rh^{105} have been previously examined by several groups of investigators (1)[2], with the use of conventional absorption methods. Observations on the characteristic radiations of Rh^{105} were also reported upon briefly by the writers (2), who found a beta ray of energy ~0.6 Mev. and a gamma ray of energy ~0.3 Mev. Approximately the same beta ray energy had been previously reported by all the investigators of reference 1, and the gamma ray had been previously observed by Sullivan, Sleight, and Gladrow (1). Subsequent to all of the above-mentioned investigations, spectrometric and coincidence measurements were carried out on the radiations of Rh^{105} by Duffield and Langer (3), who accurately determined the beta ray energy as 0.570 ± 0.005 Mev., but who did not observe any gamma rays. Following the report by Duffield and Langer (3), the writers obtained a second source of Rh^{105} for further study. The results were essentially the same as those first obtained (2). The discussion which is to follow will concern itself with data resulting from observations on both sources.

PROCEDURE AND RESULTS

The 36-hr. rhodium (105) was grown from its 4.5-hr. ruthenium parent when metallic ruthenium was irradiated by slow neutrons in the Oak Ridge pile. For the first sample of rhodium, the time of irradiation was 24 hr. This time was reduced to 10 hr. when the second

* Assisted by the joint program of the ONR and the AEC.

[1] Bartol Research Foundation of The Franklin Institute, Swarthmore, Pa.

[2] The boldface numbers in parentheses refer to the references appended to this paper.

quantity of material was irradiated almost a year later. The same chemical procedure was employed in the case of both sources. The ruthenium target material was purified before exposure by distillation of RuO_4 from a perchloric-sulfuric acid solution of chemically pure $RuCl_3$. After irradiation in the pile, Ru was dissolved in a mixture of 10 parts conc. HCl, 1 part conc. HNO_3, at 160° C. Rhodium carrier was added to the Ru solution, and RuO_4 was distilled from a perchloric-sulfuric acid solution. Inactive $RuCl_3$ was added to the residue and another RuO_4 distillation effected. The residue in the distillation flask was diluted to 1 *M* in acid and treated while hot with magnesium

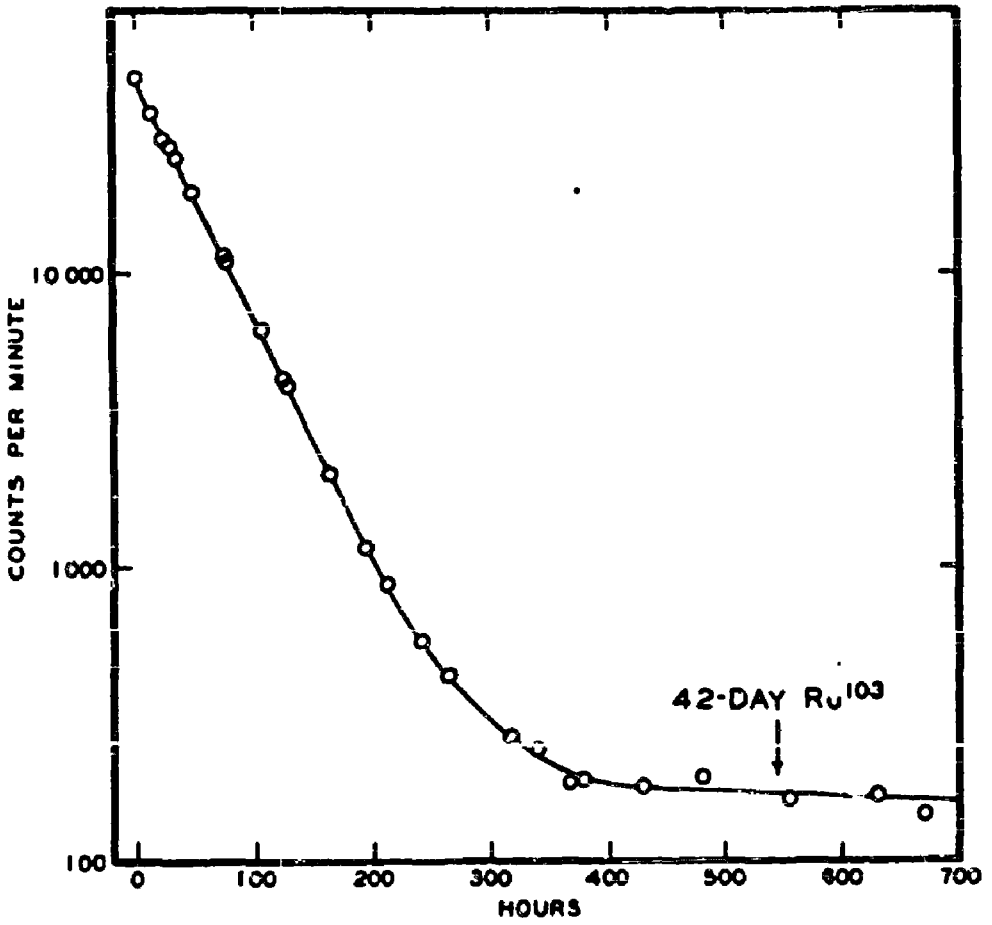

FIG. 1. Half-period of the total activity of Rh^{106}.

powder to precipitate rhodium. After dissolving excess magnesium in HCl, the suspension was filtered, the rhodium washed with HCl, hot water, alcohol, and ether, then dried.

The activity of the 36-hr. rhodium was followed for more than 300 hr. as shown in Fig. 1. The half-period taken from the slope of the curve was calculated to be 36.8 hr. A faint residual activity of long half-period is clearly present, and this is assigned to the presence of a trace of the 42-day Ru^{103}. This decay curve was considered as good evidence for high purity of the source. Using a thin source of the

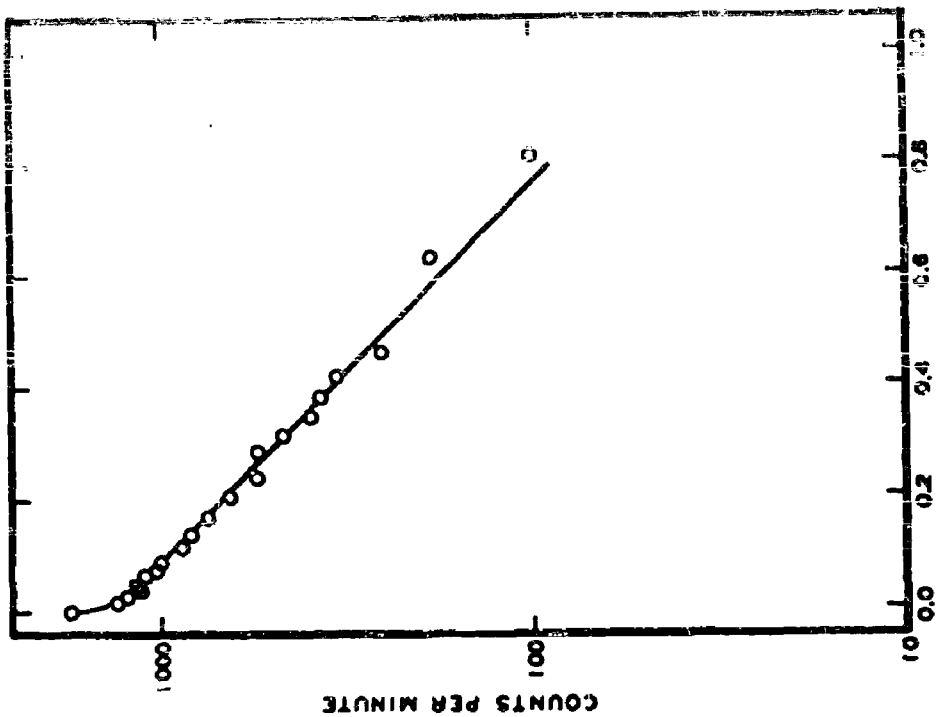

FIG. 3. Absorption in lead of the quantum radiations emitted in the disintegration of Rh^{105}.

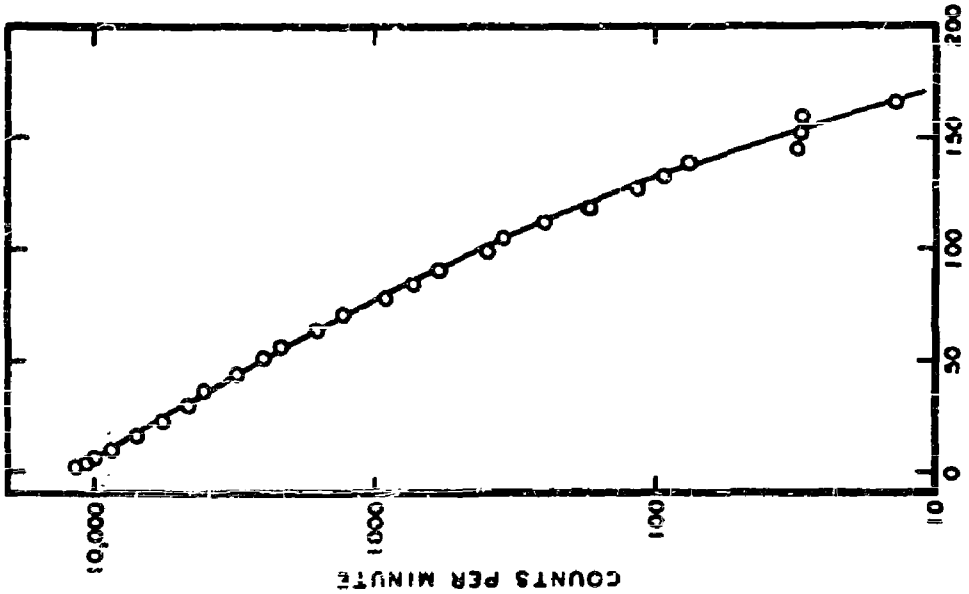

FIG. 2. Absorption in aluminum of the beta rays of the 36-hr. Rh^{105}.

purified Rh^{105}, the beta ray activity was absorbed in aluminum in a thin window "bubble" counter as shown in Fig. 2. The absorption limit occurs at 170 mg./cm.^{2}, corresponding to a maximum beta ray energy of 0.55 Mev.[4].

To investigate the nature of the quantum radiations emitted in the decay of Rh^{105}, an absorption curve in lead was carried out before a single Geiger-Mueller counter. Just sufficient aluminum was placed before the counter at the outset of the measurements to stop all of the beta rays being emitted by the source. In this way, only the quantum radiations were counted. This lead-absorption curve of the gamma radiation is shown in Fig. 3, where two components are clearly present. The softer component is in the region of X-rays or bremsstrahlung

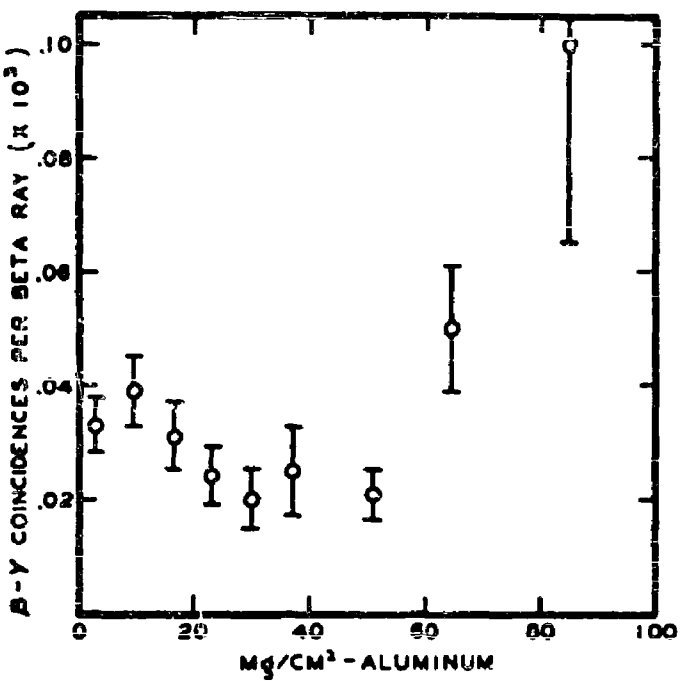

FIG. 4. The beta-gamma coincidence rate of Rh^{105} as a function of the surface density of aluminum placed before the beta ray counter.

whereas the harder component has an energy calculated from the slope of the curve as 0.36 Mev. The quantum radiations indicated by this curve are in good agreement with the findings of Sullivan, Sleight, and Gladrow (1).

When a source of the purified Rh^{105} was placed between two Geiger counters in coincidence, the beta-gamma coincidence curve of Fig. 4 was obtained. The coincidence rate was very small, and the points beyond 60 mg./cm.^{2} are essentially without meaning, because of their great statistical probable errors. The general trend of the points below 60 mg./cm.^{2} is downward, indicating that the gamma ray of Rh^{105} is coupled with an inner beta ray group. The gamma ray counter of the beta-gamma coincidence counting arrangement was calibrated

by the beta-gamma coincidence rate of Sc^{46}. From the calibration, it was calculated that the beta-gamma coincidence rate of Rh^{105} at zero absorber thickness ($\sim 0.04 \times 10^{-3}$ coincidence per beta ray) is what would be expected, were gamma rays of energy ~ 0.3 Mev. coupled with not more than 8 per cent of the beta rays.

The data of the first four figures of this paper were taken with the use of the first source of Rh^{105} obtained from Oak Ridge.

Since a question had arisen whether quantum radiations were present at all in the decay of rhodium (105) (3), the second source of radioactive material was procured from Oak Ridge for a more careful consideration of the gamma ray activity. The target material was irradiated for only 10 hr. in the pile, and after chemical purification, was placed between two blocks of aluminum, each having a surface

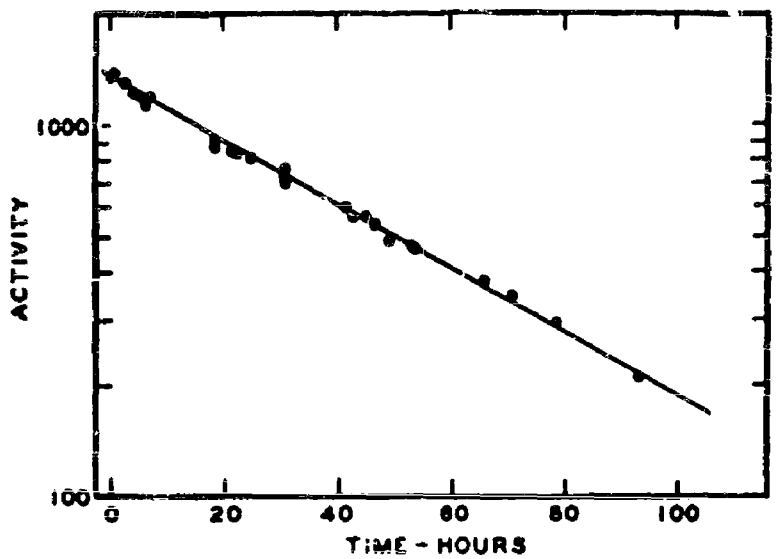

FIG. 5. Half-period of the gamma ray activity of the second source of Rh^{105}.

density of 1.7 g./cm.^{2}. This aluminum thickness was, of course, far more than sufficient to stop the beta rays of Rh^{105}. Adjacent to either aluminum block was placed a Geiger-Mueller tube, having glass walls of thickness 0.1 cm. and copper cathodes of wall thickness 0.013 cm. In one counter, the half-period of the quantum radiations being emitted by the source of Rh^{105} was measured; with the other, absorption curves in lead of the gamma rays were obtained. The decay curve of the gamma ray activity of Rh^{105} was followed for three half-periods and is shown in Fig. 5. The half-period, taken from the slope of the curve is 35 ± 1 hr. Two lead absorption curves for the gamma rays of Rh^{105} are shown in Fig. 6. The first of these curves was taken at the beginning of the decay curve of Fig. 5, and the second curve was obtained forty hours later. The quantum energy taken from the slope of the curves is 0.3 Mev. These curves differ from that of Fig. 3 in that the

softer component has now disappeared and the slope of the curve for the hard component is such as to suggest a quantum energy of 0.30 Mev. rather than 0.36 Mev. Absence of the softer component is explained by the fact that the thick block of aluminum was used before the gamma ray counter in the second measurement. The change in slope to give the differing quantum energies is explained by the fact that the geometries of the two sets of lead absorption measurements were vastly different. It is thought that the same gamma ray is certainly involved in both instances.

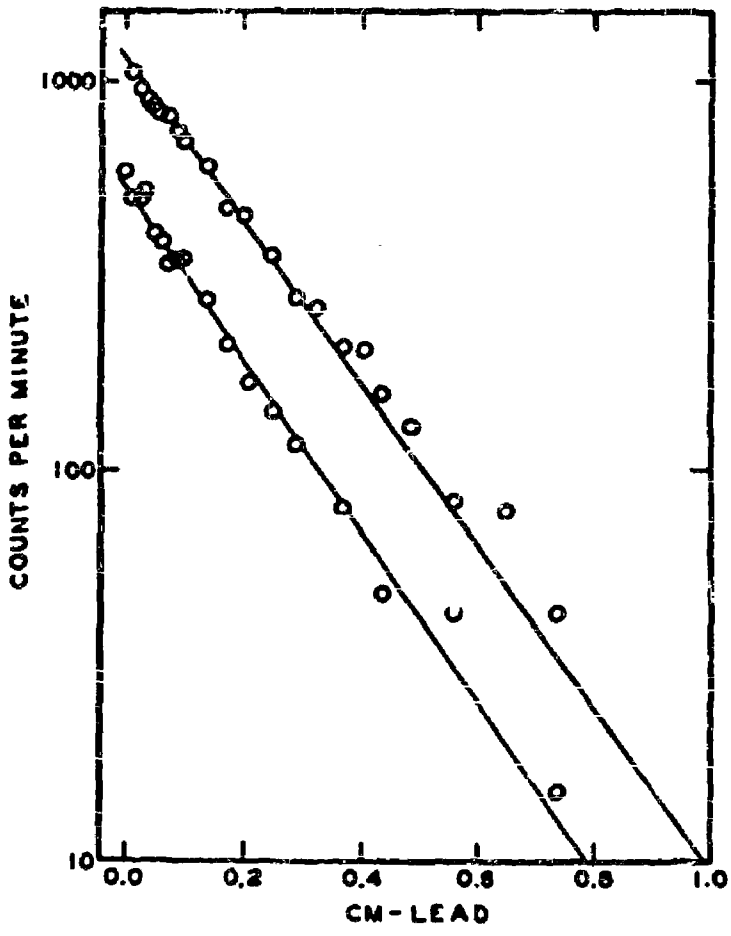

FIG. 6. Absorption in lead of the gamma rays emitted in the disintegration of the second source of Rh^{105}.

The question arose whether the presence of quantum radiations might be accounted for by bremsstrahlung effects. This seemed to be an unlikely explanation for the presence of the gamma rays, because the mean energy of the beta rays from Rh^{105} is only 0.2 Mev.[3]. However, to show positively that the results are not in any way related to the presence of bremsstrahlung, comparative measurements were carried out, using the beta spectrum of RaE. The source of Rh^{105}, the gamma ray activity of which had been followed for three half-periods, was placed before a thin window "bubble" counter. The beta ray counting

rate was observed, and after 0.1 cm. of lead had been placed before the counter, the gamma ray activity was likewise noted. The source of Rh^{105} was removed; a source of Ra (D + E + F) was positioned to give the same beta ray counting rate as was previously observed for Rh^{105}, and the same sheet of lead was placed over the counter to observe the residual counting rate. The data are given in Table I where it is

TABLE I. *Gross Counting Rates (per minute).*

Background	Ra (D + E + F)	Rh^{105}
37.5 ± 3	39 ± 4.5	116 ± 4

clear that although the counting rate from Ra (D + E + F) did not exceed the background count, that of Rh^{105} was three times greater. Were the quantum radiations which were detected in the counter originating from bremsstrahlung production in the lead sheet, the counting rate from Ra (D + E + F) should have been the larger, because the beta rays of RaE have a maximum energy of 1.17 Mev.

Acknowledgment

The writers wish to acknowledge the continued interest of Dr. W. F. G. Swann, Director of the Bartol Research Foundation.

REFERENCES

(1). NISHINA, YASAKI, KIMURA, AND IKAWA, *Phys. Rev.*, Vol. 59, p. 323 (1941); *Phys. Rev.*, Vol. 59, p. 677 (1941). SULLIVAN, SLEIGHT, AND GLADROW, Plutonium Project Report CC-1493 (March, 1944), quoted by Seaborg and Perlman, *Rev. Mod. Phys.*, Vol. 20, p. 585 (1948). E. BOHR AND N. HOLE, *Arkiv. f. Mat., Astr., o. Fys.*, Vol. 32A, paper number 15 (1948).

(2) C. E. MANDEVILLE AND E. SHAPIRO, *Phys. Rev.*, Vol. 80, p. 125 (1950).

(3) R. B. DUFFIELD AND L. M. LANGER, *Phys. Rev.*, Vol. 81, p. 203 (1951).

(4) L. E. GLENDENIN, *Nucleonics*, Vol. 2, No. 1, p. 12 (1948).

Reprinted from THE REVIEW OF SCIENTIFIC INSTRUMENTS, Vol. 23, No. 2, 95-96, February, 1952
Printed in U. S. A.

Delay Times in G-M Counters.* Letter V

W. C. PORTER AND W. E. RAMSEY
Bartol Research Foundation of the Franklin Institute,
Swarthmore, Pennsylvania
(Received June 11, 1951)

IN the study of delayed nuclear reactions, consideration must be given to the time required for circuits and counters to respond. It is the purpose of this experiment to show that G-M counters, as small as those used here, can have a maximum delay time which is no greater than 4×10^{-8} sec. Work performed in this laboratory by A. Stevenson on *Coincidence Time Delays in Geiger Counters*[1] has been extended. The method employed in these investigations consisted of measuring the double coincident rate as a function of the time separation of the coincident discharges. The procedure was such that the maximum time difference to be expected in the observed distribution corresponds to the formation of an ion pair near the wire of counter 2 and the simultaneous formation of an ion pair at the cathode of counter 1 (Fig. 1). Several circuit changes have been made so that time differences as short as 1×10^{-8} sec can be reliably measured. The geometry of the experiment was similar to that used by Stevenson.

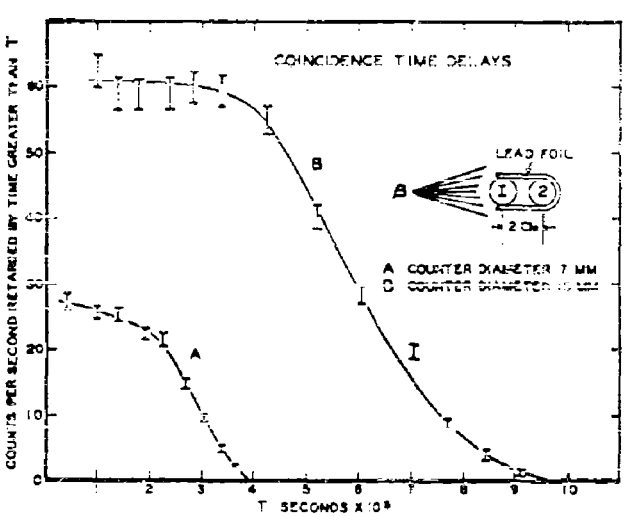

FIG. 1.

In low values of electric fields electron mobilities are constant, and thus one might expect that if the counter diameter were halved, the delay time would be quartered. However, in the electric fields which exist in these argon-ether counters, the electron velocity, not the mobility, is constant over the greater portion of the path;[3] therefore, when the counter diameter is halved, the maximum delay time is halved also. Calculations based on this constant velocity were made for these small counters (7-mm diameter) and resulted in maximum transit times of 4.4×10^{-8} sec. Figure 1, curve A, shows that the maximum measured delay time for these small counters is 4.0×10^{-8} sec. Curve B is for the same counters that Stevenson[1] used and shows the leveling-off in the number of counts in the short time region, thus extending his data to shorter times and showing the existence of the maximum in the distribution curve suggested by his data. Both of these curves indicate that there is a most probable time of delay. The values may be found by taking the first derivatives of the curves shown.

In conclusion, decreasing the diameter of these counters decreases the maximum time delay proportionally, thereby increasing the usefulness of counters for measurements in the short time region. This experiment also further verifies the fact that electron velocities are constant in argon-ether for values of electric fields found in these counters.

* Assisted by the joint program of the ONR and AEC.
[1] A. Stevenson, Rev. Sci. Instr. **23**, 93 (1952).
[3] A. Stevenson, Rev. Sci. Instr. **23**, 93 (1952).

Reprinted from THE REVIEW OF SCIENTIFIC INSTRUMENTS. Vol. 23, No. 2, 95, February, 1952
Printed in U. S. A.

General Observations on Discharge Lag in Counters.* Letter IV

W. E. RAMSEY
Bartol Research Foundation of the Franklin Institute.
Swarthmore, Pennsylvania
(Received June 11, 1951)

IT is obvious from the observations Stevenson has published in two preceding papers that the initial lag in a counter may be reduced by the proper choice of gas mixture. The form of his velocity curves also makes it possible to anticipate the approximate magnitude of the improvement to be gained by a reduction in counter diameter for the two gas mixtures investigated. In addition, it is clear that in coincidence work these lags would place no limitation on very short time applications provided the initiating electrons in coincident counters are created at the same distance from the counter wires. In this case each coincident channel is lagged by the same amount, and any measured lag indicates the correct retardation in the formation of the electrons.[1] This fact adds importance to scintillation G-M counters of the type now being developed by C. E. Mandeville. When such counters are used in coincidence, transit lags cancel out, since the electrons produced in similar counters both start from the cathode.

While the electron velocity measurements of Stevenson do not give values of E/p for the intense fields near the wire, they make it possible to estimate maximum times with fair accuracy. A consideration of the field in a tube indicates that over most of its path an electron is moving at nearly constant velocity. The maximum lag (Fig. 1) is 9.6×10^{-8} sec. This measurement gives an average velocity of 7.8×10^{6} cm/sec, a value which is acceptable if the degree of constancy observed over the region

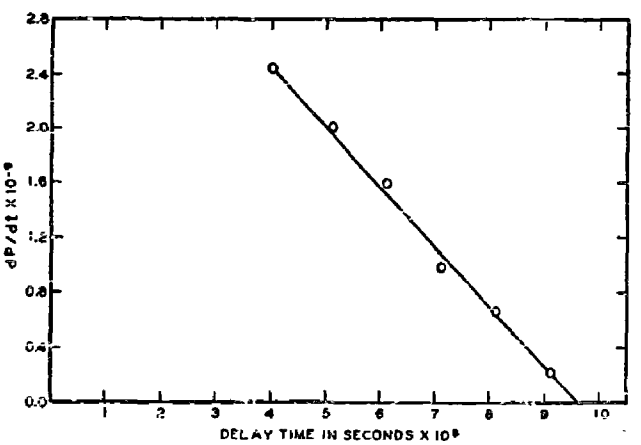

FIG. 1. Distribution function (Stevenson's data).

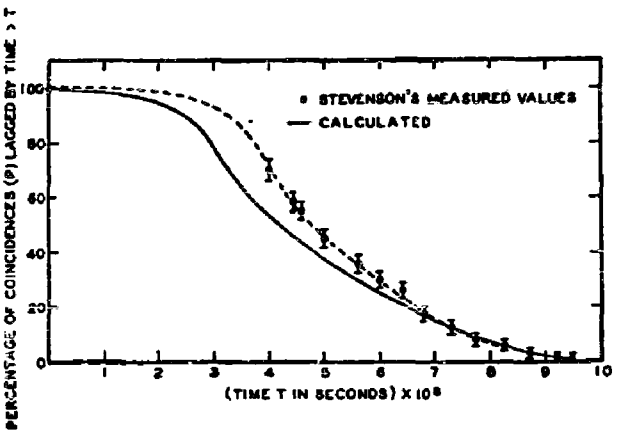

Fig. 2. Solid line calculated from $P=S\{1-e^{-2\epsilon\alpha k_1(r-vt)}\}-T\{1-e^{-3\epsilon k_1(r-vt)}\}$, where $S=\epsilon\alpha kre^{-\epsilon\alpha k_1 vt}$, $T=\frac{1}{2}\epsilon\alpha kre^{-2\epsilon\alpha k_1 vt}$, ϵ = specific ionization at atmospheric pressure; $\alpha=p/p_0$ where p = total pressure of gas, p_0 = atmospheric pressure; $\epsilon\alpha k_1$ = average number of ions per beta-particle; v = constant velocity of 7.8×10^{6} cm per sec; and r = radius of counter.

$E/P=3.0$ to $E/P=8.5$ is maintained to E/P of about fifteen. Very near the wire where E/P is large, a sharp rise in velocity should occur. However, the transit time in this region is negligible.

An exact calculation of the distribution of lags in time is impossible, because the scattering of β-particles in the counters results in an unknown distribution of path lengths. However, the general nature of the picture can be anticipated if one assumes a constant velocity and at most, small angle scattering. The problem also may be solved in the special case where scattering is sufficiently complete to give β-particles a uniform angular distribution in each tube. Little scattering was assumed in arriving at the expression for P in Fig. 2. This expression is in fair agreement with Stevenson's data. A consideration of first derivatives indicates that the distribution function has a maximum in the neighborhood of 3.0×10^{-8} sec. The experimental data (Fig. 1, Stevenson's second letter) suggests that a maximum should occur between $t=0$ and $t=4.0\times10^{-8}$ sec.

* Assisted by the joint program of the ONR and AEC.

[1] This statement implies that the initial currents in the counters are equal or are sufficiently large to trigger the circuit in the time concerned. Actually, current time studies in the short time region indicate that as far as current is involved, a properly constructed coincidence unit should permit the measurement of retardations down to 10^{-8} sec.

Reprinted from THE REVIEW OF SCIENTIFIC INSTRUMENTS, Vol. 23, No. 2, 94, February, 1952
Printed in U. S. A.

Short Double Coincidence Resolving Times for G-M Tubes. Letter III*

C. E. MANDEVILLE
Bartol Research Foundation of the Franklin Institute, Swarthmore, Pennsylvania
(Received June 11, 1951)

IN the two preceding letters[1] of this issue of the *Review of Scientific Instruments*, results are given upon which the writer wishes to make some comments. Stevenson has shown by direct measurement that electron velocities vary widely, depending upon the organic gas used in self-quenching tubes, and in particular that the velocity is about a factor of two greater in the argon-ether mixture than in the argon-butane one. This fact was also noted in 1947 by an indirect method when G-M tubes of the same dimensions as those of Stevenson's were employed in genuine coincidence loss measurements.[2,3] At that time, it was found that the argon-butane mixture could not be used without loss at a coincidence resolving time of less than 0.2 microsecond,[2] whereas the resolving time could be reduced to 0.08 microsecond without loss, using the argon-ether mixture.[3] This observation of difference in behavior of ether and butane is in complete agreement with those of the first of the two preceding letters. The coincidence loss measurements[3] were made in a G-M tube arrangement quite similar to that of Stevenson's second letter. The beta-rays penetrated the two counters uniformly over their entire volume, and the walls of each counter had a uniform thickness of 25 mg/cm². The observation of no coincidence loss in argon-ether at 0.08 microsecond agrees with the conclusion of Stevenson's second note which shows that the maximum delay time in the argon-ether mixture is $<10^{-7}$ sec. In another note,[4] it was stated that no genuine coincidence loss was observed in the beta-gamma coincidence rate of Au^{198} when the coincidence resolving time was decreased to 0.035 ± 0.005 microsecond. In this coincidence counting arrangement, the gamma-ray counter was an argon-ether tube of the glass-Aquadag type, having a diameter of 1.3 cm. The beta-ray tube was the thin "bubble" end-window type, having a cathode diameter of 0.9 cm. The beta-rays were fired along the axis of the cathode, parallel to the central wire. In making the beta-gamma measurements on Au^{198}, fifty to sixty coincidences were observed at each resolving time as the resolving time was reduced from one microsecond to 0.035 microsecond in steps of 0.25 microsecond. The coincidence rate at 0.035 microsecond was about twenty percent less than that at one microsecond, but the decrease was attributed to statistical probable error and was not regarded as evidence of a metastable state in Au^{198} or as an indication of genuine coincidence loss arising from time delays in the coincident G-M tubes.

The observation of relatively small genuine coincidence loss at 0.035 microsecond is consistent with the data of Stevenson's second note, because the counter diameters were smaller than those of his measurements. During the past four years, a considerable number of radio elements have been investigated in this laboratory by the coincidence method. In observing immediate coincidences, a coincidence resolving time of 0.10 microsecond was consistently employed to insure no genuine coincidence loss. The counters used to obtain the data of Stevenson's second letter were chosen at random from the supply of a counters used by the writer during the course of the coincidence investigations of radioactive decay schemes.

It is the purpose of this letter to emphasize the fact that under suitable conditions, very short coincidence resolving times may be used with no coincidence loss, in connection with coincident G-M tubes. Resolving times of $<10^{-7}$ sec are easily obtainable with argon-ether tubes of diameter 1.5 cm. Smaller diameters should give resolving times of $\sim10^{-8}$ sec without loss.

Since the time of the earlier measurements[3,4] at resolving times of ≤0.08 microsecond, many private communications of disbelief have been received. Papers on delay times in G-M tubes have been written, but no reference is made to the fact that the short resolving times[3,4] must indicate very small time delays in Bartol counters. Review articles on counters often devote several sections to time delays in G-M tubes and to the problem of short resolving times, but the measurements at $<10^{-7}$ sec are never discussed. It should perhaps be remarked that Bartol counters of the type utilized by Stevenson have been used in double coincidence in at least two university physics laboratories in circuits of resolving time $\leq10^{-7}$ sec without genuine coincidence loss.

* Assisted by the joint program of the ONR and AEC.
[1] Alden Stevenson, Rev. Sci. Instr. 23, 93 (1952); Rev. Sci. Instr. 23, 93 (1952).
[2] Mandeville and Scherb, unpublished data (1947).
[3] Mandeville and Scherb, Phys. Rev. 73, 90 (1948); Phys. Rev. 73, 639 (1948).
[4] Mandeville and Scherb, Phys. Rev. 73, 634 (1948).

Reprinted from THE REVIEW OF SCIENTIFIC INSTRUMENTS, Vol. 23, No. 2, 93–94, February, 1952
Printed in U. S. A.

Coincidence Time Delays in Geiger Counters.*
Letter II

ALDEN STEVENSON
Bartol Research Foundation of the Franklin Institute, Swarthmore, Pennsylvania
(Received June 11, 1951)

IN high speed coincidence counting employing Geiger-Mueller tubes, it is desirable to make the resolving time of the circuits as short as possible in order to record nuclear events separated by short times as well as to reduce the number of accidental coincidences. Clearly the ideal situation would be one in which the time between the creation of an ion in a counter and the initiation of the avalanche would be the same for both counters. If such indeed were the case, avalanches begun in two counters A and B, Fig. 1, by an ionizing ray of great speed would show no time interval between them. Actually, the variation in position where ion pairs may be formed in the two Geiger tubes and the finite transit time needed for the electrons to drift to the avalanche region bring about departures from the ideal case. If, therefore, we should have a means for measuring the time interval between the two counter discharges caused by a single ionizing ray, we should be able to obtain information on the distribution of time delays to be expected from two counters. The experiment then consisted in measuring the number of coincidences recorded whose separation in time was larger than a certain value. Letting $f(t)$ be the percentage of the total coincidence counting rate observed to have a time delay greater than t, Fig. 1 shows $f(t)$ plotted against t.

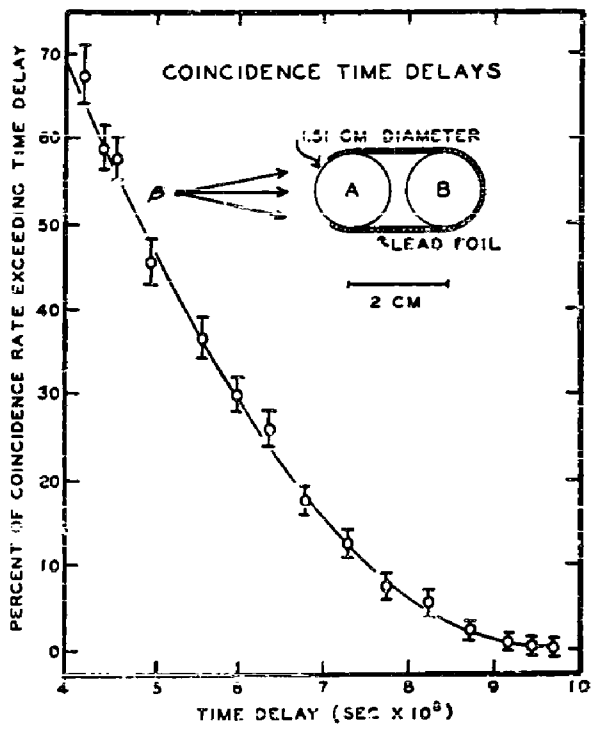

FIG. 1. The coincidence rate as a function of the delay time.

The Geiger tubes used were 1.5 cm in diameter and filled with the argon-ether mixture to a total pressure of 7 cm Hg. They were operated at 70 volts above the threshold. The central wires of the counters were made of tungsten and had a diameter of 0.003 in. The delay times between two Geiger tube pulses resulting in a coincidence were measured by employing a modification of a circuit developed by W. E. Ramsey.[1] The circuit, designed to be operated by the first 0.2-volt change of the counter wire potential, functions as an electronic switch. The discharge pulse from one Geiger tube causes a known plate current to flow in a vacuum tube until this current is shut off by the discharge of the second Geiger tube. Hence, the integrated charge on a condenser in the vacuum tube plate is directly proportional to the time elapsed between counter discharges. Of course, a certain time is necessary for an avalanche to develop to the point of operating an electronic circuit. Quite apart from the fact that this time may be expected to be the same for both counters, an independent investigation by W. E. Ramsey (as yet unpublished) indicates that the time necessary to charge the counter wire to a potential of 0.2 volt is very short compared to 4×10^{-8} sec. By employing a coaxial delay line of variable length, simulated Geiger pulses could be imposed on the timing circuit in such a way as to provide calibration and a convenient check.

The procedure was such that the maximum difference to be expected in the plotted distribution corresponds to an ion pair formed near the wire of counter B and a simultaneous pair formed at the cathode of tube A. One can conclude from the evidence of the experiment that the transit time of an electron from the cathode to the avalanche region is not in excess of 10^{-7} sec. It is not unreasonable to suppose in the light of the previous velocity measurements, that by choosing good gas mixtures and reducing the cathode diameter, one could decrease the maximum coincidence delay time to about 10^{-8} sec or less.

The author wishes to express his appreciation to Mr. Ramsey for his constant interest and advice during the course of the research.

* Assisted by the joint program of the ONR and AEC.
[1] W. E. Ramsey, Phys. Rev. 57, 1022 (1940).

Reprinted from THE REVIEW OF SCIENTIFIC INSTRUMENTS, Vol. 23, No. 2, 93, February, 1952
Printed in U. S. A.

Electron Velocities in Geiger Counter Gas Mixtures.* Letter I

ALDEN STEVENSON
Bartol Research Foundation of the Franklin Institute, Swarthmore, Pennsylvania
(Received June 11, 1951)

LACKING quantitative theoretical prediction, experimentally determined plots of electron velocities as a function of field intensity have become increasingly valuable in selecting gas mixtures for use in Geiger counters with short delay times. With this in mind there was developed a new method for measuring these velocities, involving a simplicity of design which would afford a convenient technique.

A schematic diagram of the apparatus is shown in Fig. 1. The three principal electrodes A, B, and C, made of spun copper, were mounted inside a 3-inch diameter Pyrex tube. The anode wire leads of counters 1 and 2 were placed in such a way as to reduce their mutual electrostatic coupling. By imposing a field of 200 volts/cm between electrodes A and B, electrons created in the gas by the ionization of beta-rays that have passed through the thin window were accelerated toward B. Some of these electrons were admitted simultaneously through the two slits in B. One such electron may initiate a discharge in counter 2 when it arrives at the wire. Another after passing through the slit opposite the fine wire grid of counter 1 moves in a uniform field until it arrives at C. By using a suitable timing circuit to measure the elapsed time between the pulse from counter 2 and that from 1, the transit time from B to C was directly established. Care was taken to make the counters of the same dimensions to keep their discharge characteristics similar. Uncertainty in the origin of the electrons between A and B caused an observed distribution of about 20 percent at the shortest transit times measured.

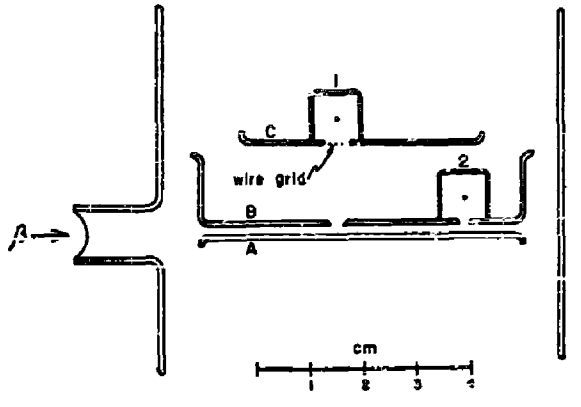

FIG. 1. Schematic diagram of the coincidence counting arrangement used to measure electron velocities.

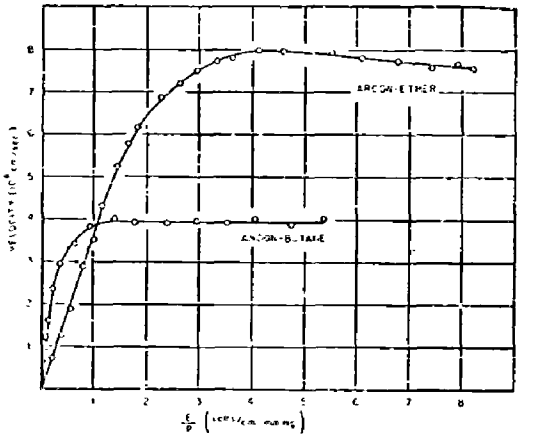

FIG. 2. Velocity of electrons as a function of E/p and the counter gas.

The experimental results are given in Fig. 2. The partial pressures of the two gas mixtures used were: 61-mm argon with 11-mm ether and 103-mm argon with 17-mm butane. The curves clearly indicate the superiority of argon-ether mixture over the argon-butane mixture—a result established qualitatively by coincidence resolving-time measurements made at the Bartol Foundation.[1] Other evidence of the leveling-off of electron velocity curves as well as actual decreases in velocity for higher values of E/p have been recorded by Rossi and Staub.[2] The upper limit of the value of the field obtainable was imposed by arcing across between two internal leads (not shown) to the electrodes. By care in design, the procedure should be capable of measuring velocities up to 15 or 20 for E/p, thus enabling the transit time of an electron traversing a counter radius to be computed for distances considerably less than 2 mm from the anode wire.

The writer wishes to express his particular appreciation to Mr. W. E. Ramsey for having designed the experimental tube with which the investigations were carried out and for discussions and advice throughout the course of the work.

* Assisted by the joint program of the ONR and AEC.
[1] C. E. Mandeville and M. V. Scherb, unpublished data (1947).
[2] B. B. Rossi and H. H. Staub, *Ionization Chambers and Counters* (McGraw-Hill Book Company, Inc., New York, 1949), pp. 11 and 14.

Reprinted from THE PHYSICAL REVIEW, Vol. 85, No. 2, 193-196, January 15, 1952
Printed in U. S. A.

Neutrons from the Disintegration of the Separated Isotopes of Silicon by Deuterons*

C. E. MANDEVILLE, C. P. SWANN, AND S. D. CHATTERJEE†
Bartol Research Foundation of the Franklin Institute, Swarthmore, Pennsylvania

AND

D. M. VAN PATTER‡
Department of Physics and Laboratory for Nuclear Science and Engineering, Massachusetts Institute of Technology, Cambridge, Massachusetts

(Received September 14, 1951)

The neutron spectra from deuterons on silicon have been studied by the method of recoil protons and photographic plates. Thick isotopic targets of the three separated isotopes of silicon were irradiated by deuterons of energy 1.4 Mev, supplied by the Bartol Van de Graaff statitron, observations being carried out at angles of zero and ninety degrees with the incident deuterons. Q-values, from which energy levels in the residual nuclei of phosphorous may be calculated, are as follows:

Reaction	Q-values (Mev)
$Si^{28}(d,n)P^{29}$	0.29
$Si^{29}(d,n)P^{30}$	3.27, 2.52, 1.81, 1.27
$Si^{30}(d,n)P^{31}$	4.92, 4.59, 3.73, 2.70, 1.51

The estimated probable error in the Q-values is 40 kev.

THERE are three stable isotopes of silicon, Si^{28}, Si^{29}, and Si^{30}, having respectively relative abundances of 92.28 percent, 4.67 percent, and 3.05 percent. When these elements are irradiated by deuterons, neutrons are emitted in the following three reactions.

$$(1)\ Si^{28}+d\rightarrow P^{29}+n^1+Q_1,$$

$$(2)\ Si^{29}+d\rightarrow P^{30}+n^1+Q_2,$$

$$(3)\ Si^{30}+d\rightarrow P^{31}+n^1+Q_3.$$

Naturally occurring silicon has been previously bombarded with deuterons to observe the neutron spectra.[1] However, because of the element of ambiguity introduced by the presence of the mixture of isotopes, the data are difficult of interpretation. To reinvestigate the above three reactions, quantities of the separated isotopes, in the form of silicon dioxide, were obtained from the Y-12 plant, Carbide and Carbon Chemicals Division, Union Carbide and Carbon Corporation, Oak Ridge, Tennessee. The mass analyses of the various targets are shown in Table I.

* Assisted by the joint program of the ONR and AEC.

† Calcutta, India. Guest physicist, Bartol Research Foundation, 1951.

‡ The contribution of D. M. Van Patter to this article consists of the preparation of the Appendix.

[1] R. A. Peck, Jr., Phys. Rev. 73, 947 (1948).

TABLE I. Isotopic analysis of target materials.

Si^{28}		Si^{29}		Si^{30}	
Isotope	Percent	Isotope	Percent	Isotope	Percent
28	99.4	28	29.1	28	40.97
29	0.4	29	68.6	29	2.44
30	0.2	30	2.2	30	56.59

Thick isotopic targets of the separated isotopes of silicon were irradiated by deuterons of energy 1.40 Mev, supplied by the Bartol Van de Graaff statitron. The neutrons emitted in the three reactions above were recorded in Eastman NTA plates located at zero and ninety degrees with the incident deuterons.

In evaluating the energies of the neutron groups of all of the three reactions above, two procedures have been employed. One has been to apply the range-energy relation of Lattes, Fowler, and Cuer[2] to NTA plates, increasing the observed energy by two percent to allow for an acceptance angle of twelve degrees in the forward direction; the other has consisted in decreasing the result of the first method by an amount indicated by a recently obtained calibration curve[3] for NTA plates, and increasing it to take into account the use of a thick target.[4] The latter procedure has been considered to give the preferable result. The procedures of evaluation described above will be referred to respectively as Method I and Method II.

$Si^{28}(d,n)P^{29}$

The energy spectrum of the acceptable recoil protons of the neutrons emitted in the reaction $Si^{28}(d,n)P^{29}$ is shown in Fig. 1. Observations were carried out at zero degrees and ninety degrees in the laboratory system of coordinate axes. As indicated in the figure, two groups of neutrons appear at both angles of observation. The group of lower energy is assigned to the reaction $C^{12}(d,n)N^{13}$. The more energetic is thought to be related to the formation of P^{29} in its ground state. In the forward direction, high energy neutrons of low intensity

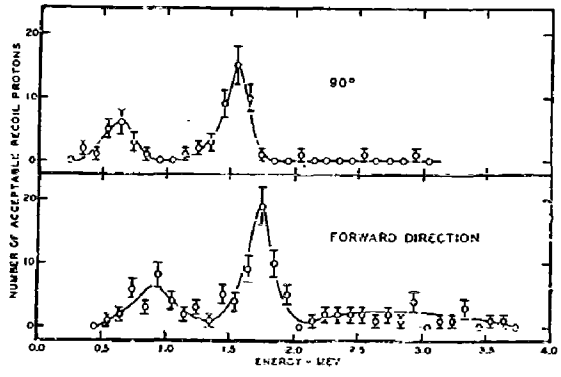

FIG. 1. Recoil protons knocked on in the forward direction by the neutrons from $Si^{28}(d,n)P^{29}$.

[2] Lattes, Fowler, and Cuer, Proc. Phys. Soc. (London) 59, 883 (1947).
[3] Richards, Johnson, Ajzenberg, and Laubenstein, Phys. Rev. 83, 994 (1951).
[4] S. C. Snowdon (to be published).

TABLE II. Ground-state Q-values for $Si^{28}(d,n)P^{29}$.

	Method I	Method II
Q-value (Mev)	0.36±0.04	0.29±0.04

are present. These are thought to result from the bombardment of "low Z" contaminants on the walls of the vacuum tube and of the magnet box between the poles of the beam focusing magnet of the Van de Graaff statitron. Plates in the forward direction are sensitive to neutrons emanating from these points, whereas the plates at ninety degrees to the beam are perpendicular to their direction of emission and hence do not record their recoil protons in the acceptable sense. This point is born out by the fact that no appreciable evidence of the presence of neutrons beyond those of the ground state is apparent in the data obtained at ninety degrees. The data of Fig. 1 are summarized in Table II.

The Q-values of Table II are means of those calculated at each of the two angles of observation. It is to be noted that they are in disagreement with the previously reported Q-value of -0.80 ± 0.10 Mev,[1] and with those values calculated from other reactions and from mass values (see Appendix).

$Si^{29}(d,n)P^{30}$

The spectra of acceptable recoil protons of the neutrons emanating from $Si^{29}(d,n)P^{30}$ are shown in Fig. 2. The most energetic group[5] is assigned to $N^{14}(d,n)O^{15}$,

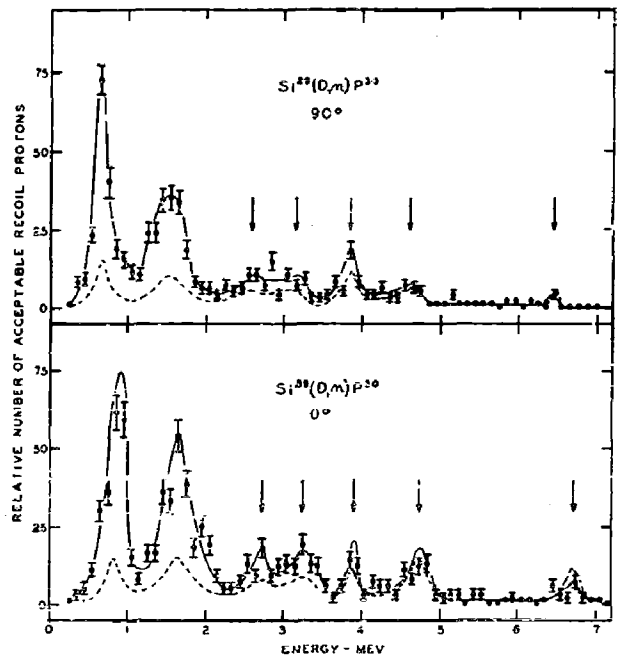

FIG. 2. Energy spectrum of the acceptable recoil protons of the neutrons from the reaction $Si^{29}(d,n)P^{30}$.

[5] The neutron group of the nitrogen reaction appears at zero degrees and ninety degrees in the data relating to $Si^{29}(d,n)P^{30}$ and in the forward direction alone in measurements on $Si^{30}(d,n)P^{31}$. The absence of this group at ninety degrees in the latter reaction

the least energetic one to $C^{12}(d,n)N^{13}$. The ground-state group of the reaction $Si^{28}(d,n)P^{29}$, the reaction of the preceding discussion, is also clearly present. The intermediate groups are assigned to the reaction $Si^{29}(d,n)P^{30}$. The data of Fig. 2 are summarized in Table III.

The energy levels of P^{30} in Table III are calculated from the preferred values of Method II.

$Si^{30}(d,n)P^{31}$

The acceptable recoil proton groups of the neutrons from $Si^{30}(d,n)P^{31}$ are shown in Fig. 3.[6] Here again, the most energetic group, appearing at 6.75 Mev in the forward direction, is assigned to $N^{14}(d,n)O^{15}$; the least energetic one to $C^{12}(d,n)N^{13}$. Again, the ground-state group of $Si^{28}(d,n)P^{29}$ is present. The remaining groups are assigned to $Si^{30}(d,n)P^{31}$. The data of Fig. 3 are summarized in Table IV.§

The nuclear energy levels of P^{31} have been calculated from the preferred Q-values of Method II.

TABLE III. Q-Values of $Si^{29}(d,n)P^{30}$ and energy levels of P^{30}.

Q-values (Mev) Method I	Q-values (Mev) Method II	Excitation levels of P^{30}
1.41±0.04	1.27±0.04	2.00±0.06
1.97±0.04	1.81±0.04	1.46±0.06
2.68±0.04	2.52±0.04	0.75±0.06
3.51±0.04	3.27±0.04	0.00

CONCLUSIONS

The energies of the neutron groups from deuterons on the separated isotopes of silicon have been measured. In many instances the calculated energy levels of the residual nuclei of phosphorous agree with those already obtained (see reference 1, Table II). The bearing of the measurements upon the masses and reaction energies of the silicon region are discussed in the appendix.

The writers wish to acknowledge the continued interest of Dr. W. F. G. Swann, Director of the Bartol Research Foundation.

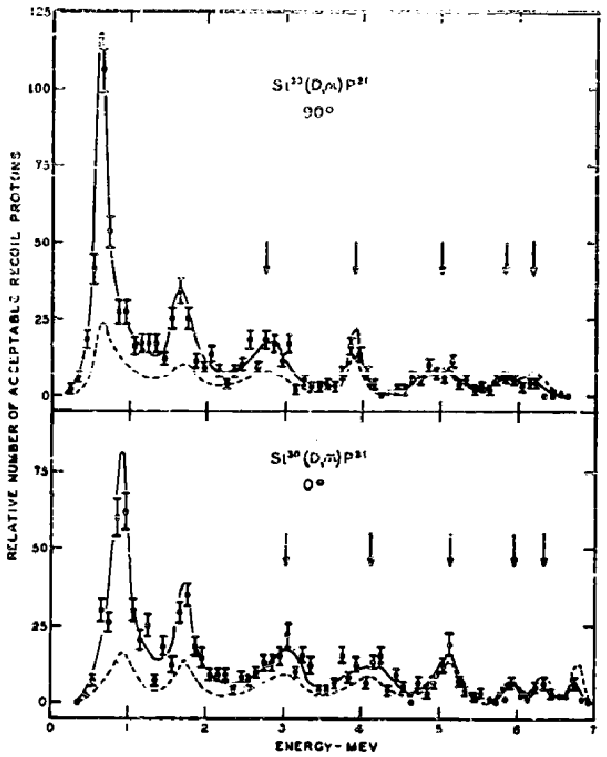

FIG. 3. Recoil protons of the neutrons emitted in the reaction $Si^{30}(d,n)P^{31}$.

APPENDIX: DISCUSSION OF RESULTS

Recent precise measurements[7,8] of nuclear Q-values involving nuclei with $Z=10$ to 16 have led to a revision of masses in that region.[9,10] However, in many cases, the most accurate method of estimating a given reaction energy involves the use of mass differences rather than a table of masses. It is of interest to compare the Q-values of the ground states measured by Mandeville, Swann, and Chatterjee with the reaction energies which can be predicted from the measurements of other workers.

The Reaction $Si^{28}(d,n)P^{29}$.—The end point of the beta-transition $P^{29}\xrightarrow{\beta^+}Si^{29}$ has been measured as 3.63±0.07 Mev[11] by means of cloud chamber and magnetic field. Except for the results of the present paper relating to reaction $Si^{28}(d,n)P^{29}$, the beta-transition above is the only link connecting the nucleus of P^{29} with other nuclei. Combining the total disintegration energy of the beta transition, 4.65±0.07 Mev, with the reaction energy of the

TABLE IV. Q-values of $Si^{30}(d,n)P^{31}$ and energy levels of P^{31}.

Q-values (Mev) Method I	Q-values (Mev) Method II	Excitation levels of P^{31} (Mev)
1.64±0.04	1.51±0.04	3.41±0.06
2.28±0.04	2.70±0.04	2.22±0.06
3.95±0.04	3.73±0.04	1.19±0.06
4.79±0.04	4.59±0.04	0.33±0.06
5.16±0.04	4.92±0.04	0.00

is not considered significant, because statistical difficulties are encountered in accumulating acceptable long tracks. From the several spectra, an average Q-value of 5.11±0.04 Mev is calculated for $N^{14}(d,n)O^{15}$, using Method II of the text. This result is in good agreement with the previously reported energy release of 5.15±0.05 Mev [W. M. Gibson and D. L. Livesey, Proc. Phys. Soc. (London) 60, 523 (1948)].

[6] The broken line of Figs. 2 and 3 represents the actual distribution of neutron energies corrected for variation with energy of the n-p scattering cross section and acceptance probability.

§ *Note added in proof:* In each of the three figures, the data at zero and ninety degrees have not been normalized to take into account plate area scanned. No information is thus presented concerning the angular distributions of the neutron groups. The fluctuation of the intensity of the carbon group relative to those of the other neutron groups is thought to be related to statitron performance. Excessive sparking and breakdown in the vacuum tube appear to increase the carbon contamination.

[7] Strait, Van Patter, Buechner, and Sperduto, Phys. Rev. 81, 747 (1951).

[8] W. W. Buechner, *et al.*, M.I.T. report, Laboratory for Nuclear Science and Engineering (May 31, 1951).

[9] H. T. Motz, Phys. Rev. 81, 1061 (1951).

[10] A. H. Wapstra, to be published.

[11] White, Creutz, Delsasso, and Wilson, Phys. Rev. 59, 63 (1941).

TABLE AI. Q-values in Mev.

Reaction	Observed	Calculated from nuclear reactions	Calculated from masses
$Si^{28}(d,n)P^{29}$	0.29±0.04	0.81±0.07	0.81±0.09
$Si^{29}(d,n)P^{30}$	3.27±0.04	3.25±0.18	3.24±0.11
$Si^{30}(d,n)P^{31}$	4.92±0.04	5.08±0.02	5.03±0.06

reaction $Si^{28}(d,p)Si^{29}$, 6.246±0.007 Mev,[7] and with the neutron-proton mass difference of 0.782±0.001 Mev,[12] a reaction energy 0.81±0.07 Mev may be calculated for the reaction $Si^{28}(d,n)P^{29}$.

The Reaction $Si^{29}(d,n)P^{30}$.—The Q-value for the formation of P^{30} in the ground state in the reaction $Si^{29}(d,n)P^{30}$ may be calculated from each of two independent cycles of nuclear reactions.

I. (a) $P^{31}+\gamma \rightarrow P^{30}+n-(12.37\pm0.2)$ Mev[13,14]
(b) $P^{31}+p \rightarrow Si^{28}+He^4+(1.909\pm0.015)$ Mev[15]
(c) $Si^{28}+d \rightarrow Si^{29}+p+(6.246\pm0.007)$ Mev[7]
(d) $2d \rightarrow He^4+(23.834\pm0.007)$ Mev[12]

$Q=(2d-He^4)-1.909$ Mev -6.246 Mev -12.37 Mev
$=3.31\pm0.20$ Mev

II. (a) $Si^{29}+d \rightarrow Si^{30}+p+(8.388\pm0.013)$ Mev[8]
(b) $P^{30} \xrightarrow{\beta^+} Si^{30}+(4.52\pm0.35)$ Mev[16]
(c) $n \xrightarrow{\beta^-} p+(0.782\pm0.001)$ Mev[12]

$Q=(p-n)-4.52$ Mev $+8.388$ Mev
$=3.09\pm0.35$ Mev

A weighted average of results I and II is 3.25±0.18 Mev.

The Reaction $Si^{30}(d,n)P^{31}$.—In the case of the reaction $Si^{30}(d,n)P^{31}$, precise estimates of the energy release can be made by two independent methods.

I. (a) $Si^{30}+d \rightarrow Si^{31}+p+(4.367\pm0.010)$ Mev[7]
(b) $Si^{31} \xrightarrow{\beta^-} P^{31}+(1.51\pm0.01)$ Mev[17]
(c) $n \xrightarrow{\beta^-} p+(0.782\pm0.001)$ Mev[12]

$Q=(p-n)+4.367$ Mev $+1.51$ Mev
$=5.095\pm0.015$ Mev

II. (a) $Si^{29}+d \rightarrow Si^{30}+p+(8.388\pm0.013)$ Mev[8]
(b) $Si^{28}+d \rightarrow Si^{29}+p+(6.246\pm0.007)$ Mev[7]
(c) $P^{31}+p \rightarrow Si^{28}+He^4+(1.909\pm0.015)$ Mev[15]
(d) $d \rightarrow p+n-(2.225\pm0.002)$ Mev[12]
(e) $2d \rightarrow He^4+(23.834\pm0.007)$ Mev[12]

$Q=(2d-He^4)+(d-n-p)-6.246$ Mev
-8.388 Mev -1.909 Mev
$=5.066\pm0.022$ Mev

An arithmetical average of the results of I and II is 5.08±0.02 Mev.

The foregoing calculated values are listed in Table AI of this Appendix together with values estimated from a table of binding energies recently computed by Wapstra.[10] The agreement between these values is not surprising, because Wapstra's binding energies are based to a large extent upon nuclear Q-values.

It may be seen from this table that the observed Q-value for the reaction $Si^{29}(d,n)P^{30}$ is in agreement with other measurements, and, in fact, establishes the mass of P^{30} with greater precision than was previously possible. The observed energy release, 4.92±0.04 Mev, for the reaction $Si^{30}(d,n)P^{31}$ is somewhat lower than the more accurate predicted value of 5.08±0.02 Mev; however, it seems probable that the ground-state group of the reaction has been observed. In the case of $Si^{28}(d,n)P^{29}$, the observed energy release of 0.29±0.04 Mev is in distinct disagreement with the estimated value of 0.81±0.07 Mev. This discrepancy can be attributed to either an inaccuracy in the early measurement[11] of the end point of the transition $P^{29} \xrightarrow{\beta^+} Si^{29}$ or to the fact that the ground state of the reaction $Si^{28}(d,n)P^{29}$ has not been observed in the measurements of the present paper.

[12] Li, Whaling, Fowler, and Lauritsen, Phys. Rev. 83, 512 (1951).
[13] McElbinney, Hanson, Becker, Duffield, and Diven, Phys. Rev. 75, 542 (1949).
[14] A. Katz and L. Penfold, Phys. Rev. 81, 815 (1951).
[15] D. M. Van Patter and P. M. Endt, preliminary value.
[16] C. Magnan, Ann. phys. 15, 5 (1941).
[17] H. W. Newson, Phys. Rev. 51, 624 (1937).

Reprinted from THE REVIEW OF SCIENTIFIC INSTRUMENTS, Vol. 22, No. 12, 878-885, December, 1951
Printed in U. S. A.

Trajectories in an Axial Focusing Double Lens Spectrometer*

S. C. SNOWDON
Bartol Research Foundation of the Franklin Institute, Swarthmore, Pennsylvania

(Received May 16, 1951)

The trajectories of an electron with zero canonical angular momentum ($p_\varphi-(erA_\varphi/c)=0$) have been computed with third-order accuracy for a $1/(1+x^2)$ axial field shape. By suitably matching the above solutions with a set of similar solutions obtained by shifting the origin, it is possible to obtain the complete zero canonical angular momentum trajectories corresponding to the double lens problem in which the axial field shape approximates rather closely one that is physically realizable. The numerical computations illustrate several typical trajectories. Design considerations are given to illustrate the utility and limitations of the theory.

INTRODUCTION

IT is of interest to consider the electron trajectories in a magnetic field whose variation along the axis is given by two juxtaposed sections of a $1/(1+x^2)$ distribution since it may be shown that the actual axial field distribution of a double lens spectrometer (Fig. 1) may be approximated by the above double bell-shaped field (Fig. 2 and Table I).

The motion of an electron in an axially symmetric magnetic field has been discussed by Zworykin, *et al*[1] who showed that for the case of zero canonical angular momentum the equation of the radial component of the trajectory is

$$(A_0^2-A_\varphi^2)\frac{d^2\rho}{dz^2}+\frac{1}{2}\left(\frac{\partial A_\varphi^2}{\partial\rho}-\frac{d\rho}{dz}\frac{\partial A_\varphi^2}{\partial z}\right)\times\left[1+\left(\frac{d\rho}{dz}\right)^2\right]=0, \quad (1)$$

where ρ is the radial distance, z is the axial distance, A_φ is the vector potential of the magnetic field, and A_0 is a constant equal to the uniform field ($H\rho$) value of an electron of energy $e\Phi$. If the relativistic mass variation is taken into account, it may be shown that

$$A_0=(2m_0c^2\Phi/e+\Phi^2)^{\frac{1}{2}}. \quad (2)$$

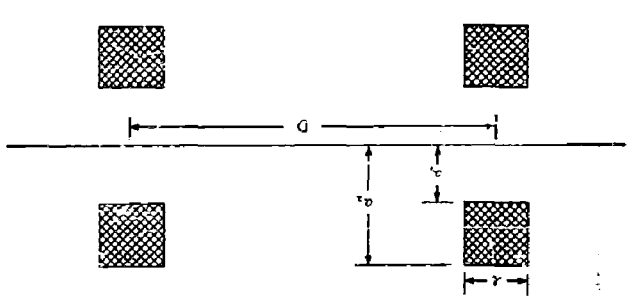

FIG. 1. General size, cross section, and location of the two identical coils used in the double lens spectrometer. The dimensions are as follows: $a_1=8.36$ in., $a_2=17.5$ in., $l=9.125$ in., and $D=53.0$ in. Other similar designs may be obtained by multiplying all distances by a constant factor.

The azimuthal motion may be derived from the radial motion through the equation:

$$\rho\frac{d\varphi}{d\rho}=A_\varphi\left[1+\left(\frac{d\rho}{dz}\right)^2\right]^{\frac{1}{2}}\cdot[A_0^2-A_\varphi^2]^{\frac{1}{2}}, \quad (3)$$

where φ designates the azimuth angle.

The vector potential A_φ may be expanded in powers of ρ as

$$A_\varphi=\tfrac{1}{2}\rho H(z)-\tfrac{1}{16}\rho^3H''(z)+(1/384)\rho^5H(z)^{(IV)}+\cdots, \quad (4)$$

where $H(z)$ is the field on the axis.

Agnew and Anderson[2] have given a special case of the first-order or paraxial trajectories in the double bell-shaped field to be considered here. These first-order calculations are the result of linearizing Eq. (1) for small values of ρ. Because of this linearity, their trajectories do not include the concept of a ring focus which is essentially a nonlinear phenomenon. Since a third-order calculation includes a first approximation of the nonlinearity involved in Eq. (1), the following third order calculations give an improved notion of the nature of the trajectories in the double bell-shaped axial field. For the range of initial angles under consideration, 0° to 40°, it is reasonable to suppose that the trajectories resulting from this third-order calculation are not greatly at variance with the exact trajectories in the double bell-shaped field. No estimate of the fifth-order calculations are given because of their complexity. Furthermore, since it is intended that the double lens spectrometer field trajectories are to be approximated by those of the double bell-shaped field and since the actual double lens axial field is only approximately given by the double bell-shaped field, there is added justification for not considering an approximation beyond the third order.

In particular, since an electron starting out on the axis must necessarily have zero canonical angular momentum, the trajectories will be arranged so that only the focusing of a point source of electrons on the axis will be considered. The focusing of a point source off axis, in general, requires a consideration of all values of

* Assisted by the joint program of the ONR and AEC.

[1] Zworykin, *et al.*, *Electron Optics and the Electron Microscope* (John Wiley and Sons, Inc., New York), p. 504.

[2] H. M. Agnew and H. L. Anderson, Rev. Sci. Instr. **20**, 869 (1949).

TABLE I. Axial magnetic field of coils shown in Fig. 1.

z	0.00	4.00	8.00	12.00	16.00	20.00	24.00
	1.000	0.898	0.685	0.479	0.309	0.220	0.178
z	28.0	32.0	36.0	40.0	44.0	48.0	52.0
	0.170	0.199	0.269	0.380	0.602	0.838	0.990

the canonical angular momentum constant. One might choose to ask how the zero canonical angular momentum trajectories associated with the off axis point source behave and, in this manner, get some idea of the nature of the focusing of these points. We have chosen to omit this consideration.

Finally by replacing A_φ in Eq. (1) by the series expansion given by Eq. (4) and subsequently approximating Eq. (1) in such a manner that only the terms in ρ and $d\rho/dz$ up to and including the third power appear, a differential equation will result which will give the third-order radial trajectories as distinct from the first-order or paraxial trajectories.

SINGLE BELL-SHAPED FIELD TRAJECTORIES

As already discussed, the bell-shaped field used will be taken as

$$H(z)=H_0/(1+z^2/a^2). \tag{5}$$

For convenience the following symbols are introduced:

a = the half-breadth at half-maximum of the axial magnetic field distribution,
H_0 = the maximum value of the axial magnetic field,
y = the radial coordinate of the electron in units of a,
x = the axial coordinate of the electron in units of a,
φ = the angular displacement of the electron around the axis,
h = the axial magnetic field in units of H_0.

In addition, a measure of the strength of the magnetic field relative to the momentum of the electron is defined as:

$$k=aH_0/2A_0. \tag{6}$$

Equation (1), in the approximation being considered, becomes

$$y''+k^2h^2y=(k^2hh''/2-k^4h^4)y^3+k^2hh'y'y^2-k^2h^2(y')^2y, \tag{7}$$

where the prime designates a derivative with respect to x and

$$h=1/(1+x^2).$$

To solve Eq. (7) let

$$y=\lambda P+\mu Q+\lambda^3R+\lambda^2\mu S+\lambda\mu^2T+\mu^3U. \tag{8}$$

The paraxial or first-order solution would result from assuming that only the first two terms were present. Substituting Eq. (8) into Eq. (7) gives the following linear equations upon equating the coefficients of similar terms in λ and μ.

$$P''+k^2h^2P=0 \text{ with } P=0,\quad P'=1 \text{ at } x=0, \tag{9}$$

$$Q''+k^2h^2Q=0 \text{ with } Q=1,\quad Q'=0 \text{ at } x=0, \tag{10}$$

$$R''+k^2h^2R=(k^2hh''/2-k^4h^4)P^3 +k^2hh'P'P^2-k^2h^2(P')^2P \text{ with } R=R'=0 \text{ at } x=0, \tag{11}$$

$$S''+k^2h^2S=3k^2(hh''-2k^2h^4)P^2Q/2 +k^2hh'(2QPP'+P^2Q') -k^2h^2[Q(P')^2+2PQ'P'] \text{ with } S=S'=0 \text{ at } x=0, \tag{12}$$

$$T''+k^2h^2T=3k^2(hh''-2k^2h^4)Q^2P/2 +k^2hh'(2PQQ'+Q^2P') -k^2h^2[P(Q')^2+2QQ'P'] \text{ with } T=T'=0 \text{ at } x=0, \tag{13}$$

$$U''+k^2h^2U=k^2(hh''-2k^2h^4)Q^3/2 +k^2hh'Q'Q^2-k^2h^2(Q')^2Q \text{ with } U=U'=0 \text{ at } x=0. \tag{14}$$

The conditions at $x=0$ were chosen in order that $\lambda=\partial y/\partial x$, and $\mu=y$ at $x=0$. This makes the functions (Q, S, U) even in x and the functions (P, R, T) odd in x.

To solve Eqs. (9)–(14) it is convenient to introduce the variable θ through the relation:

$$x=\tan\theta. \tag{15}$$

Equations (9) and (10) are easily solved, the solutions being given in Eqs. (20) and (21). Substituting these

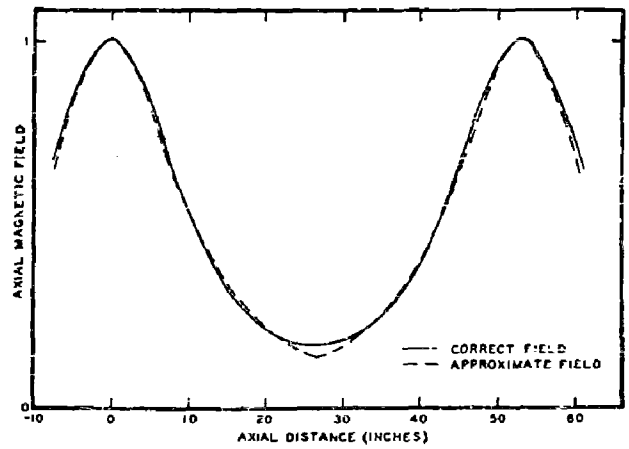

FIG. 2. Axial magnetic fields. (a) From $-\infty<x<2.5$, $h=1/(1+x^2)$, from $2.5<x<\infty$, $h=1/[1+(x-2.5)^2]$. (b) Magnetic field, normalized to unity at $x=0$, calculated for the coils shown in Fig. 1 using equations in Deutsch, Elliott, and Evans, Rev. Sci. Instr. 15, 178 (1944). The coil separation is set at $5a$, to coincide with (a). For the best fit with the coils shown in Fig. 1, the scale factor a was taken to be 10.60 in.

solutions into Eqs. (11)–(14) and defining $r=R\cos\theta$, $s=S\cos\theta$, $t=T\cos\theta$, $u=U\cos\theta$ gives:

$$\frac{d^2r}{d\theta^2}+(1+k^2)r = -\frac{k^2}{2(1+k^2)^{\frac{1}{2}}}(1+\cos2\theta)\sin(1+k^2)^{\frac{1}{2}}\theta - \frac{k^2}{2(1+k^2)}\sin2\theta(\cos(1+k^2)^{\frac{1}{2}}\theta - \cos3(1+k^2)^{\frac{1}{2}}\theta), \quad (16)$$

$$\frac{d^2s}{d\theta^2}+(1+k^2)s = -\frac{k^2}{2}(1+\cos2\theta)\cos(1+k^2)^{\frac{1}{2}}\theta + \frac{k^2}{2(1+k^2)^{\frac{1}{2}}}\sin2\theta(\sin(1+k^2)^{\frac{1}{2}}\theta - 3\sin3(1+k^2)^{\frac{1}{2}}\theta), \quad (17)$$

$$\frac{d^2t}{d\theta^2}+(1+k^2)t = -\frac{k^2(1+k^2)^{\frac{1}{2}}}{2}(1+\cos2\theta)\sin(1+k^2)^{\frac{1}{2}}\theta - \frac{k^2}{2}\sin2\theta(\cos(1+k^2)^{\frac{1}{2}}\theta+3\cos3(1+k^2)^{\frac{1}{2}}\theta), \quad (18)$$

$$\frac{d^2u}{d\theta^2}+(1+k^2)u = -\frac{k^2(1+k^2)}{2}(1+\cos2\theta)\cos(1+k^2)^{\frac{1}{2}}\theta + \frac{k^2(1+k^2)^{\frac{1}{2}}}{2}\sin2\theta(\sin(1+k^2)^{\frac{1}{2}}\theta + \sin3(1+k^2)^{\frac{1}{2}}\theta). \quad (19)$$

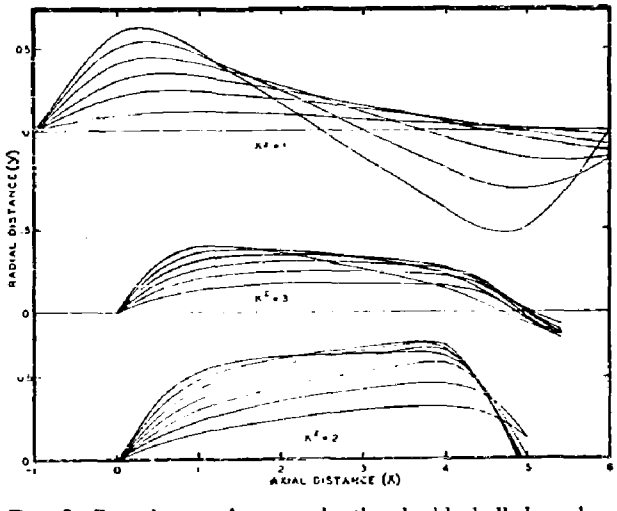

FIG. 3. Complete trajectories in the double bell-shaped axial magnetic field for $k^2=2$ and $k^2=3$ each with $x_1=0$ and for $k^2=1$ with $x_1=-1.030$.

It will be noticed that an even operator acts on the functions (r, s, t, u) to produce either even or odd functions. In these cases it can be shown that the particular integrals may be chosen to have the symmetry of the inhomogeneous part of the equation. Complementary solutions, Eqs. (20) and (21), then are added to allow the conditions at $\theta=0$ to be satisfied. By assuming the form of the particular integral, the coefficients may be determined by substitution into the differential equation. A check on the resulting solution was obtained by using the fact that the differential operator is self-adjoint, thus allowing the complementary solutions to be used as integrating factors in solving the equations by direct integration. The results are:

$$P=\frac{\sin(1+k^2)^{\frac{1}{2}}\theta}{(1+k^2)^{\frac{1}{2}}\cos\theta}, \quad (20)$$

$$Q=\frac{\cos(1+k^2)^{\frac{1}{2}}\theta}{\cos\theta}, \quad (21)$$

$$R=\frac{1}{8(1+k^2)^{\frac{1}{2}}(4k^2+3)\cos\theta} \times\{2k^2(1+k^2)^{\frac{1}{2}}(4k^2+3)\theta\cos(1+k^2)^{\frac{1}{2}}\theta - (16k^4+17k^2+3)\sin(1+k^2)^{\frac{1}{2}}\theta\} - \frac{3}{8}\frac{\cos2\theta}{(1+k^2)^{\frac{1}{2}}(4k^2+3)}\cdot\frac{\sin3(1+k^2)^{\frac{1}{2}}\theta}{\cos\theta} + \frac{\sin2\theta}{8(1+k^2)(4k^2+3)\cos\theta} \times\{k^2(4k^2+3)\cos(1+k^2)^{\frac{1}{2}}\theta - (2k^2+3)\cos3(1+k^2)^{\frac{1}{2}}\theta\}, \quad (22)$$

$$S=\frac{-1}{8(1+k^2)^{\frac{1}{2}}(4k^2+3\cos\theta} \times\{2k^2(4k^2+3)\theta\sin(1+k^2)^{\frac{1}{2}}\theta + 9(1+k^2)^{\frac{1}{2}}\cos(1+k^2)^{\frac{1}{2}}\theta\} + \frac{9\cos2\theta}{8(4k^2+3)\cos\theta} \cdot\cos3(1+k^2)^{\frac{1}{2}}\theta - \frac{\sin2\theta}{8(1+k^2)^{\frac{1}{2}}(4k^2+3)\cos\theta} \times\{k^2(4k^2+3)\sin(1+k^2)^{\frac{1}{2}}\theta - 3(2k^2+3)\sin3(1+k^2)^{\frac{1}{2}}\theta\}, \quad (23)$$

$$T=-\frac{1}{8(1+k^2)^{\frac{1}{2}}(4k^2+3)\cos\theta}$$
$$\times\{2k^2(1+k^2)^{\frac{1}{2}}(4k^2+3)\theta\cos(1+k^2)^{\frac{1}{2}}\theta$$
$$-(16k^4-3k^2-9)\sin(1+k^2)^{\frac{1}{2}}\theta\}$$
$$-\frac{9(1+k^2)^{\frac{1}{2}}\cos2\theta}{8(4k^2+3)\cos\theta}\cdot\sin3(1+k^2)^{\frac{1}{2}}\theta$$
$$+\frac{\sin2\theta}{8(4k^2+3)\cos\theta}\{k^2(4k^2+3)\cos(1+k^2)^{\frac{1}{2}}\theta$$
$$+3(2k^2+3)\cos3(1+k^2)^{\frac{1}{2}}\theta\}, \quad (24)$$

$$U=-\frac{(1+k^2)^{\frac{1}{2}}}{8(4k^2+3)\cos\theta}\{2k^2(4k^2+3)\theta\sin(1+k^2)^{\frac{1}{2}}\theta$$
$$-3(1+k^2)^{\frac{1}{2}}\cos(1+k^2)^{\frac{1}{2}}\theta\}-\frac{3(1+k^2)\cos2\theta}{8(4k^2+3)\cos\theta}$$
$$\cdot\cos3(1+k^2)^{\frac{1}{2}}\theta-\frac{(1+k^2)^{\frac{1}{2}}\sin2\theta}{8(4k^2+3)\cos\theta}$$
$$\times\{k^2(4k^2+3)\sin(1+k^2)^{\frac{1}{2}}\theta$$
$$+(2k^2+3)\sin3(1+k^2)^{\frac{1}{2}}\theta\}. \quad (25)$$

Equations (20)–(25) together with Eqs. (8) and (15) constitute the complete third-order solution of the trajectories of the bell-shaped field. For a given k, a trajectory is defined by the number pair (λ_1, μ_1) where λ_1 and μ_1 are, respectively, the particular choices of the slope and value of the trajectory at the origin. An alternative designation of the trajectories may be made using the number pair (λ, x_1) where x_1 is the initial position of the electron starting out on the axis and λ is the corresponding slope at x_1. To convert from (λ, x_1) to (λ_1, μ_1) it is necessary to solve the pair of equations:

$$y(\lambda_1, \mu_1; x_1)=0; \quad y'(\lambda_1, \mu_1; x_1)=\lambda. \quad (26)$$

This will give $\lambda_1(\lambda, x_1)$ and $\mu_1(\lambda, x_1)$ which may be inserted into Eq. (8) for the number pair (λ, μ) to give the trajectory beginning at $x=x_1$, $y=0$ with a slope λ. The simple bell-shaped field trajectories, of course, do not form as close an approximation to the actual single coil trajectories as do the double bell-shaped field trajectories to the actual double coil trajectories. For this reason, it is not possible to check the single lens solution with the careful single lens computations of Keller, Koenigsberg, and Paskin.[3]

DOUBLE BELL-SHAPED FIELD TRAJECTORIES

If the center of the first coil (see Fig. 1) is at $x=0$ and the center of the second coil is at $x=2x_0$, then let region I be defined by $-\infty<x<x_0$ and region II be defined by $x_0<x<\infty$. For the same k in each region (same ampere-turns in each coil), let the radial trajectory be designated in region I by $y_{\rm I}=y(k, \lambda_1, \mu_1; x)$ and in region II by $y_{\rm II}=y(k, \lambda_2, \mu_2; x-2x_0)$. The conditions for smooth matching of the trajectories at $x=x_0$ may be stated as:

$$y(k, \lambda_1, \mu_1; x_0)=y(k, \lambda_2, \mu_2; -x_0), \quad (27)$$

and

$$y'(k, \lambda_1, \mu_1; x_0)=y'(k, \lambda_2, \mu_2; -x_0). \quad (28)$$

For a fixed k and x_0 it is desired to know λ_2 and μ_2 in terms of λ_1 and μ_1. Then, since the solution of Eq. (26) gives λ_1 and μ_1 in terms of λ and x_1, it is possible to obtain λ_2 and μ_2 in terms of λ and x_1. Thus, one picks a value x_1 where the electron starts out on the axis with a slope λ. From this, λ_1, μ_1, λ_2, μ_2 may be determined by solving Eqs. (26)–(28). By the use of Eqs. (8), (15), and (20)–(25) the complete trajectory may be drawn.

The sample trajectories are drawn for $k^2=0.75$ with $x_0=-1.030$ and -0.684, for $k^2=1.000$ with $x_1=-1.030$, and for $k^2=2.000$ and 3.000 each with $x_1=0.000$. In each case the value of x_0 was taken to be 2.500. The values of the initial slope λ range from 0.100 to 0.800. Table III gives the results of a graphical solution of Eqs. (26), (27) and (28). By using the tabulated values of the functions (P, Q, R, S, T, U) in Table II, it then is possible to construct the complete trajectories (Table IV and Figs. 3 and 4.

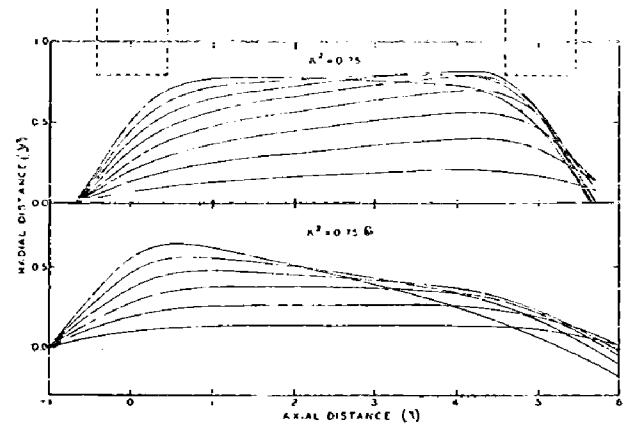

FIG. 4. Complete trajectories in the double bell-shaped axial magnetic field for $k^2=0.75$ with $x_1=-1.030$ and $x_1=-0.684$. Dotted lines indicate position of coils.

Discussion

An examination of the trajectories in Figs. 3 and 4 shows that some cases do not display suitable ring foci. This situation arose because it was not known a priori what values of k^2 and x_1 to choose before starting the calculation. The trajectories for $k^2=2$ and 3 with $x_1=0$ were calculated first because the computations are considerably reduced if x_1 is set equal to zero. For $k^2=3$ the trajectories between $\lambda=0.5$ and 0.7 come to a good focus at $x=5.25$, $y=-0.12$. For $k^2=2$ the trajectories between $\lambda=0.4$ and 0.7 come to a reasonably good focus at $x=4.4$, $y=0.48$. A value of k^2 somewhat nearer to 3

[3] J. M. Keller, E. Koenigsberg, and A. Paskin, Rev. Sci. Instr. 21, 715 (1950).

TABLE II. Functions used in computing trajectories. The derivatives were calculated by taking the derivative of the functions rather than by using differences. Differences not shown gave rough check.

θ	x		P				Q			
		k^2	0.750	1.000	2.000	3.000	0.750	1.000	2.000	3.000
0.000	0.000		0.000	0.000	0.000	0.000	1.000	1.000	1.000	1.000
0.200	0.203		0.202	0.201	0.200	0.199	0.985	0.980	0.960	0.940
0.400	0.423		0.414	0.411	0.400	0.389	0.937	0.917	0.835	0.757
0.600	0.684		0.653	0.643	0.603	0.565	0.850	0.801	0.614	0.439
0.800	1.030		0.946	0.919	0.815	0.717	0.764	0.610	0.264	−0.042
1.000	1.557		1.356	1.293	1.055	0.842	0.451	0.289	−0.297	−0.770
1.100	1.965		1.655	1.550	1.202	0.891	0.254	0.034	−0.724	−1.297
1.190	2.498		2.034	1.890	1.370	0.928	−0.009	−0.301	−1.267	−1.947

θ	x	P'				Q'			
0.600	0.684	0.883				−0.381			
0.800	1.030	0.814	0.755	0.535	0.329	−0.451	−0.587	−1.054	−1.414
1.190	2.498	0.701	0.611	0.298	0.051	−0.495	−0.626	−1.005	−1.185

θ	x		R				S			
		k^2	0.750	1.000	2.000	3.000	0.750	1.000	2.000	3.000
0.000	0.000		0.000	0.000	0.000	0.000	0.000	0.000	0.000	0.000
0.200	0.203		−0.001	−0.001	−0.003	−0.004	−0.016	−0.030	−0.042	−0.621
0.400	0.423		−0.010	−0.013	−0.024	−0.035	−0.071	−0.094	−0.181	−0.261
0.600	0.684		−0.037	−0.049	−0.091	−0.129	−0.184	−0.238	−0.425	−0.570
0.800	1.030		−0.104	−0.134	−0.234	−0.308	−0.365	−0.458	−0.722	−0.857
1.000	1.557		−0.241	−0.298	−0.483	−0.585	−0.621	−0.745	−0.979	−0.969
1.100	1.965		−0.357	−0.442	−0.668	−0.770	−0.788	−0.919	−1.074	−0.938
1.190	2.498		−0.510	−0.623	−0.894	−0.985	−0.982	−1.112	−1.146	−0.861

θ	x	R'				S'			
0.600	0.684	−0.147				−0.496			
0.800	1.030	−0.230	−0.289	−0.460	−0.549	−0.525	−0.617	−0.707	−0.530
1.190	2.498	−0.287	−0.337	−0.407	−0.380	−0.345	−0.338	−0.105	0.159

θ	x		T				U			
		k^2	0.750	1.000	2.000	3.000	0.750	1.000	2.000	3.000
0.000	0.000		0.000	0.000	0.000	0.000	0.000	0.000	0.000	0.000
0.200	0.203		−0.005	−0.008	−0.018	−0.029	−0.026	−0.039	−0.116	−0.231
0.400	0.423		−0.039	−0.052	−0.114	−0.184	−0.096	−0.145	−0.426	−0.834
0.600	0.684		−0.105	−0.139	−0.279	−0.440	−0.197	−0.298	−0.860	−1.647
0.800	1.030		−0.188	−0.242	−0.469	−0.772	−0.325	−0.491	−1.396	−2.587
1.000	1.557		−0.274	−0.348	−0.737	−1.392	−0.501	−0.757	−2.090	−3.605
1.100	1.965		−0.324	−0.415	−0.978	−1.958	−0.630	−0.950	−2.543	−4.112
1.190	2.498		−0.385	−0.504	−1.329	−2.722	−0.793	−1.193	−3.061	−4.553

θ	x	T'				U'			
0.600	0.684	−0.267				−0.388			
0.800	1.030	−0.205	−0.250	−0.495	−1.008	−0.352	−0.532	−1.452	−2.404
1.190	2.498	−0.114	−0.171	−0.680	−1.427	−0.303	−0.448	−0.913	−0.669

than 2 would undoubtedly give a good point focus on the axis since, at the focus, y is negative for $k^2=3$ and positive for $k^2=2$.

It was then realized that rather a large power dissipation in the coils would result from using these trajectories since the magnetic field from $x=-\infty$ to $x=0$ and from $x=5$ to $x=\infty$ is not utilized. For example, if $k^2=3$ is used, about 200 kw would be needed to focus a 12-Mev electron. To remedy this, the trajectories for $k^2=1$ and $x_1=-1.030$ ($\theta_1=-0.800$) were computed. A rather poor focus of the trajectories between $\lambda=0.1$ and 0.33 was obtained at $x=4.2$, $y=0.05$. In order to include the higher angle trajectories in the focus, a lower value of $k^2=0.75$ was tried with the same $x_1=-1.030$. The situation improved somewhat, a rather poor focus being obtained for the trajectories between $\lambda=0.1$ and 0.4 at $x=5.7$, $y=0.05$. Keeping the same value of $k^2=0.75$, the initial point x_1 was set at -0.684 ($\theta_1=-0.600$). A fair

TABLE III. Matching conditions for the various trajectories with $x_0=2.500$. In the cases where $x_1=0$ the values of λ_1 and μ_1 are easily determined to be $\lambda_1=\lambda$, and $\mu_1=0$.

		$k^2=0.750$; $x_1=0.684$					$k^2=0.750$; $x_1=-1.030$		
λ	λ_1	μ_1	λ_2	μ_2	λ	λ_1	μ_1	λ_2	μ_2
0.100	0.085	0.065	−0.088	0.174	0.100	0.070	0.095	−0.070	0.101
0.200	0.169	0.130	−0.191	0.332	0.200	0.138	0.189	−0.138	0.183
0.300	0.251	0.196	−0.316	0.458	0.300	0.202	0.282	−0.195	0.229
0.400	0.330	0.260	−0.469	0.542	0.400	0.260	0.373	−0.232	0.229
0.500	0.406	0.323	−0.619	0.571	0.500	0.310	0.464	0.240	0.169
0.600	0.478	0.386	−0.705	0.569	0.600	0.355	0.553	−0.226	0.056
0.700	0.545	0.446	−0.675	0.532					
0.800	0.608	0.509	−0.552	0.465					

		$k^2=1.000$; $x_1=-1.030$			$k^2=2.000$ $x_1=0.000$			$k^2=3.000$ $x_1=0.000$		
λ	λ_1	μ_1	λ_2	μ_2	λ	λ_2	μ_2	λ	λ_2	μ_2
0.100	0.061	0.092	−0.044	0.009	0.200	−0.393	0.138	0.200	−0.231	0.012
0.220	0.129	0.201	−0.088	0.000	0.300	−0.686	0.134	0.300	−0.325	0.008
0.330	0.185	0.299	−0.100	−0.052	0.400	−0.969	0.010	0.400	−0.381	−0.005
0.440	0.231	0.396	−0.073	−0.169	0.500	−1.092	−0.089	0.500	−0.381	−0.021
0.560	0.267	0.498	0.024	−0.362	0.600	−1.113	−0.132	0.600	−0.319	−0.040
0.670	0.287	0.590	0.287	−0.590	0.700	−1.090	−0.127	0.700	−0.186	−0.074
					0.800	−0.985	−0.063			

focus for the trajectories between $\lambda=0.4$ and 0.7 was obtained at $x=4.95$, $y=0.55$. From the manner in which the trajectories seemed to be shifting with k^2 and x_1 a slightly better focus would probably occur for $k^2=1$ and $x_1=-0.547$ ($\theta_1=-0.500$), however, it was felt that the small improvements that would occur might be nullified by the inexactness of the theory so that further computations were not carried out. The chief result, apart from an understanding of the nature of the trajectories, is that the maximum radial excursion of the usable electron trajectories is $y_{max}=0.83$ and that this occurs at $x=4.0$ assuming that the trajectories for $k^2=0.75$ and $x_1=-0.685$ are adopted. It should be noted that the inside diameter of the coils occurs at 0.788 as may be seen from the next section. Therefore, the latter trajectories are somewhat outside the minimum radius that the vacuum chamber is allowed to have. However, in view of small experimental changes that may be made in the choice of k^2 and x_1, it is believed that an adequate design may now be formulated.

DOUBLE LENS SPECTROMETER

In order that the theory of the bell-shaped field trajectories shall be a reasonable approximation to the actual trajectories in a double lens spectrometer, it is necessary that the actual coil configuration shall give a field along the axis that rather closely approximates the double bell-shaped field. Figure 2 shows that this may be done. The first coil design that was under consideration was to be made using 2.000-in.×0.0625-in. copper bus bar for the current carrying element and 0.375 in. sq copper tubing for the cooling. There were to be 4 copper bus coils of 126 turns using 0.010-in. insulation and 3-sq copper tubing spirals sandwiched between for cooling. Two additional cooling coils were then to be placed on the outside.

This gave a cross section for the coil of 9.125 in. by 9.140 in. The inside diameter was taken to be 8.360 in. Figure 2 shows that the actual field could be approximated by the double bell-shaped field if the separation between the coils were taken as 53.0 in. Since the dimensionless measure of the coil separation was taken to be 5.000, this required that the unit of distance, a, be taken as 10.6 in. Thus, in Fig. 4 all the dimensionless measures of distance should be multiplied by 10.6 in. to give the actual distances in inches. If a design using 3000 amp/in.^{2} as the maximum allowable current density is under consideration, then the power consumption in the coils is 160 kw total, and the maximum energy electron that may be focused is about 22 Mev. The value of $H_0=4700$ gauss and the value of $A_0=72{,}400$ gauss-cm.

If one were to consider a design where 10 Mev is the maximum electron energy, and where a more conservative value of 2000 amps/in.^{2} is taken for the maximum allowable current density, then all the above dimensionless considerations hold; it is only necessary to find the new unit of distance, a. Letting primes designate the values in the previous example, it may be shown that:

$$(a/a')^2=kj'A_0/k'jA_0', \tag{29}$$

and if P designates the total power consumption,

$$P/P'=j^2a^3/j'^2a'^3. \tag{30}$$

For the new example, $j/j'=\frac{2}{3}$, and since $A_0=34{,}600$ gauss-cm for a 10-Mev electron, $A_0/A_0'=0.478$. Therefore, $a=0.85a'=9.0$ in. and the power required is $P=(2/3)^2\times(0.85)^3\times160=43$ kw. This figure is about a factor of two higher than that required by a comparable uniform field design but might be bettered somewhat if more of the magnetic field beyond $x=5$ were utilized

TABLE IV. Complete trajectories for $x_0=2.500$. The errors involved in the calculation are indicated by the fact that some entries do not equal zero exactly (i.e., $x=-0.684$, $k^2=0.75$, and $x=-1.030$, $k^2=0.75$, and $k^2=1.000$).

λ \ x	−1.030	−0.684	−0.423	−0.203	0.000	0.203	0.423	0.684	1.030	1.557	1.965
$k^2=0.75$											
0.100		0.000	0.026	0.047	0.065	0.081	0.096	0.111	0.126	0.144	0.156
0.200		0.000	0.052	0.094	0.130	0.162	0.191	0.219	0.248	0.283	0.305
0.300		0.000	0.078	0.142	0.196	0.243	0.285	0.325	0.364	0.411	0.442
0.400		0.000	0.104	0.188	0.260	0.321	0.375	0.424	0.471	0.524	0.559
0.500		0.000	0.130	0.235	0.323	0.398	0.462	0.516	0.566	0.620	0.653
0.600		0.000	0.156	0.282	0.386	0.473	0.544	0.601	0.648	0.694	0.721
0.700		−0.002	0.179	0.325	0.446	0.544	0.620	0.675	0.715	0.746	0.763
0.800		0.000	0.208	0.374	0.509	0.617	0.695	0.744	0.769	0.775	0.773
$k^2=0.75$											
0.100	0.000	0.035	0.060	0.078	0.095	0.108	0.118	0.126	0.133	0.137	0.139
0.200	0.000	0.069	0.119	0.158	0.189	0.213	0.233	0.248	0.258	0.265	0.266
0.300	0.000	0.103	0.178	0.236	0.282	0.317	0.344	0.363	0.374	0.377	0.374
0.400	0.000	0.137	0.238	0.314	0.373	0.418	0.449	0.467	0.474	0.466	0.454
0.500	0.000	0.172	0.296	0.391	0.464	0.516	0.548	0.561	0.555	0.528	0.501
0.600	−0.002	0.205	0.355	0.469	0.553	0.611	0.640	0.643	0.620	0.564	0.516
$k^2=1.000$											
0.100	0.000	0.034	0.059	0.078	0.092	0.102	0.109	0.112	0.111	0.104	0.093
0.220	0.000	0.076	0.130	0.171	0.201	0.223	0.236	0.240	0.235	0.214	0.195
0.330	0.000	0.113	0.194	0.255	0.299	0.329	0.345	0.346	0.330	0.290	0.254
0.440	0.000	0.154	0.260	0.339	0.396	0.430	0.443	0.433	0.403	0.334	0.274
0.560	0.000	0.192	0.329	0.429	0.498	0.536	0.542	0.516	0.454	0.340	0.247
0.670	0.001	0.231	0.394	0.512	0.590	0.626	0.619	0.569	0.473	0.307	0.175
$k^2=2.000$											
0.200					0.000	0.040	0.080	0.120	0.161	0.207	0.235
0.300					0.000	0.060	0.119	0.178	0.237	0.302	0.341
0.400					0.000	0.080	0.159	0.235	0.311	0.391	0.438
0.500					0.000	0.100	0.197	0.290	0.378	0.467	0.518
0.600					0.000	0.119	0.235	0.342	0.438	0.529	0.577
0.700					0.000	0.139	0.272	0.391	0.490	0.573	0.613
0.800					0.000	0.159	0.308	0.436	0.532	0.597	0.620
$k^2=3.000$											
0.2000					0.000	0.040	0.078	0.112	0.141	0.164	0.172
0.3000					0.000	0.060	0.116	0.166	0.207	0.237	0.247
0.4000					0.000	0.079	0.154	0.218	0.267	0.299	0.307
0.5000					0.000	0.099	0.190	0.266	0.320	0.348	0.349
0.6000					0.000	0.118	0.226	0.311	0.364	0.379	0.368
0.7000					0.000	0.138	0.261	0.351	0.397	0.388	0.360
0.8000											

This would mean an investigation of the trajectories for somewhat lower values of λ and k^2 for various values of x_1 to see if a suitable ring focus could be obtained at $x>5.0$.

As a compensation for this higher power figure, it may be shown that the resolution of the double lens spectrometer is about eight times that of the uniform field type for the same transmission. Consider the focusing of the rays between $\lambda=0.4$ and $\lambda=0.7$ (5.5 percent of a sphere transmission). Figure 4 shows that these come to a ring focus within a range of about 0.03 in y for $k^2=0.75$. The momentum dispersion may be estimated as follows: from Fig. 3 for $k^2=1$, it may be seen that, for the mean trajectory ($\lambda=0.55$), $y=-0.36$ at $x=5$; Fig. 4 for $k^2=0.75$ gives $y=0.13$ at $x=5$. Since the ring focus will occur in the neighborhood of $x=5$, it is reasonable to assume that the shift in y for the mean trajectory at $x=5$ will be about the same as for the actual trajectories used (i.e., those more nearly like Fig. 4 for $k^2=0.75$ and $x_1=-0.685$). The change in the radial position of the ring focus for a given percentage change in the momentum then is measured by $A_0\partial\rho/\partial\lambda_0$ and for the above figures, this is $3.43a$ where, a, is the unit of distance associated with the design. A measure of the resolution may be taken as this dispersion divided by $0.03a$, or 114. If the trajectories of the uniform field spectrometer are drawn and similar estimates made, the figure corresponding to $0.03a$ is $0.02a$ and the figure corresponding to $3.43a$ is $0.275a$. Therefore, a measure of the momentum resolution similar to the above figure is 13.8. The ratio of these two resolutions is about eight. The actual ratio may be somewhat smaller than this since more of the magnetic field is utilized in the $x_1=1.030$ trajectories than in the $x_1=-0.685$ tra-

TABLE IV.—*Continued.*

2.498	3.035	3.443	3.970	4.316	4.577	4.797	5.000	5.203	5.423	5.684	6.030
0.171	0.185	0.194	0.203	0.204	0.199	0.189	0.174	0.153	0.126	0.089	
0.333	0.359	0.377	0.394	0.395	0.385	0.364	0.332	0.287	0.228	0.150	
0.478	0.511	0.535	0.558	0.560	0.545	0.511	0.458	0.384	0.288	0.163	
0.578	0.638	0.666	0.693	0.695	0.672	0.622	0.542	0.434	0.296	0.119	
0.693	0.731	0.758	0.784	0.782	0.748	0.677	0.571	0.430	0.255	0.034	
0.753	0.783	0.805	0.825	0.814	0.768	0.683	0.569	0.402	0.208	−0.035	
0.780	0.795	0.805	0.808	0.787	0.736	0.651	0.532	0.382	0.198	−0.031	
0.767	0.758	0.748	0.725	0.691	0.639	0.564	0.465	0.343	0.194	0.008	
0.141	0.140	0.140	0.137	0.131	0.124	0.114	0.101	0.085	0.066	0.040	0.005
0.267	0.266	0.263	0.255	0.243	0.228	0.208	0.183	0.152	0.114	0.064	−0.004
0.368	0.360	0.352	0.335	0.316	0.293	0.264	0.229	0.185	0.132	0.064	−0.028
0.437	0.416	0.398	0.368	0.339	0.308	0.271	0.229	0.178	0.117	0.040	−0.063
0.463	0.422	0.388	0.338	0.296	0.256	0.215	0.169	0.118	0.059	−0.014	−0.110
0.450	0.382	0.327	0.251	0.195	0.146	0.101	0.056	0.010	−0.041	−0.100	−0.174
0.083	0.068	0.059	0.046	0.036	0.027	0.018	0.009	0.000	−0.009	−0.021	−0.035
0.167	0.137	0.114	0.081	0.058	0.037	0.018	0.000	−0.017	−0.036	−0.057	−0.081
0.204	0.153	0.114	0.060	0.022	−0.009	−0.031	−0.052	−0.071	−0.089	−0.106	−0.123
0.194	0.112	0.049	−0.034	−0.087	−0.124	−0.151	−0.169	−0.180	−0.184	−0.180	−0.167
0.119	−0.003	−0.098	−0.219	−0.291	−0.335	−0.358	−0.362	−0.348	−0.315	−0.261	−0.176
0.000	−0.175	−0.308	−0.473	−0.569	−0.619	−0.625	−0.590	−0.512	−0.394	−0.231	−0.001
0.266	0.296	0.313	0.320	0.303	0.265	0.209	0.138				
0.386	0.427	0.452	0.464	0.434	0.364	0.261	0.134				
0.491	0.540	0.570	0.572	0.503	0.372	0.200	0.010				
0.573	0.625	0.563	0.634	0.525	0.346	0.132	−0.089				
0.629	0.676	0.698	0.662	0.530	0.330	0.099	−0.132				
0.653	0.688	0.701	0.655	0.522	0.325	0.102	−0.127				
0.636	0.653	0.653	0.605	0.494	0.330	0.137	−0.063				
0.178	0.180	0.177	0.161	0.134	0.098	0.057	0.012	−0.035	−0.081	−0.124	
0.252	0.252	0.247	0.221	0.182	0.131	0.071	0.008	−0.058	−0.120	−0.176	
0.309	0.304	0.292	0.257	0.220	0.145	0.071	−0.005	−0.071	−0.143	−0.206	
0.341	0.326	0.307	0.259	0.200	0.131	0.058	−0.021	−0.095	−0.161	−0.215	
0.344	0.314	0.284	0.224	0.160	0.094	0.028	−0.040	−0.098	−0.152	−0.191	
0.312	0.259	0.213	0.137	0.074	0.017	−0.031	−0.074	−0.105	−0.127	−0.134	

jectories. The actual resolution of the double lens spectrometer could be calculated rather than estimated as above, if the equation for the trajectories $y_{II}[k, \lambda_2(\lambda), \mu_2(\lambda); x]$ were linearized in the region of the ring focus. This seemed like an unreasonably long process so was not attempted.

If a design based on the above calculations is used, it is reasonable to suppose that the most desirable trajectories can be made to fall within the vacuum chamber. The exact trajectories can then be investigated by either of two techniques. One method makes use of the fact that a length of 0.003 in. copper wire carrying a suitable current traces out the exact trajectory of the electron.[4] A second method, described by Slatis,[5] makes use of photographic plates. These methods will also determine the trajectories of the off axis source points. Finally, as regards the azimuthal variation, Eq. (3), it was felt that this could be handled easily by experiment. No calculation of $\varphi(x)$ was undertaken since it would only serve to determine the rotation of the helical baffles. A first-order estimate of this rotation may be found in Agnew and Anderson.[2] This should be sufficient since the only purpose of these baffles is to discriminate between electron and positrons.

[4] V. K. Rasmussen, Jr., Cal. Inst. Tech. thesis (1950). Method suggested by C. Y. Chao.

[5] H. Slatis, Arkiv. f. Mat. Astron. o. Fys. 32A, No. 20 (1945), also H. Slatis and K. Siegbahn, P. R. 75, 1955 (1949).

ACKNOWLEDGMENTS

The author wishes to acknowledge the computing assistance of Mr. S. Forbes and Mrs. E. A. Seaman. Likewise, the continued interest of Dr. W. F. G. Swann, Director of the Bartol Foundation, was appreciated.

Reprinted from THE PHYSICAL REVIEW Vol. 84, No. 6, 1252-1253, December 15, 1951
Printed in U. S. A.

Absence of a Detectable Diurnal Variation in the Frequency of Heavy Primaries and Nuclear Disintegrations at 80,000 Feet*

GORDON W. MCCLURE AND MARTIN A. POMERANTZ
Bartol Research Foundation of the Franklin Institute, Swarthmore, Pennsylvania
(Received November 1, 1951)

A BALLOON-BORNE ionization chamber of the type previously employed to measure the variation of burst frequency with altitude at geomagnetic latitudes 52°N[1] and 69°N[2] has been sent aloft at night at Minneapolis, Minnesota, with the cooperation of ONR Project Skyhook in an attempt to detect a possible diurnal fluctuation in the intensity of the burst-producing radiation.

As in former flights, the instrument was calibrated by means of a built-in Po$-\alpha$ source, and was adjusted to respond to bursts of ionization $\geq$1.0 Po$-\alpha$. Our standard method of burst-telemetering and recording was used. Altitude data were supplied by General Mills Aeronautical Research Laboratory. To maintain the internal temperature at a safe level during the night, the gondola was wrapped in a 3-inch layer of cellulose padding and was heated electrically by storage batteries.

According to preflight plans, the instrument was to reach about 80,000 feet shortly after sundown and remain near that level until the following afternoon. Had this performance been realized, data from the Minnesota flight alone would have sufficed to establish the magnitude of the diurnal effect. Actually, the balloon altitude dropped rather rapidly after midnight and did not increase again at daybreak; consequently, it was necessary to compare the night counting rates at Minneapolis (geomag. lat. 55°N) with the day rates recorded at Swarthmore (geomag. lat. 52°N). The necessity of relying on the data from a single night flight is not regarded as a serious source of error, since variations in the data obtained from different instruments in numerous flights at Swarthmore and Ft. Churchill have been within the statistical uncertainties.

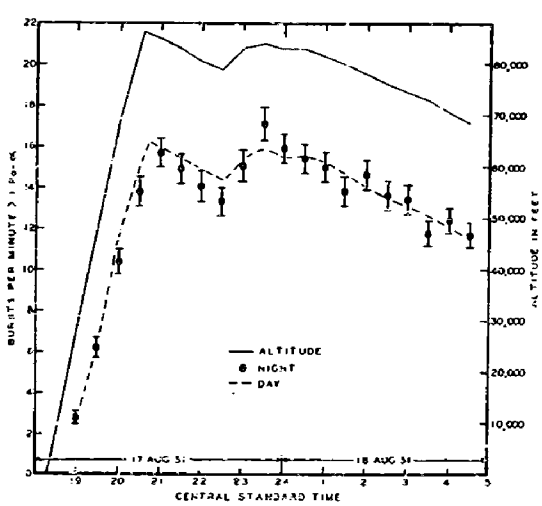

FIG. 1. Altitude *vs* time curve (solid line) for night flight at geomagnetic latitude 55°N and counting rates (solid circles) obtained with ionization chamber biased to record bursts $\geq$ 1 Po$-\alpha$. Counting rates averaged from four daytime flights (dashed curve) at corresponding altitudes show no significant deviations from night rates.

The latitude effect between Swarthmore and Minneapolis for this type of instrument is regarded as negligible in the light of previous measurements which have established that the daytime burst rates are the same at 52°N and 69°N at all altitudes up to 100,000 feet.

The altitudes and burst rates recorded during the night flight are plotted in Fig. 1. The dashed curve represents the counting rates averaged from four daytime flights at corresponding altitudes. The night counting rates are in excellent agreement with the day rates at all altitudes attained between sunset and sunrise. If a diurnal variation in the burst rate exists at all, its magnitude does not exceed the combined statistical and systematic uncertainties which are estimated as $\pm$5 percent.

According to a previous analysis[1] of the daytime results, 37 percent of the bursts at 80,000 feet are caused by primary heavy nuclei of charge $Z\geq 8$ and the remainder by nuclear disintegrations occurring in the chamber walls. Excluding the possibility that the intensities of the heavy nuclei and of the star-producing radiation vary from night to day in opposite senses (an increase in one being partially compensated by a decrease in the other), it is concluded that the heavy nucleus intensity does not change by more than $\pm$13 percent, nor the frequency of stars by more than $\pm$9 percent from night to day.

Photographic emulsion results[3] have indicated that the diurnal variation in the frequency of stars at balloon altitudes is smaller than 5 percent. On the other hand, the available emulsion data concerning heavy nuclei[3-5] seem to show a nighttime drop in intensity of 50 to 70 percent below the daytime value for nuclei with $Z\geq 10$.

If the emulsion evidence is correct on both points, the ion chamber rates should have been 18 to 26 percent lower during the night, at 80,000 feet. Such an effect is not observed and indeed lies considerably outside the range of the systematic and statistical uncertainties in the present results.

We are grateful to Mr. A. T. Bauman for the arrangement and supervision of the balloon flight, and to the National Geographic Society for continued support.

* Assisted by the joint program of the ONR and AEC.
[1] G. W. McClure and M. A. Pomerantz, Phys. Rev. 79, 911 (1950).
[2] Results to be published.
[3] J. J. Lord and M. Schein, Phys. Rev. 78, 484 (1950).
[4] J. J. Lord and M. Schein, Phys. Rev. 80, 304 (1950).
[5] Freier, Ney, Naugle, and Anderson, Phys. Rev. 79, 206 (1950).

Reprinted from THE REVIEW OF SCIENTIFIC INSTRUMENTS, Vol. 22, No. 11, 855-856 November, 1951
Printed in U. S. A.

The Spectrograms of Some Ultraviolet Scintillators*

H. O. ALBRECHT AND C. E. MANDEVILLE
Bartol Research Foundation of the Franklin Institute, Swarthmore, Pennsylvania
(Received May 25, 1951)

IN seven earlier publications,[1-4] the writers have described the detection of scintillations from crystals in photosensitive G-M tubes. Detectable scintillations are produced when the crystals are irradiated by alpha-, beta-, and gamma-rays. Since the cathode response of the photon counters is peaked in the ultraviolet, it has been necessary to prepare phosphors which would scintillate in that region. A considerable number of efficient ultraviolet scintillators have already been reported,[1-4] but a detailed discussion of their emission characteristics has not been given. The ultraviolet emission from several of these scintillators has been determined in a small Hilger quartz spectrograph, using Eastman 103a-0 plates.† Spectrograms resulting from alphas on CaF_2, NaCl-Ag, and NaBr-Ag are given in Fig. 1 where the exposed plates are themselves reproduced. Some of the scintillators did not give sufficient intensity for good photographic reproduction even after a considerable time of exposure. Accordingly, their spectra have been drawn along with those of the above three mentioned phosphors and are shown in Fig. 2. The third spectrogram of Fig. 2 is that of the *phosphorescence* from alphas on NaCl-Ag. To obtain this spectrum, the phosphor was irradiated for 1/120 of a second, allowed to decay for 1/120 sec, exposed before the slit of the spectrograph for 1/120 sec, and allowed to decay for another 1/120 sec before again being irradiated. This procedure was followed for sixteen hours.

From the spectrograms presented, it is evident that efficient ultraviolet scintillators exist in quantity for use with scintillation Geiger counters or with photomultipliers having their peak response in the ultraviolet. It is to be noted that the emission spectrum of Corning 9741 glass is included among the spectrograms of Fig. 2. This glass is a highly efficient ultraviolet transmitter and is used in the construction of the walls of scintillation G-M tubes. Its emission spectrum became of particular interest when it was found that alpha-particles could be counted by detection in scintillation Geiger counters of ultraviolet emitted from the glass walls themselves. For example, when 10 millicuries of polonium were brought near a scintillation Geiger counter, although no scintillating phosphors were present to be bombarded, a counting rate of $\sim 10^6$ counts per minute was observed. From the geometry, it was estimated that this corresponded to a detection efficiency of $\sim 10^{-4}$ percent. When the same source was housed in a bottle of ordinary soft glass and placed over an RCA-5819 photomultiplier tube, an even higher detection efficiency was noted.

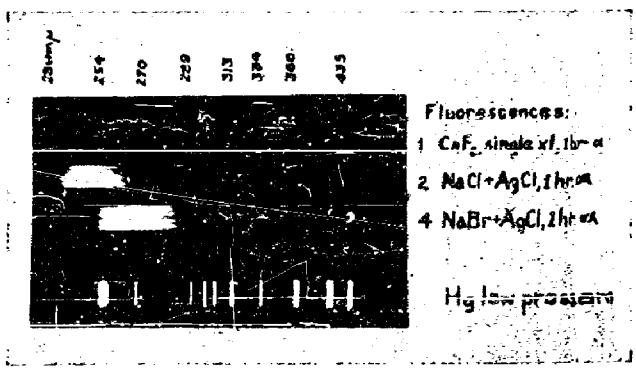

FIG. 1. Ultraviolet emission of alphas on CaF_2, NaCl-Ag, and NaBr-Ag. This is an actual photographic reproduction of the exposed plates.

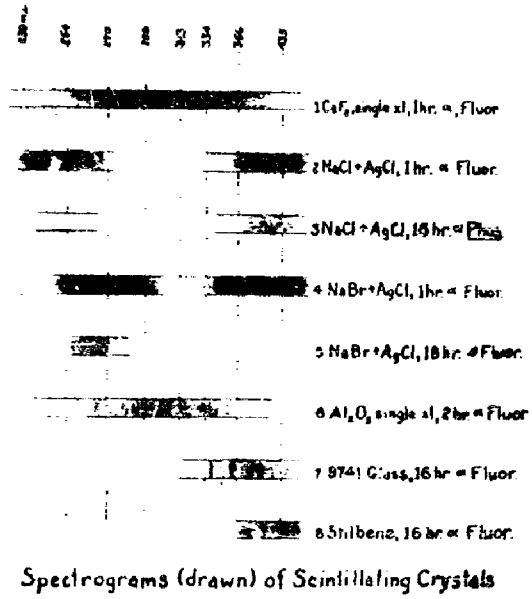

FIG. 2. Spectrograms of some ultraviolet scintillators. Owing to intensity problems, these spectra have been drawn.

* Assisted by the joint program of the ONR and AEC.
[1] C. E. Mandeville and H. O. Albrecht, Phys. Rev. 79, 1010 (1950); 80, 117 (1950); 80, 299 (1950); 80, 300 (1950).
[2] C. E. Mandeville, Nucleonics 7, No. 4, 92 (1950).
[3] C. E. Mandeville and M. V. Scherb, Nucleonics 7, No. 5, 34 (1950).
[4] H. O. Albrecht and C. E. Mandeville, Phys. Rev. 81, 163 (1951).
† These are partial spectra. Both the long and short wave limits (3300 AU–4500 AU) of the recorded spectrograms have been determined to a great extent by the sensitivity of the photographic plates.

Distribution List

Professional

Dr. W. F. G. Swann, Director, Bartol Research Foundation of the Franklin Institute, Swarthmore, Pennsylvania

Professor C. C. Lauritsen, Department of Physics
California Institute of Technology, Pasadena, California

Professor C. D. Anderson, Department of Physics
California Institute of Technology, Pasadena, California

Professor R. B. Brode, Department of Physics
University of California, Berkeley 4, California

Professor E. O. Lawrence, Radiation Laboratory
University of California, Berkeley 4, California

Professor J. R. Richardson, Department of Physics
University of California (Los Angeles) Los Angeles 24, California

Professor E. C. Creutz, Department of Physics
Carnegie Institute of Technology, Schenley Park, Pittsburgh 13, Pennsylvania

Dr. M. A. Tuve, Department of Terrestrial Magnetism
Carnegie Institute of Washington, Washington, D. C.

Dr. R. S. Shankland, Case Institute of Technology
Department of Physics, University Circle, Cleveland 6, Ohio

Professor S. K. Allison, Institute of Nuclear Studies
University of Chicago, Chicago, Illinois

Professor J. Rainwater, Columbia University,
Nevis Cyclotron Laboratories, P. O. Box 117,
Irvington-on-Hudson, New York

Professor R. R. Wilson, Laboratory of Nuclear Studies
Cornell University, Durham, North Carolina

Professor W. M. Nielson, Department of Physics
Duke University, Durham, North Carolina

Dr. Guy Suits, Research Laboratory, General Electric Company
Schenectady, New York

Dr. Zoltan Bay, Department of Physics,
George Washington University, Washington, D. C.

Professor N. F. Ramsey, Department of Physics
Harvard University, Cambridge, Massachusetts

Director, Nuclear Laboratory, Harvard University,
Cambridge, Massachusetts

Professor F. W. Loomis, Department of Physics,
University of Illinois, Urbana, Illinois

Professor A. C. G. Mitchell, Department of Physics,
Indiana University, Bloomington, Indiana

Professor J. A. Van Allen, Department of Physics,
State University of Iowa, Iowa City, Iowa

Professor J. D. Stranathan, Department of Physics,
University of Kansas, Lawrence, Kansas

Professor J. M. Cork, Department of Physics,
University of Michigan, Ann Arbor, Michigan

Professor W. E. Hazen, Department of Physics,
University of Michigan, Ann Arbor, Michigan

Professor J. H. Williams, Department of Physics,
University of Minnesota, Minneapolis, Minnesota

Professor E. P. Ney, Department of Physics,
University of Minnesota, Minneapolis, Minnesota

Professor Truman S. Gray, Servo-Mechanisms Laboratory,
Massachusetts Institute of Technology,
Cambridge 39, Massachusetts

Professor J. R. Zacharias, Laboratory of Nuclear Science and
Engineering, Massachusetts Institute of Technology,
Cambridge 39, Massachusetts (2)

Professor S. A. Korff, Department of Physics,
New York University, University Heights, New York 53, New York

Professor B. Waldman, Nuclear Physics Laboratory,
University of Notre Dame, Notre Dame, Indiana

Professor J. N. Cooper, Department of Physics,
Ohio State University, Columbus 10, Ohio

Professor W. E. Stephens, Department of Physics,
University of Pennsylvania, Philadelphia 4, Pennsylvania

Professor A. J. Allen, Department of Physics,
University of Pittsburgh, Pittsburgh, Pennsylvania

Professor C. T. Reynolds, Department of Physics,
Princeton University, Princeton, New Jersey

Professor H. C. White, Department of Physics,
Princeton University, Princeton, New Jersey

Professor Leticia del Rosario, Department of Physics,
Gobierno De Puerto Rico, Universidad De Puerto Rico,
Rio Piedras, Puerto Rico

Professor K. Lark-Horowitz, Department of Physics,
Purdue University, Lafayette, Indiana

Professor T. W. Bonner, Department of Physics,
Rice Institute, Houston, Texas

Professor R. E. Marshak, Department of Physics,
University of Rochester, Rochester, New York

Professor Charles A. Whitmer, Chairman,
Department of Physics, Rutgers University,
New Brunswick, New Jersey

Professor E. L. Ginzton, Microwave Laboratory,
Stanford University, Palo Alto, California

Professor F. Bloch, Department of Physics,
Stanford University, Palo Alto, California

Professor J. D. Trimmer, Department of Physics,
University of Tennessee, Knoxville, Tennessee

Professor A. L. Hughes, Department of Physics,
Washington University, St. Louis, Missouri

Professor R. D. Sard, Department of Physics,
Washington University, St. Louis, Missouri

Professor J. H. Manley, Department of Physics,
University of Washington, Seattle 5, Washington

Dr. J. W. Coltman, Research Laboratories, Westinghouse
Electric Corporation, East Pittsburgh, Pennsylvania

Professor R. G. Herb, Department of Physics,
University of Wisconsin, Madison 6, Wisconsin

Professor W. W. Watson, Department of Physics,
Sloane Physics Laboratory, Yale University,
New Haven, Connecticut (?)

Chief of Naval Research, Attn: Nuclear Physics Branch
Navy Department, Washington 25, D. C. (2)

Director, Naval Research Laboratory
Attn: Technical Information Officer, Washington 25, D. C. (9)

Director, Office of Naval Research
Chicago Branch Office, 844 North Rush St., Chicago 11, Illinois

Director, Office of Naval Research, San Francisco
Branch Office, 801 Donahue Street, San Francisco 24, California

Director, Office of Naval Research, New York
Branch Office, 346 Broadway, New York 13, New York

Director, Office of Naval Research, Pasadena
Branch Office, 1030 E. Green Street, Pasadena 1, California

Officer in Charge, Office of Naval Research, Navy No. 100,
Fleet Post Office, New York, New York (10)

Superintendent, Nucleonics Division, Naval Research Laboratory,
Anacostia, Washington, D. C.

Chief of the Bureau of Ships, Att: Code 390, Navy Department,
Washington 25, D. C.

Chief of the Bureau of Ships, Att: Code 330, Navy Department,
Washington 25, D. C.

Chief of the Bureau of Ordnance, Att: Ram, Navy Department,
Washington 25, D. C.

Chief of the Bureau of Ordnance, Att: ReSa, Navy Department,
Washington 25, D. C.

Chief of the Bureau of Aeronautics, Att: RS-5,
Navy Department, Washington 25, D. C.

Chief, Bureau of Aeronautics, Att: Technical Library
Navy Department, Washington 25, D. C.

Commanding Officer, Naval Radiological Defense Laboratory,
San Francisco Naval Shipyard, San Francisco, California

Chief of Naval Operations, Att: Op 36, Navy Department,
Washington 25, D. C.

Commander, U. S. Naval Ordnance Test Station,
Technical Library, Inyokern, China Lake, California

Commanding General, Air Force Cambridge Research Center,
Attn: Geophysics Research Library,
230 Albany Street, Cambridge 39, Massachusetts

Sandia Corporation, Sandia Base, Albuquerque, New Mexico
Classified Document Division, Attn: [illegible]

U. S. Atomic Energy Commission, Oak Ridge Division of Technical Information and Declassification Service, New York Operations Office, P. O. Box 30, Ansonia Station, New York 23, New York

National Bureau of Standards Library, Room 203,
Northwest Building, Washington 25, D. C.

National Science Foundation
2144 California Street, Washington 25, D. C.

Director, Office of Ordnance Research,
2127 Myrtle Drive, Durham, North Carolina

Foreign

Doctor Cesar Lattes
Scientific Director, Brazilian Center of Physical Research,
Rio de Janeiro, Brazil